1-1-1974

Optical studies of the crystallization and deformation of polyethylene terephthalate.

Ashok Misra
University of Massachusetts Amherst

OPTICAL STUDIES OF THE CRYSTALLIZATION AND DEFORMATION OF POLYETHYLENE TEREPHTHALATE

A Dissertation Presented

By

ASHOK MISRA

Submitted to the Graduate School of the
University of Massachusetts in partial fulfillment
of the requirements for the degree of

DOCTOR OF PHILOSOPHY

February 1974

Major Subject: Polymer Science & Engineering

OPTICAL STUDIES OF THE CRYSTALLIZATION AND DEFORMATION OF POLYETHYLENE TEREPHTHALATE

A Dissertation

By

ASHOK MISRA

Approved as to style and content by:

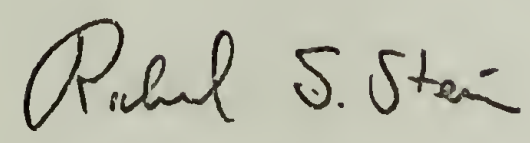

R. S. Stein, Chairman of Committee

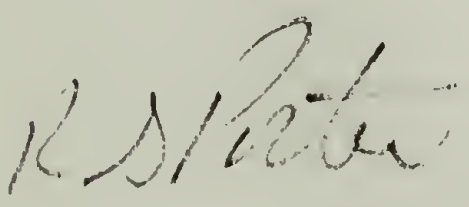

R. S. Porter, Member

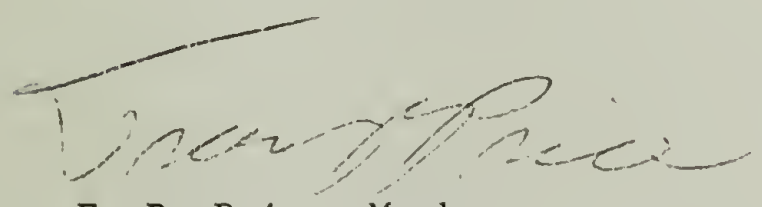

F. P. Price, Member

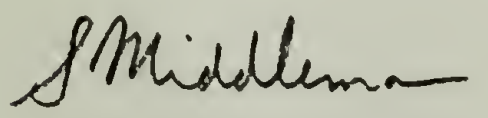

S. Middleman, Member

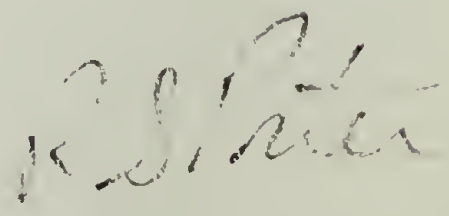

R. S. Porter, Department Head

February, 1974

DEDICATION

To my parents.

ACKNOWLEDGMENT

I wish to thank my advisor, Professor Richard S. Stein, for his guidance and encouragement throughout the course of this research. Thanks must also go to the other members of my committee for their availability, suggestions and constructive criticisms.

Helpful discussions with Professor Fraser P. Price, Professor Garth L. Wilkes and Robert Prud'homme are gratefully acknowledged.

I also wish to thank Dr. George C. Adams of du Pont for providing samples for this study and for his suggestions.

Lastly I wish to thank Mrs. Nancy MacLeay for the preparation of the manuscript.

OPTICAL STUDIES OF THE CRYSTALLIZATION AND DEFORMATION OF POLYETHYLENE TEREPHTHALATE

Ashok Misra

ABSTRACT

Low angle light scattering (LALS) theories have been developed for explaining scattering patterns obtained from solid polymer films which help in identifying the shape and the orientation of the crystalline morphology. In the present investigation these theories are extended to study the early stages of crystallization and the strain induced crystallization of polyethylene terephthalate (PET).

Light scattering patterns obtained with H_V polarization during the early stages of crystallization of PET exhibit a monotonic decrease in intensity which corresponds to a rod-like superstructure. With time, the pattern changes to that corresponding to a sheaf-like structure. Finally a spherulitic type pattern results with a maximum at some angle characteristic of the size of the spherulite. Thus it is shown that spherulites develop from rod-like precursors which evolve into sheaf-like structures and then eventually to spherulites. A series of V_V scattering patterns show a circular symmetry in the early stages changing to a two-fold symmetry at longer times. However, the V_V scattered intensity passes through a maximum during the course of crystallization. These observations are explained qualitatively on the basis of a recent theory.

A model containing two rate constants is presented for the development of spherulites from sheaves. One, G_R, is a radial spherulite growth rate while the other, G_S, describes the rate of increase of the apex angle of the sheaf. On the basis of this model, Avrami kinetics are developed which predict a change in the Avrami constant n from 5 to 3 as the sheaf develops into a spherulite. H_V light scattering patterns are calculated according to this model and are found to compare favorably with those found during the early stages of crystallization of PET.

The location of spherulite centers in a polyethylene sample is analysed. The size of spherulites in a volume-filled film is characterized by the distance to their boundaries. The regularity in size is characterized by a "truncation parameter", $\langle\sigma^2/\bar{a}^2\rangle$, where σ^2 is the variance. The value of $\langle\sigma^2/\bar{a}^2\rangle$ for a polyethylene sample is found to be lower than that based upon the assumption of random location of nuclei. Consequently, experimentally observed spherulites are more regular than those generated by random location. Experimental values may be duplicated by a model in which nuclei are excluded from regions within a certain distance of a given nucleus. Reasons for this non-random distribution of spherulites are discussed.

Strain induced crystallization of polyethylene terephthalate is studied by stretching quenched amorphous films at temperatures below and above its glass transition. Changes in birefringence, density, low angle light scattering and wide angle X-ray diffraction (XRD) are observed. Stretching below Tg is accompanied by necking where the necked region has a high degree of orientation as measured by birefringence and crystallinity as measured by density. The H_V, V_V and H_H scattering patterns show

the existance of a rod-like superstructure with a preferred orientation in the stretching direction. Annealing under constraint shows no significant changes while annealing with shrinkage results in the formation of rows of ellipsoidal spherulites where the rows are along the stretching direction and the long axis of ellipsoids are normal to it. Annealing also results in an increase in crystallinity and leads to an increase in the perfection of the crystalline structure as seen by XRD. Above Tg observations are made as a function of elongation and stretching temperature. With the temperature constant, orientation and crystallinity increase with elongation. LALS shows the formation of ellipsoidal spherulites with their long axis normal to the direction of stretching. Light micrographs confirm the LALS observations in both the cases.

TABLE OF CONTENTS

PREFACE

This dissertation has been divided into two categories, a) Unoriented Systems and b) Oriented Systems. In all there are five chapters, any of which may be read independently. Most of the work done was related to polyethylene terephthalate which justifies the title. However, work presented in Chapter III is on polyethylene.

Portions of Chapters I and III have been published. Chapter II is presented in the form of the published manuscript. Co-authors in the published work have been acknowledged. Chapters IV and V have not been published yet. However, manuscripts for their publications are under preparation.

CHAPTER I

EARLY STAGES OF CRYSTALLIZATION OF POLYETHYLENE TEREPHTHALATE

Introduction

Crystallization kinetics of polyethylene terephthalate (PET) have been studied by several investigators.[1-9] Recently the low angle light scattering technique[10,11] has been used to follow the kinetics of spherulitic crystallization[9,12,13] and it has proved a convenient method for measuring spherulite growth rates.

Barnov[11] and van Antwerpen[9] used light scattering to determine spherulitic growth rates for PET over a wide range of crystallization temperatures. They show that a plot of spherulitic radius versus crystallization time has a linear growth rate region which finally levels off to a constant radius value. However, they did not study the superstructure prior to the formation of spherulites. In the present investigation the main emphasis was to study the superstructure in the early stages of crystallization under conditions where crystallization is slow by light scattering. Portions of this chapter have been published.[14]

Experimental

Sample Preparation. Samples were prepared from 13 mil thick amorphous film of PET obtained through the courtesy of the Film Division of E. I. duPont de Nemours & Co. The film was characterized as:

Weight average molecular weight, M_w (light scattering) = 41,000

Number average molecular weight, M_n (osmometry) = 27,800

Mark-Houwink relations:

$$[\eta]_{TFA} = 4.33 \times 10^{-4} M_w^{0.68}$$

$$[\eta]_{TCE/Phenol} = 2.29 \times 10^{-4} M_w^{0.73}$$

Pieces of the film were pressed between microscope cover glasses of thickness 1.7 mil and heated to 290°C for 15 minutes in a silicone oil bath. They were then rapidly transferred to a crystallizing bath at 110°C for a predetermined period of time after which they were quenched into another silicone oil bath cooled to 0°C by an ice water mixture. Samples prepared in this fashion are convenient because they can be used directly for several optical studies.

Photographic Light Scattering. Light scattering patterns were obtained for cross polarization (H_V) as well as parallel polarization (V_V). The photographic apparatus with a Spectra-Physics He-Ne laser has been previously described.[15] A schematic diagram of the apparatus is shown in Figure 1.

During the early stages of crystallization there were two problems in obtaining the H_V scattering patterns: (1) the patterns were large in size and the entire pattern could not be recorded with the ordinarily used sample-to-film distance (≈15 cm). (2) The scattering intensity was low. In some cases the intensity was too low to be seen but could be recorded with a sufficiently long exposure time. To solve these two problems the photographic light scattering set up was modified such that the sample-to-film distance could be reduced to about 2 cm. thus making it possible to record scattering up to a 45° scattering angle. The reducing of sample-to-film distance also increased the intensity thus

reducing the exposure time required to take a picture. The intensity increases inversely with the square of the sample-to-film distance. Patterns were recorded on Polaroid type 57 film.

Results and Discussion

Photographic Light Scattering Studies. The low-angle light scattering patterns arising from spherulites are quite well understood.[10,11] Because of the reciprocal relationship between the size of the scattering pattern and the size of the scattering spherulite, the scattering pattern is large (but of low intensity) in early stages of the crystallization, and becomes smaller and more intense as spherulites grow. Consequently, this method is well suited for the study of early stages of the crystallization process provided that the sample-to-film distance is sufficiently small so as to record scattering at larger angles and the exposure time is long enough to record weak intensities. Polyethylene terephthalate is a good polymer for such studies in that it may be readily quenched from the crystallizing temperature to below its glass temperature where the crystallization rate is negligible. Thus, quenched films can be studied at leisure at room temperature utilizing exposure times that are as long as is necessary to record weak scattering intensities. It is estimated that it should be possible to examine spherulites only a few thousand Angstroms in diameter when they are not much bigger than their constituent crystals.

H_V Scattering Patterns. The scattering of light by incomplete spherulites having sheaf-like texture has been described.[16] It has been shown that the predictions of a two-dimensional "fan" model, Figure 2,

yield H_v scattering patterns ranging from the typical "four-leaf clover" characteristic of perfect spherulites where the fan angle, β, equals 90° to "rod-like" scattering patterns[17] as β becomes small. The spherulite H_v scattering patterns of perfect spherulites have zero intensity at scattering angle $\theta = 0°$ and a maximum at a value of θ characteristic of the spherulite diameter. On the other hand, the scattering from randomly oriented rods exhibits a maximum intensity at $\theta = 0°$ and a monotonically decreasing intensity with increasing values of θ. Thus, one might expect to see a changing character of the pattern as the spherulites evolve, provided the time required for the formation of spherulites is slow enough. For PET, crystallization from the melt at 110°C, was found to be suitable for such a study.

A series of H_v light scattering patterns during the early stages of crystallization are presented in Figure 3 as a function of crystallization time. It is seen that there is negligible scattering in sample (a) quenched from the melt. With short times of crystallization, (b) - (d), there is the development of a cross-type H_v pattern characteristic of the scattering from rod-like aggregates with their optic axes either along or perpendicular to the rod axes. It is believed that during this stage, one is observing the growth of the rod-like precursors of spherulites which are clusters of crystals of polyethylene terephthalate with correlated orientation, probably resulting from low-angle branching. These patterns are characterized by their having a maximum intensity at their center and a steady decrease in intensity along the 45° arms in going outward from the center. The rate of intensity fall-off with scattering angle increases with increasing length of the rods. The over-all intensity of the pattern increases with time as a consequence of the increasing length and number of these aggregates.

By picture (e), there is an indication of the development of lobes along these 45° axes with their centers at some distance from the center of the pattern. A comparison with theory[16] indicates that this is associated with the evolution of the rods to "sheafs" associated with an increase of the fan angle of the model of Figure 2. This process continues in the series (e) - (g) where a decrease in the intensity of the central cross and an increase in the intensity of the lobes is seen. A distinct scattering maximum is seen at some angle θ_m which decreases with increasing crystallization time characteristic of an inverse in the radius of the growing spherulite.

In (f) an increase in background scattering is evident. It is believed that this is a consequence of depolarization of the scattered light arising because of the large total amount of scattering at this stage where the dimensions of the spherulite are of the order of the wavelength of light. Also, because of the high intensity of V_V scattering at this stage, it is possible that some of the intense vertically polarized scattered light may "leak" through the horizontally oriented analyser. By (g), this radius has reached 1.4 μm. and the spherulite is relatively complete. While the intensity near the center is quite low, the lobes still maintain the "tennis racquet" shape described by Kawai, et. al. for imperfect spherulites.[18] By sample (h) which has crystallized for 45 minutes, the spherulites have grown to 4.75 μm. and no central cross is visible.

A series of light scattering patterns, in the range where a spherulitic maximum intensity is observed, is shown in Figure 4. It can be seen that the size of the patterns decreases with increasing

crystallization time up to 60 minutes after which it stays constant. Spherulite sizes were calculated from these patterns using the relationship:

$$4.1 = \left(\frac{4\pi R}{\lambda'}\right) \sin\left(\theta'_m/2\right) \qquad (1)$$

where: R = spherulitic radius

λ' is the wavelength of laser in the polymer

$$= \frac{\lambda \text{ (wavelength of laser in air)}}{\eta \text{ (refractive index of the polymer)}}$$

θ'_m is the corrected scattering angle for maximum intensity along the 45° azimuthal direction, and is related to the measured scattering angle (θ_m) and the refractive index of the polymer as $\sin \theta'_m = \sin (\theta_m)/_n$

Small values of $\sin (\theta'_m/2)$ can be approximated by $\theta_m/2$ (in radians) which results in:

$$R = \frac{4.1}{2} \quad \frac{\lambda}{\pi\theta_m} \qquad (2)$$

Spherulite sizes are plotted as a function of crystallization time in Figure 5. There are three regions of such a plot: (i) an induction region, up to 5 min. in which the patterns are not spherulitic in nature; (ii) a linear growth region from 5 - 50 min. where the spherulite radius is proportional to time; and (iii) an impingement region, beyond 50 min. where the spherulites impinge upon each other so that the radial growth rate tapers off. Beyond 60 min., little growth is seen, and this limiting radius of about 6.75 μm is dependent upon the initial density of nuclei.[13] The fact that the pattern in this region indicates some degree of

imperfection may result, in part from the truncations of the spheres arising because of impingement, as has been shown by a recent theoretical analysis.[19]

An extrapolation of the linear growth region to zero radius would lead to a negative intercept of the time axis, as has alsc been shown by Baranov, et al.[13] This apparent negative "induction time" is, of course, an artifact resulting from the incorrectness of this extrapolation because of the structure not being spherulitic at short times. At earlier times, the kinetics of growth of the rod-like and sheaf-like structures is different from that of spherulites.

The existance of sheaf-like structures between 2.75 and 5 min. has been shown earlier in Figure 3. A sheaf can be approximated by a conic sector, the radius of which may be calculated from the position of the maxima in the light scattering patterns. Photometric measurements were made for this purpose. The radii of these sheaves are seen to be along the spherulitic radial growth rate line in Figure 5. Extrapolating this straight line to zero time gives an intercept of 1 μm on the radius axis. This means that either the growth rate for the length of rods is faster than the radial growth rate or that the growth started from preformed 1 μm long rod-like nuclei.

Thus it is evident that the light scattering technique characterizes the development of spherulites from rod-like precursors at the beginning of crystallization. As crystallization proceeds the rod-like nuclei evolve into sheaflike structures and then eventually to spherulites. Because of the absence of a maximum at some angle in this early part of crystallization, it is difficult to estimate the size of the rods from the scattering photographs. However, photometric

measurement of the angular variation of intensity for these samples should serve to characterize the size of the entity and may characterize its growth.

V_V Scattering. Changes occuring in the scattering patterns obtained with the V_V mode of polarization (parallel polars) have been observed for polyethylene by Stein and Rhodes.[10] They observed that as amorphous polyethylene crystallized, the V_V scattered intensity first increased, then decreased after which it again increased. The corresponding H_V pictures showed a monotonic increase in intensity and were intense only during the second increase of the V_V intensity. They concluded that since V_V intensity depended upon the effective polarizability of the surroundings (α_s) but the H_V intensity did not, the maximum must be associated with the change in α_s with volume fraction of crystalline material.

A qualitative explanation of such an observation is quite straight forward.[20] The H_V scattering at small angles depends only upon fluctuations in the magnitude and optic axis orientation of anisotropic regions whereas the V_V scattering also depends upon fluctuations in the density or average polarizability. The V_V intensity maximum arises from the latter contribution. The origin of this average polarizability fluctuation is the difference between the average polarizability of the spherulite and that of its surrounding material. Its contribution is greatest when the polymer is about half spherulitic after which it decreases as the spherulites become volume filling due to interference. Thus the V_V scattering maximum should occur when the fraction of spherulites, ϕ_s, is approximately 0.5 and the minimum occurs around when ϕ_s is 1.0. The residual scattering

at this time arises from the anisotropy contribution. The second increase in V_V intensity as well as the increase in H_V intensity is associated with the increase in the anisotropy as the spherulites become more crystalline internally as a consequence of secondary crystallization.

An investigation similar to that of Stein and Rhodes[10] was carried out in this study for the isothermal crystallization of polyethylene terephthalate. Samples were crystallized at 110°C from the melt. The half-time crystallization under these conditions is about 15 minutes.[6] A series of V_V scattering patterns as a function of crystallization time is presented in Figure 6. Sample-to-film distance and the exposure times were the same for all pictures. It can be seen that the V_V intensity increases up to 10 minutes of crystallization, decreases between 10 and 30 minutes and then begins to increase again. It should be noted that from a study of H_V patterns it is known that the structure becomes spherulitic at 5 minutes. These observations are in agreement with the explanation given above. Since half-time of crystallization is about 15 minutes,[6] ϕ_s would be approximately 0.5 at 10 minutes. Also from Figure 5 it is seen that the increase in spherulitic radius is small after 60 minutes thus ϕ_s would be around one at this time. Examination under the microscope confirms that at 10 minutes the polymer is approximately half filled with spherulites and is completely filled at 1 hour as shown in Figures 7a and b respectively.

Recently a statistical theory has been developed by Stein and Yoon[20] which can explain quantitatively why the V_V scattered intensity passes through a maximum during crystallization. According to this theory the V_V intensity is a function of volume fraction of spherulites ϕ_s, polarizability of the surrounding medium α_m, tangential and radial

polarizabilities of the spherulite (α_t and α_r respectively) and the radius of the spherulite R. The expression for the V_V intensity is given as:[20]

$$I_{V_V} = K_1 V\pi R^3 B(\phi_s) \cos^2\rho_1 (3/u^3)^2 \times \{(\alpha_t - \alpha_d)(2 \sin U - U \cos U - \text{Si } U) + (\alpha_r - \alpha_d)(\text{Si } U - \sin U) + (\alpha_r - \alpha_t)[\cos^2(\theta/2)/\cos\theta] \cos^2\mu\ (4 \sin U - U \cos U - 3 \text{ Si } U)\}^2 \quad (3)$$

where $B(\phi_s)$ is a concentration dependent factor given as:

$$B(\phi_s) = \frac{\left[\cos^2\rho_1[\phi_s(1-\phi_s)(\alpha_t - \alpha_m)(\frac{2}{3}\alpha_r + \frac{1}{3}\alpha_t - \alpha_m) + \phi_s(\frac{1}{5} - \phi_s/9)(\alpha_r - \alpha_t)^2] + \sin^2\rho_1\ \phi_s/15\ (\alpha_r - \alpha_t)^2\right]}{\left[\cos^2\rho_1[(1-\phi_s)^2(\alpha_t - \alpha_m)(\frac{2}{3}\alpha_r + \frac{1}{3}\alpha_t - \alpha_m) + (\alpha_r - \alpha_t)^2(\frac{1}{5} - \frac{2\phi_s}{9} + \frac{\phi_s^2}{9})] + \sin^2\rho_1 \frac{\phi_s}{15}(\alpha_r - \alpha_t)^2\right]} \quad (4)$$

and, $U = (\frac{4\pi R}{\lambda}) \sin(\theta/2)$ $\qquad$ $\text{Si } U = \int_0^U \frac{\sin x}{x}\, dx$ $\qquad$ (5)

$$\alpha_t - \alpha_d = (\alpha_t - \alpha_m)(1-\phi_s) - (\phi_s/3)(\alpha_r - \alpha_t) \quad (6)$$

$$\alpha_r - \alpha_d = (\alpha_t - \alpha_m)(1-\phi_s) + [1-(\phi_s/3)](\alpha_r - \alpha_t) \quad (7)$$

When plotted as a function of ϕ_s, the V_V intensity will pass through a maximum if the polarizability of the surrounding is not between the

radial and tangential polarizabilities of the spherulites. In other words, either $\alpha_m < \alpha_t, \alpha_r$; or $\alpha_m > \alpha_t, \alpha_r$ which implies that $(\alpha_r - \alpha_m) \times (\alpha_t - \alpha_m) > 0$. This is usually true for crystalline polymers and is true for PET since a maximum in the V_v intensity as a function of crystallization time has been observed (Figure 4). It should be pointed out that the difference between the tangential and radial polarizabilities $(\alpha_t - \alpha_r)$ may increase during crystallization due to the increase in the crystallinity of the spherulite. This is known to be true in the case of polyethylene. Work is presently being done to see how $(\alpha_t - \alpha_r)$ varies during the crystallization of PET.[21]

The V_v intensity goes to a minimum value when ϕ_s reaches the value of unity since the terms arising from the effect of surrounding polarizibilities goes to zero. At this point the polymer in volume filled and any increase in the V_v intensity would be due to an increase in the value of $(\alpha_t - \alpha_r)$ resulting from the secondary crystallization occuring within the spherulites. If this is true a plot of crystallinity versus time would show an increase even after the spherulite radius has reached its maximum value. This second increase in the V_v intensity, if any, would be small since the increase in $(\alpha_t - \alpha_r)$ during secondary crystallization would be small.

H_v scattering, on the other hand, is a function of the volume fraction of spherulites ϕ_s, difference between the tangential and radial polarizabilities $(\alpha_t - \alpha_r)$, and the spherulitic radius. The expression for the H_v intensity is given as:[20]

$$I_{H_v} = \frac{1}{4} \phi_s K_5 \cos^2\rho_2 (\alpha_r - \alpha_t) R^3 \left(\frac{3}{U^3}\right)^2 \times \{(\alpha_r - \alpha_t)[\cos^2(\theta/2)/\cos\theta] \sin 2\mu [4 \sin U - U \cos U - 3 \mathrm{Si}\, U]\}^2 \quad (8)$$

Thus the H_v scattering intensity should increase monotonically during crystallization as can be seen in Figures 3 and 4. Any increase in H_v intensity after ϕ_s has attained a value of unity would be further indication of an increase in $(\alpha_t - \alpha_r)$ during the secondary crystallization.

Stein and Yoon theory[20] extends further to predict the shape of V_v scattering patterns during crystallization for two dimensional and three dimensional spherulites. In the two dimensional case, when the volume fraction of spherulites ϕ_s is small the scattering arises from density fluctuation and a circular pattern is predicted. As ϕ_s increases, the pattern develops a two-fold symmetry and is elongated along the polarization direction. When ϕ_s approaches unity, i.e., the spherulites become volume filling, the two-fold symmetry changes to a four-fold symmetry. On the other hand for the three dimensional case, the circular pattern is predicted as before during the early stages when ϕ_s is small. As ϕ_s increases and the spherulites become volume filling, the pattern changes, takes on a two-fold symmetry being elongated in the polarization direction, and maintains this two-fold symmetry. The actual shape of the pattern depends upon the anisotropy of the spherulite and the polarizability difference between the spherulite and its amorphous surroundings.[11,20] By comparing such a theory with the V_v scattering patterns in Figure 4 it can be concluded that PET has three-dimensional volume filling spherulites or has two-dimensional nonvolume filling spherulites. An examination under the microscope, Figure 7b, shows the polymer to have volume filling spherulites, thus they must be three dimensional.

It is seen that V_v light scattering provides information about the spherulitic crystallization process and can be used to study the

crystallization kinetics of polymers. A qualitative explanation of the changes occurring in the V_v patterns during the crystallization of PET has been presented. Quantitative work is in progress at the present time.[21] Samuels has used V_v scattering patterns from annealed isotactic polypropylene films in conjunction with refractive index and birefringence measurements to obtain information about the crystallization mechanism.[22]

References

1. M. J. Kolb and E. F. Izard, J. Appl. Phys. 20, 571 (1949).
2. W. M. Cobbs and R. B. Burton, J. Polymer Sci. 12, 275 (1953).
3. A. Keller, G. R. Lester, and L. B. Morgon, Phil. Trans. Roy. Soc. (London) A247, 1 (1954).
4. F. D. Hartley, F. W. Lord and L. B. Morgon, Phil. Trans. Roy. Soc. A247, 23, (1954).
5. L. B. Morgon, Phil. Trans. Roy. Soc. A247, 13 (1954).
6. K. G. Mayhan, W. J. James and W. Bosch, J. Appl. Polymer Sci. 9, 3605 (1965).
7. G. S. Fiedling-Russell and P. S. Pillai, Die Makromolekulare Chemie 135, 263 (1970).
8. F. van Antwerpen and D. W. van Krevelen, J. Polymer Sci. A-2, 10, 2409 (1973).
9. F. van Antwerpen and D. W. van Krevelen, J. Polymer Sci. A-2, 10, 2423 (1973).
10. R. S. Stein and M. B. Rhodes, J. Appl. Phys., 31, 1873 (1960).
11. R. Samuels, J. Polymer Sci. A-2, 9, 2165 (1971).
12. C. Picot, G. Weill and H. Benoit, J. Polymer Sci. C, 16, 3973 (1968).
13. V. G. Baranov, A. V. Kanarov and T. I. Volkov, J. Polymer Sci. C, 30, 271 (1970).
14. A. Misra, R. S. Stein, J. Polymer Sci. B, 10, 473 (1972).
15. G. C. Adams, Ph.D. Dissertation, University of Massachusetts, Amherst, Massachusetts, 1966; J. Polymer Sci., A-2, 6, 31 (1968).
16. C. Picot, R. S. Stein, M. Motegi and H. Kawai, J. Polymer Sci. A-2, 8, 2115 (1970).

17. M. B. Rhodes and R. S. Stein, J. Polymer Sci., A2, 7, 1539 (1969).

18. M. Motegi, T. Oda, M. Moritani and H. Kawai, Polymer Journal (Japan), 1, 209 (1970).

19. R. E. Prud'homme and R. S. Stein, J. Polymer Sci., A2, 8, 1683 (1973).

20. D. Y. Yoon and R. S. Stein, submitted for publication in J. Polymer Sci., A2; D. Y. Yoon, Ph.D. Dissertation, University of Massachusetts.

21. R. S. Stein, A. Misra and T. Yuasa, in preparation.

22. R. J. Samuels, submitted for publication in J. Polymer Sci. A2.

Captions for Figures

Figure 1: Schematic diagram of the photographic light scattering set up.

Figure 2: The "fan-model" of a two-dimensional sheaf-like incomplete spherulite.

Figure 3: H_v light scattering patterns during the early stages of crystallization of PET when crystallized from the melt at 110°C.

Sample to Photographic Film Distance = 3.86 cm

Sample	Crystallization Time	Relative Exposure Time
a	0	60 seconds
b	0.5 minutes	60 seconds
c	1.0 minutes	20 seconds
d	2.0 minutes	15 seconds
e	2.75 minutes	5 seconds
f	3.5 minutes	1 second
g	5.0 minutes	2 seconds
h	45.0 minutes	0.2 seconds

Figure 4: H_v light scattering patterns during the spherulitic growth of PET when crystallized from the melt at 110°C.

Sample-to-Film Distance = 15 cm.

Sample	Crystallization Time	Relative Exposure Time
a	5 minutes	1/5 second
b	10 minutes	1/10 second
c	20 minutes	1/50 second
d	30 minutes	1/100 second
e	45 minutes	1/100 second
f	60 minutes	1/100 second
g	90 minutes	1/100 second

Figure 5: A plot of spherulite radius as a function of crystallization times of PET samples crystallized from the melt at 110°C.

Figure 6: V_v light scattering patterns for PET samples crystallized from the melt at 110°C. Sample-to-film distance = 10 cm. Exposure time is the same for all pictures.

Figure 7: Photomicrograph of a PET sample crystallized from the melt at 110°C

a) For 10 minutes. Magnification = 350x

b) For 60 minutes. Magnification = 70x

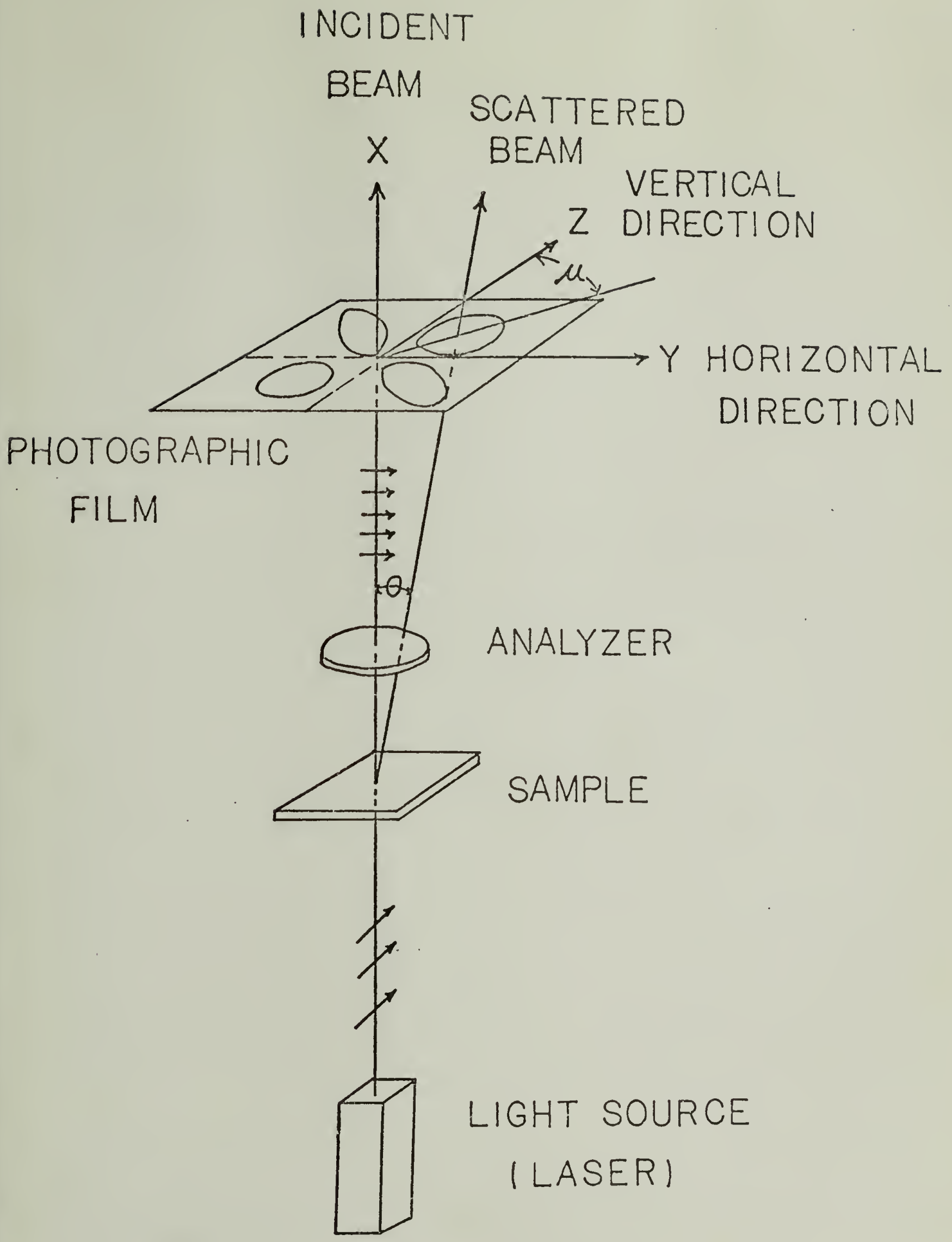
INCIDENT
BEAM
SCATTERED
BEAM
X
VERTICAL
Z DIRECTION
μ
Y HORIZONTAL
DIRECTION
PHOTOGRAPHIC
FILM
θ
ANALYZER
SAMPLE
LIGHT SOURCE
(LASER)

Figure 1

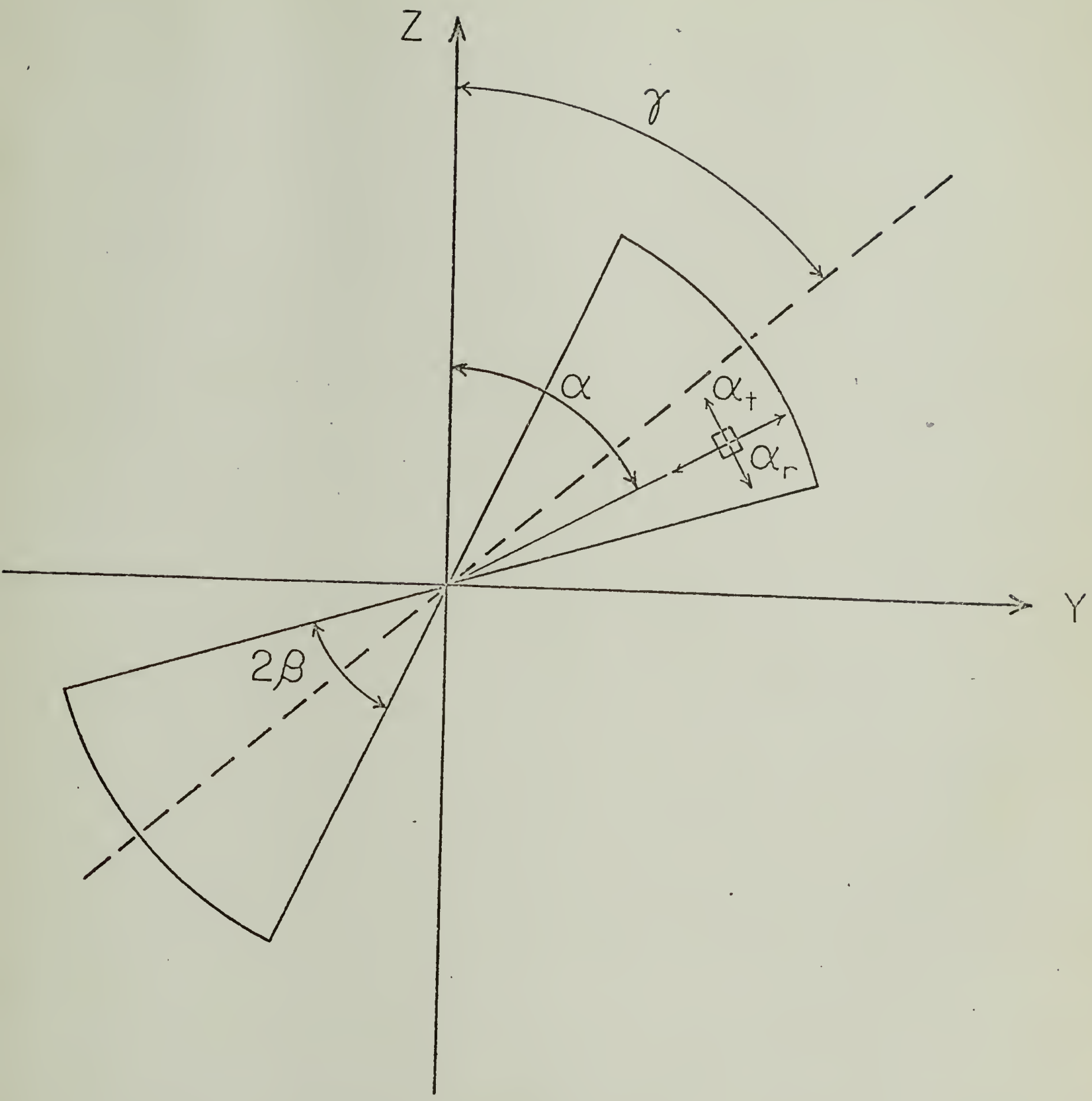

Figure 2

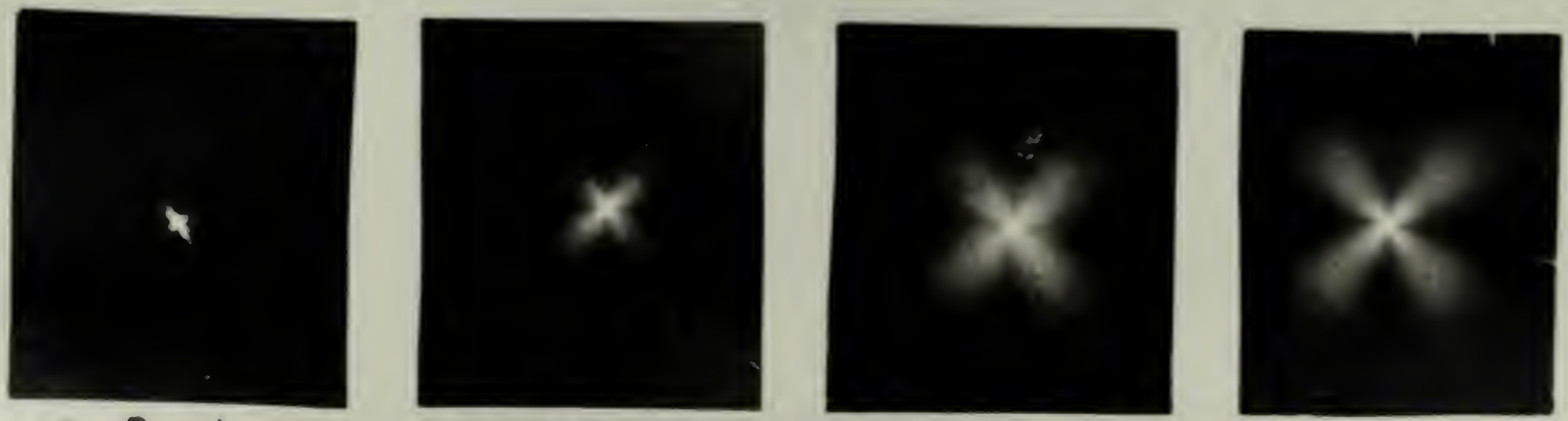
a. 0 min
b. 0·5 min
c. 1 min
d. 2 mins
5 cm
e. 2·75 mins
f. 3·5 mins
g. 5 mins
h. 45 mins

Figure 3

a. 5 mins

b. 10 mins

c. 20 mins

d. 30 mins

e. 45 mins

f. 60 mins

g. 90 mins

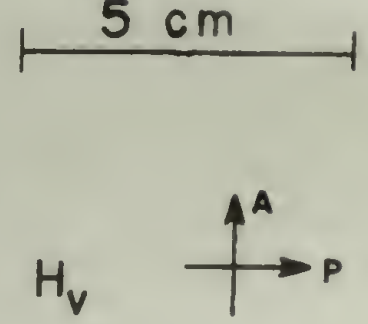

Figure 4

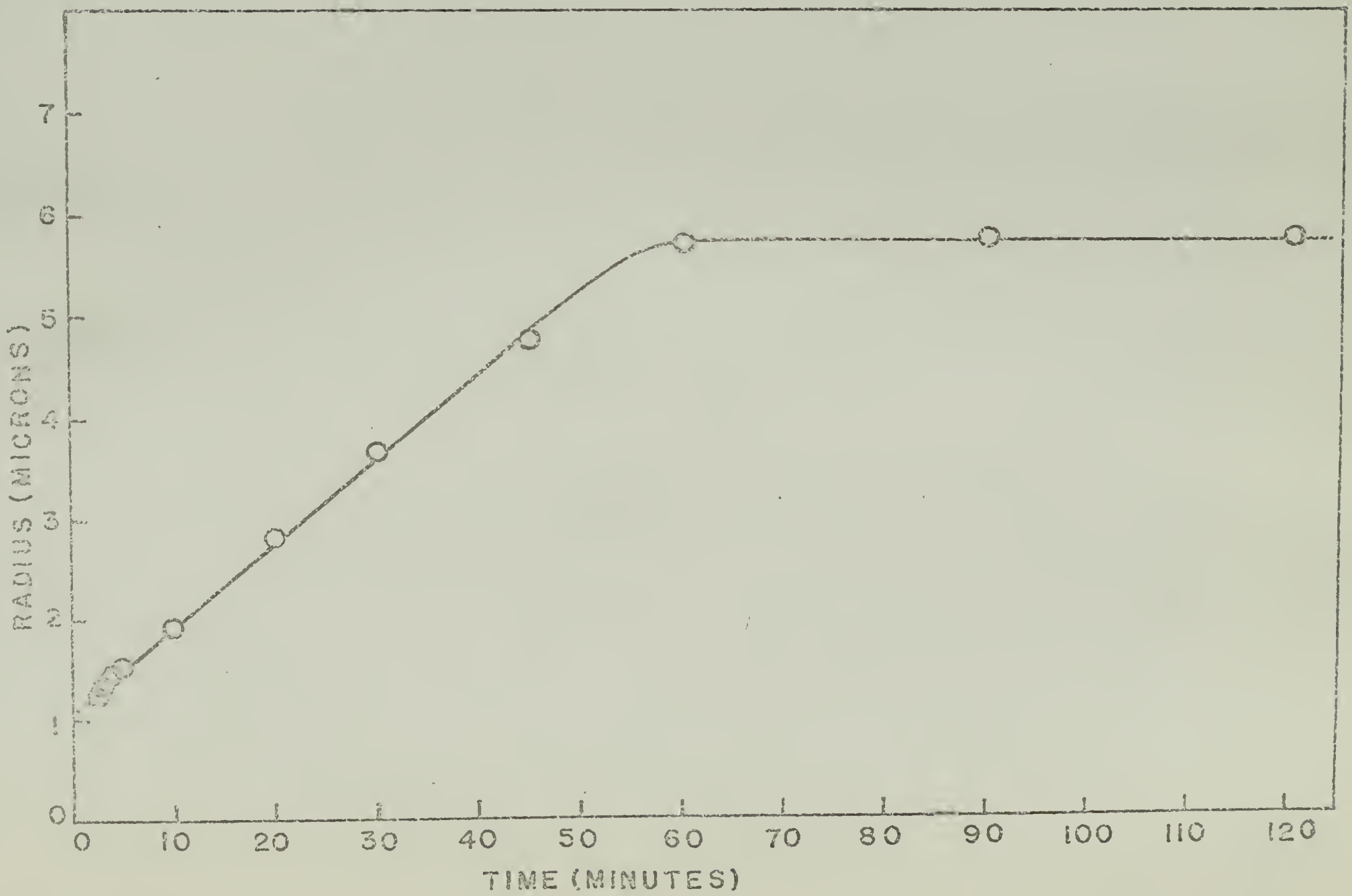
RADIUS (MICRONS)
0
1
2
3
4
5
6
7
0
10
20
30
40
50
60
70
80
90
100
110
120
TIME (MINUTES)

Figure 5

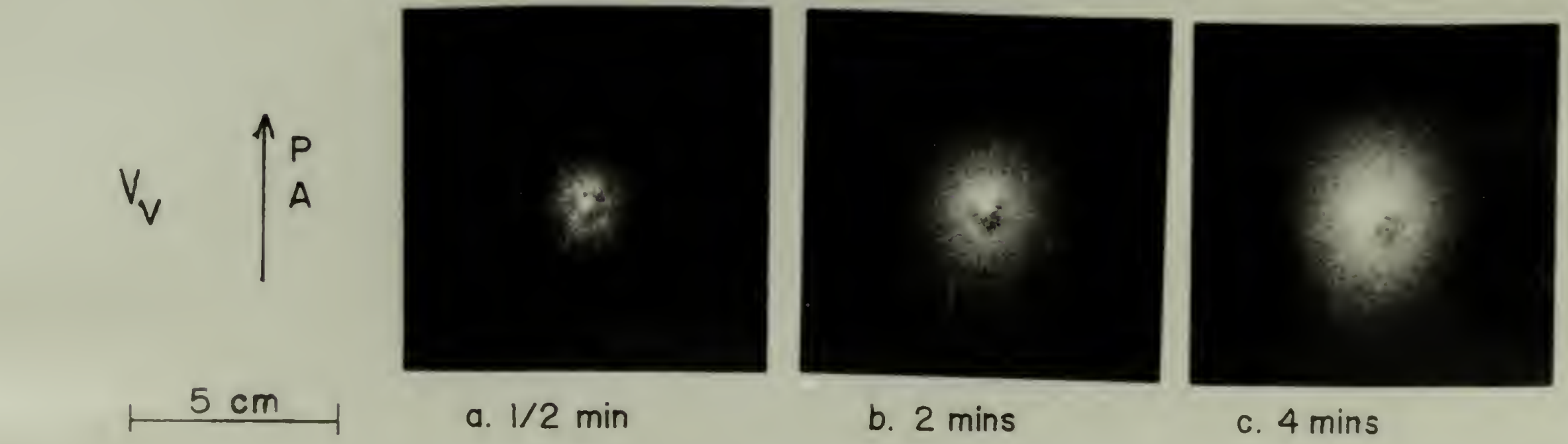
V_V
P
A
5 cm
a. 1/2 min
b. 2 mins
c. 4 mins
d. 10 mins
e. 20 mins
f. 30 mins
g. 45 mins

Figure 6

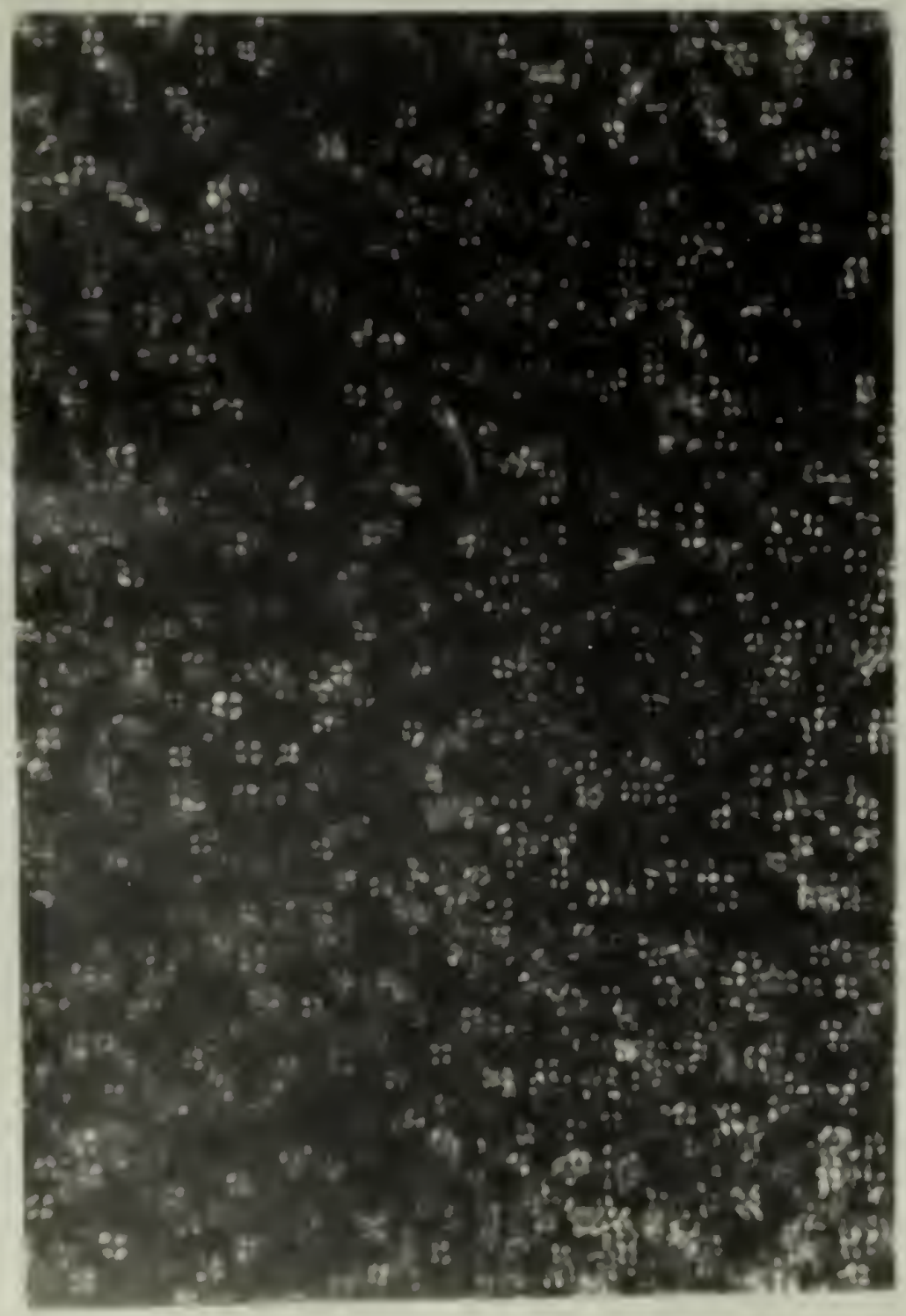

a. 10 mins 20μ

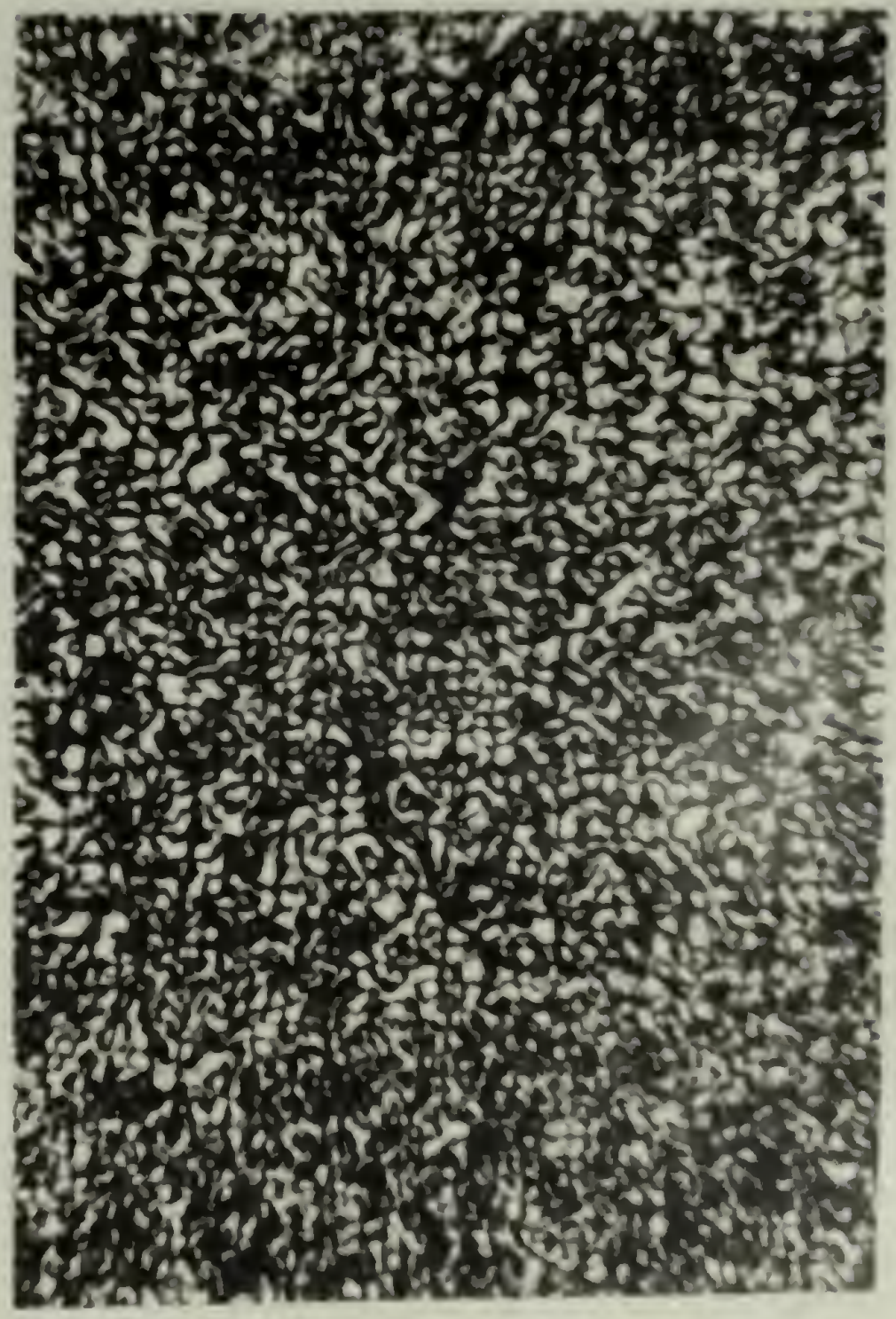

b. 60 mins 50μ

Figure 7

C H A P T E R II

THE KINETICS OF GROWTH OF DEVELOPING SPHERULITES

This chapter is a continuation of the previous one and has been published (R. S. Stein and A. Misra, J. Polymer Sci. A2, 11, 109 (1973)). It is presented here in the same form as it was published.

A model for the growth of a spherulite is proposed and on the basis of this model kinetics for the early stages of crystallization is developed. H_v light scattering patterns are calculated according to this model using the computer center facilities of University of Massachusetts. The computer program used is included in the Appendix.

Abstract

A model containing two rate constants is presented for the development of spherulites from sheafs. One, G_R, is a radial spherulite growth constant while the other, G_S, describes the rate of increase of apex angle of the sheaf. Avrami kinetics are developed based upon this model which predict a change in the Avrami constant n from 5 to 3 as the sheaf develops into a spherulite. H_v light scattering patterns are calculated according to this model and are found to favorably compare with those found during the early stages of the crystallization of polyethylene terephthalate.

Introduction

It has been recognized by many workers that spherulites first

develop as rod-like structures,[1,2] and then, by branching of lamellae, evolve into sheafs and finally spheres. Since the kinetics of growth depend upon the geometry of the growing species,[3] it is reasonable that the growth kinetics will change during this evolutionary process. If data are fitted by an Avrami type equation,[4] then one might expect the Avrami exponent to change with time. This is often empirically allowed for by inserting an induction time in the kinetic equations. This device is not always satisfactory since one sometimes finds a negative induction time.[5,6]

The Model

It has been suggested that at early stages of crystallization, the partially developed spherulite can be approximated by a conic sector [Fig. (1)].[7,8] Such models can, for example, be used to account for light scattering patterns observed at early stages of crystallization.[6] As crystallization continues, these sheaves will grow radially, probably at a rate equal to the radial growth rate of the spherulite, $G_R = \partial r/\partial t$. As a result of branching the sheaf will grow sidwards so that the apex angle β increases at some rate $G_S = \partial\beta/\partial t$ which will generally be different from the radial growth rate. This lateral growth will continue until a complete spherulite develops. While this is certainly an over-simplified model of spherulite development, it is of interest to explore its predictions of crystallization kinetics. We shall see that from the predicted dimensional changes of these sheaf-like structures, it is possible to calculate light scattering patterns which may be compared with experimental patterns[6] obtained during the course of crystallization.

Kinetic Calculations

Let us first review the formulation of the kinetics of growth of a complete spherulite, assuming heterogeneous nucleation. At a time when the spherulite has a radius, r, its surface area A_S is $4\pi r^2$. We shall assume that if no truncation by other spherulites occurs, the rate of increase of the volume of a spherulite will be proportional to its surface area

$$\frac{dV_s}{dt} = 4\pi r^2 \frac{dr}{dt}$$

$$= 4\pi r^2 G_R \qquad (1)$$

If truncation occurs because of impingement with other spherulites, this rate is decreased by a fraction f_s which at least at early stages of crystallization is $(1-\phi_S)$ where ϕ_S is the volume fraction of spherulitic material.[9] The total rate of increase of volume of spherulites will be N_S times that given in Eqn. (1), where N_S is the number of spherulites present, assuming they all start growing instantaneously. Thus the change in volume fraction of spherulites is:

$$\frac{d\phi_S}{dt} = 4\pi r^2 G_R (N_S/V)(1-\phi_S) \qquad (2)$$

where V is the volume of the crystallizing system.

Now if the radial growth rate is constant, $r = G_R t$ so:

$$\frac{d\phi_S}{1-\phi_S} = 4\pi\, G_R{}^3 (N_S/V) t^2\, dt$$

$$= k_S\, t^2\, dt \qquad (3)$$

where $k_S = 4\pi\, G_R{}^3 (N_S/V)$.

Thus, upon integrating:

$$-\ln(1-\phi_S) = k_S\, t^3/3 \qquad (4)$$

or

$$\phi_S = 1 - \exp[-k_S t^3/3] \qquad (5)$$

The volume fraction of crystalline material is then:

$$\phi_C = \phi_{SC}\, \{1 - \exp[-k_S t^3/3]\} \qquad (6)$$

where ϕ_{SC} is the volume fraction of crystals within the spherulite. This is assumed constant and it is also assumed that all of the crystallization is within the spherulites. The consequences of allowing ϕ_{SC} to vary with time have been explored elsewhere.[10-12]

Equation (6) expresses the familiar result of an Avrami exponent of 3 for three-dimensional growth with heterogeneous nucleation.[3,4] We shall now explore the consequences of the growth of incomplete spherulites.

For a conic spherulitic sector of the sort shown in Fig. 1, the volume is:

$$V_S = \frac{4}{3}\pi r^3 (1-\cos\beta) \tag{7}$$

If both r and β can change, the rate of change in volume is:

$$\frac{dV_S}{dt} = \frac{\partial V_S}{\partial r}\frac{dr}{dt} + \frac{\partial V_S}{\partial \beta}\frac{d\beta}{dt} \tag{8}$$

From (7) it is apparent that:

$$\frac{\partial V_S}{\partial r} = 4\pi r^2 (1-\cos\beta) \tag{9}$$

and

$$\frac{\partial V_S}{\partial \beta} = \frac{4}{3}\pi r^3 \sin^3\beta \tag{10}$$

If we assume a constant lateral growth rate of G_S, Eqn. (8) becomes:

$$\frac{dV_S}{dt} = 4\pi r^2 [(1-\cos\beta)G_R + \frac{1}{3} r \sin\beta . G_S] \tag{11}$$

If now $\beta = G_S t$, then by proceeding as before (assuming that the decrease in crystallization rate due to truncation for the spherulite sector is $[1-\phi_S]$, the same as that for the complete spherulite) we obtain:

$$\frac{d\phi_S}{1-\phi_S} = k_S\{[1-\cos(G_S t)]t^2+1/3G_S[\sin(G_S t)]t^3\}dt \qquad (12)$$

which leads to:

$$\phi_C = \phi_{SC}\left(1-\exp[-k_S(1/3t^3 + \int_0^t\{-t^2\cos(G_S t) + 1/3\, G_S t^3 \sin(G_S t)\}dt]\right) \qquad (13)$$

$$= \phi_{SC}\{1-\exp[-(k_S/3)t^3(1-\cos[G_S t])]\}$$

for times shorter than t_c which is that necessary to develop a complete spherulite. This value of t_c is the time required for β to increase to $\pi/2$ and is $t_c = \pi/(2G_S)$. At this time the degree of crystallinity is ϕ_C^C and is given by:

$$\phi_C^C = \phi_{SC}\{1-\exp[-(k_S/3)t_C^3]\} \qquad (14)$$

At times greater than t_C, the terms involving sidewards growth of the sector disappear from the crystallization equation and the equation for ϕ_C is identical with Eqn. (6) for a complete spherulite.

Thus for times greater than t_C, there is no effect of the initiation process on the crystallization isotherm. This is a reasonable conclusion since we have assumed that the radial growth rate is unaffected so that by the time the spherulite has become complete, its radius has reached the value that it would have if it had been complete from the beginning. The

only effect of the nucleation process which we have assumed is that the degree of crystallinity will be lower in the interval between t = 0 and t_c.

A plot of (ϕ_c/ϕ_{sc}) against $(t/t_{1/2})$ is given in Fig. 2 for a number of values of $(t_c/t_{1/2})$, where $t_{1/2}$ is the half time for crystallization of the normally developing spherulite which is:

$$t_{1/2} = [3\ell n2/k_s]^{1/3} \tag{15}$$

in terms of which Eqn. (13) may be written:

$$(\phi_c/\phi_{cs}) = 1-\exp\{-0.693(t/t_{1/2})^3[1-\cos([\pi/2][t/t_c])]\} \tag{16}$$

It is noted that increasing t_c leads to an apparent induction time which is positive. A negative induction time is not predictable by this mechanism, since the degree of crystallinity during this initial period will always be less than that of a complete spherulite.

It is possible, of course, that t_c may be appreciably greater than $t_{1/2}$ in which case the cosine term in Eqn. (16) may be expanded in a series, the first term of which gives:

$$(\phi_c/\phi_{cs}) = 1-\exp\{-0.693(t^5/t_{1/2}{}^3 t_c{}^2)\} \tag{17}$$

leading to an apparent Avrami exponent of 5. It has been pointed out by Morgan[13] that such behavior is expected for sheaf-like growth.

In general, if one has a crystallization process with an Avrami exponent, n, so that:

$$(\phi_c/\phi_{cs}) = 1-\exp[-k't^n] \tag{18}$$

then it is well known that a double logarithmic plot according to the equation:

$$\ell n\ \{-\ell n[1-(\phi_c/\phi_{cs})]\} = \ell n\ k' + n\ell n\ t \tag{19}$$

leads to a line with a slope of n. A plot of this type is presented in Fig. 3, where it is seen that one obtains essentially two straight line segments, one at shorter time with a slope close to 5 and one at longer time with a slope close to 3. The transition between the two slopes occurs at longer times with increasing values of $(t_c/t_{1/2})$.

Light Scattering Patterns

The light scattering patterns may be calculated during growth according to the proposed model using the methods of Stein and Picot[7] or Kawai, et al.[14] A series of such calculated H_v patterns is shown in Fig. 4 which may be compared with a set of experimental patterns in Fig. 5 obtained during the isothermal crystallization of polyethylene terephthalate from the melt as previously described by Misra and Stein.[6] The calculations are actually based on a two-dimensional model, but experience has indicated that the results of two and three-dimensional light scattering calculations are quite similar. It is noted that the theory is capable of describing the observed sequence of patterns. However, if one obtains the spherulite size from the H_v patterns under conditions when spherulitic structure is complete,

the extrapolated plot of spherulite size against time should be zero according to this model as a consequence of the assumption that $r = G_R t$. The observed negative induction time[5,6] would require a radial growth rate which was either initially faster than linear (Chapter 1) or else that growth started from a preformed rod-like nucleus having a finite size at $t = 0$, in which case $r = r_o + G_R t$.

At short times both the experimental and theoretical patterns exhibit intensities which monotonically decrease from the center, characteristic of rod-like structures, while at longer times the intensity increases and a maximum occurs at some angle, θ_{max}, characteristic of the radius of the incomplete spherulite. As t approaches t_C and the spherulite becomes complete, the pattern evolves toward the four-leaf clover type H_v pattern characteristic of perfect spherulites.

This trend is clearly seen in Fig. 6 where the variation in H_v scattered intensity with θ in a plane at $\mu = 45°$ to the polarizer and analyzer is plotted for various values of t/t_C. The development of a scattering maximum with increasing crystallization time is evident. This maximum becomes more intense and moves toward smaller scattering angles as the spherulites become more complete and grow in size.

Thus, we see that this simple model can account for many of the features of the early part of crystallization. It is apparent that the model may be elaborated to account for particular variations of crystallization mechanisms that are observed.

REFERENCES

1. A. Keller, J. Polymer Sci. 17, 447 (1955).
2. J. N. Hay, British Polymer J. 3, 74 (1971).
3. L. Mandelkern, Crystallization of Polymers, McGraw-Hill, New York, 1964, Chapter 8.
4. M. Avrami, J. Chem. Phys. 7, 1103 (1939); 8, 212 (1940); 9, 177 (1941).
5. V. G. Baranov, A. V. Kenarov, and T. I. Volkov, J. Polymer Sci., C, No. 30, 271 (1970).
6. A. Misra and R. S. Stein, J. Polymer Sci., B, 10, 473 (1972).
7. R. S. Stein, C. Picot, M. Motegi and H. Kawai, J. Polymer Sci., A2, 8, 2115 (1970).
8. M. Motegi, T. Oda, M. Moritani, and H. Kawai, Polymer Journal (Japan) 1, 209 (1970).
9. R. S. Stein and J. Powers, J. Polymer Sci. 56, S9 (1962).
10. S. Hoshino, E. Meineke, J. Powers, and R. S. Stein, J. Polymer Sci. A3, 3041 (1965).
11. F. P. Price, J. Polymer Sci., A3, 3079 (1965).
12. J. H. Hillier, J. Polymer Sci., A3, 3087 (1965).
13. L. B. Morgan, Philosophical Trans., Royal Soc. (London) A, 247, 13 (1954).
14. S. Tatematsu, N. Hayashi, S. Nomura and H. Kawai, Presented at the 20th Annual Meeting of the Soc. of Polymer Science, Japan, May 27, 1971; in press.

CAPTIONS FOR FIGURES

Figure 1: The sector model for spherulite growth.

Figure 2: The predicted variation of the volume fraction of crystallinity with $(t/t_{1/2})$ for various values of the relative time $(t_c/t_{1/2})$ for spherulitic completion.

Figure 3: A theoretical Avrami plot of the variation of log $\{-\log[1-(\phi_c/\phi_{cs})]\}$ against log $(t/t_{1/2})$ for various values of $(t_c/t_{1/2})$.

Figure 4: The calculated H_v light scattering contours for several values of (t/t_c) with $(t_c/t_{1/2}) = 1/3$. (a) $t/t_c = 0.4$; (b) $t/t_c = 0.6$; (c) $t/t_c = 0.8$; (d) $t/t_c = 1.0$.

Figure 5: A series of experimental H_v light scattering patterns for the isothermal crystallization of polyethylene terephthalate from the melt at 110°C where $t_{1/2} \tilde{=} 5$ min. It is estimated that $(t_c/t_{1/2}) = 15$ min. for this crystallization.

Figure 6: A calculated plot of the variation of H_v scattered intensity with scattering angle θ at an azimuthal angle $\mu = 45°$ for various values of (t/t_c) for $(t_c/t_{1/2}) = 1/3$.

Figure 1

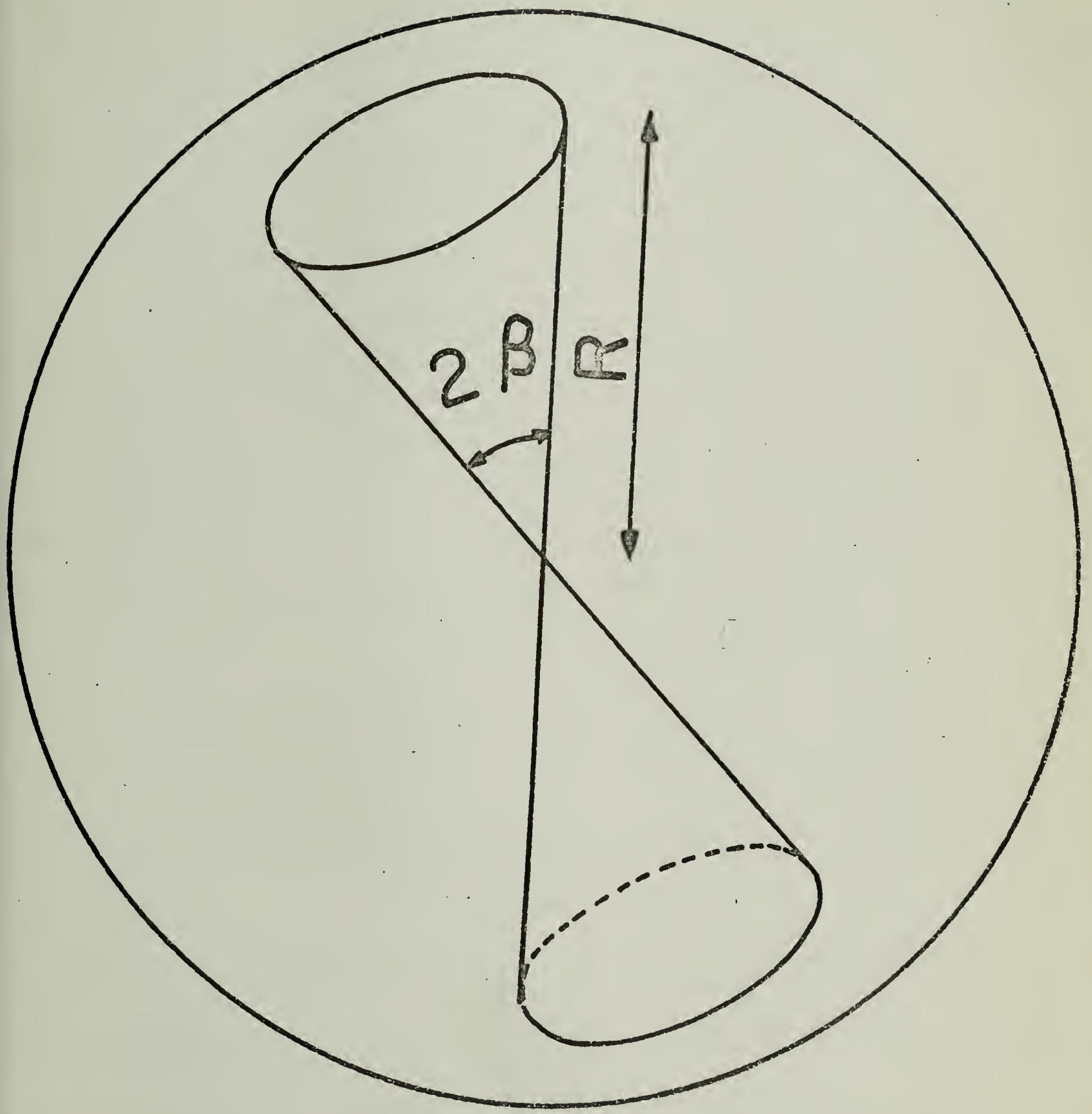

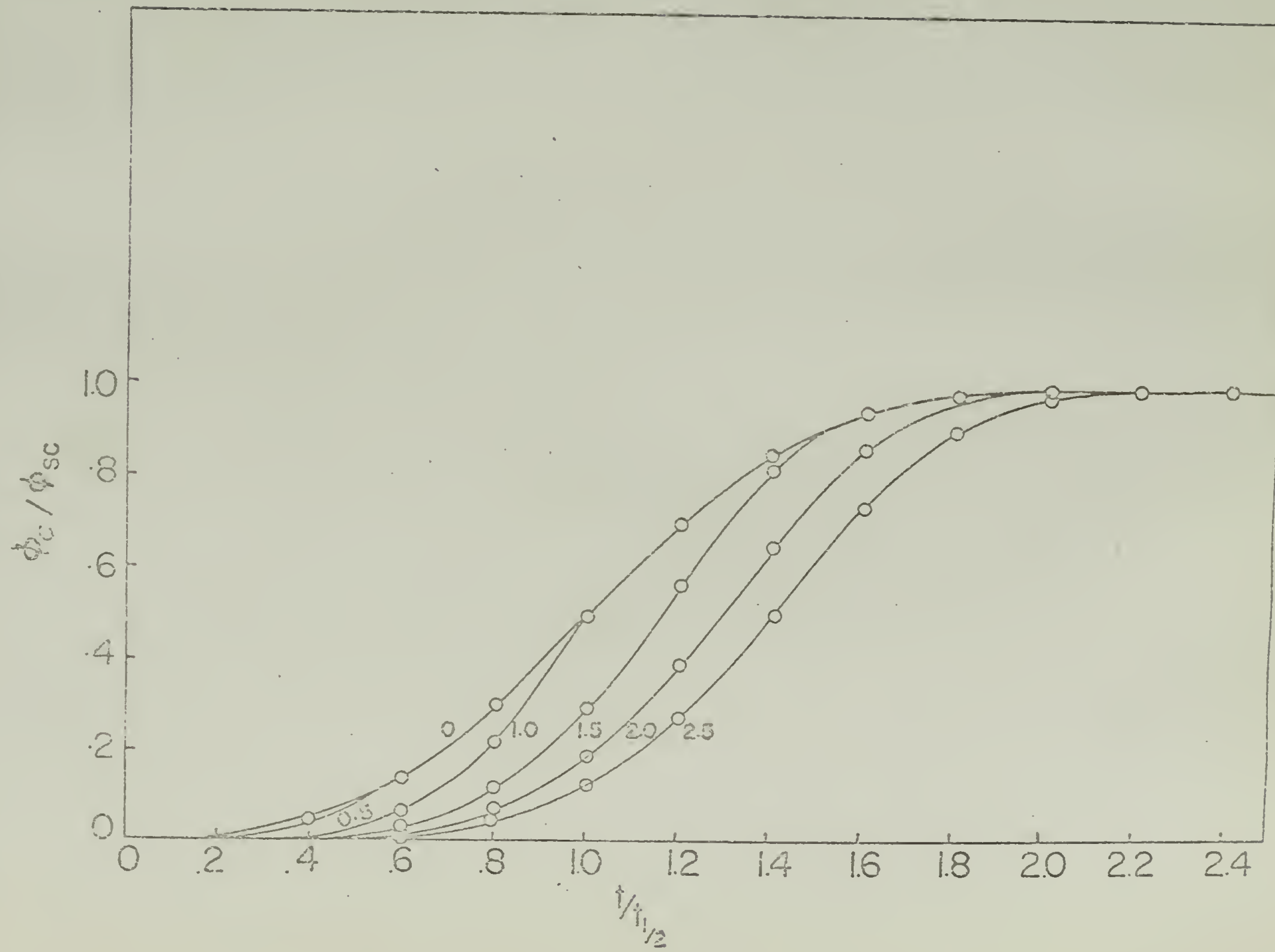
ϕ_c / ϕ_{sc}
1.0
.8
.6
.4
.2
0
0
.2
.4
.6
.8
1.0
1.2
1.4
1.6
1.8
2.0
2.2
2.4
$t/t_{1/2}$
0
0.5
1.0
1.5
2.0
2.5

Figure 2

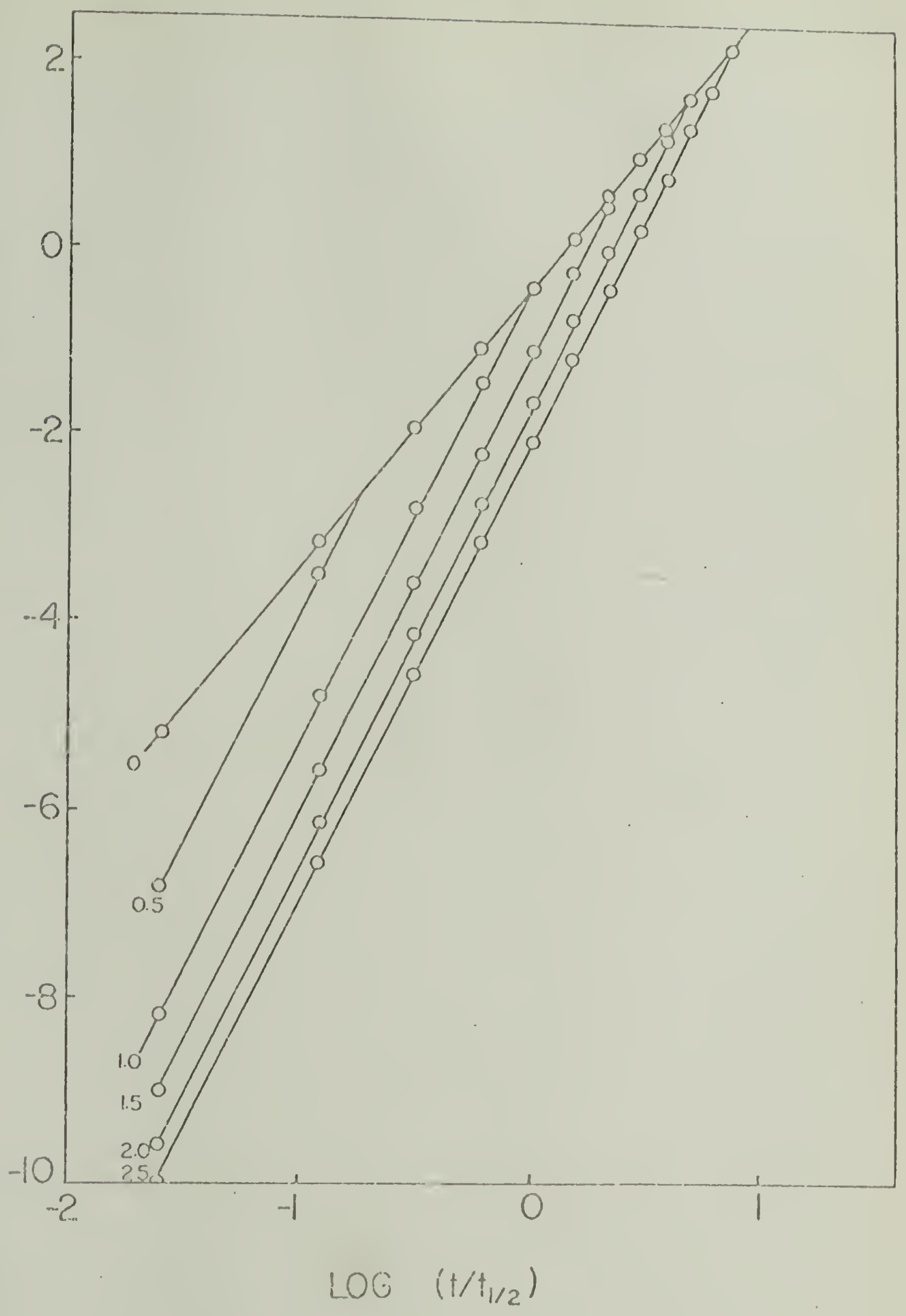

Figure 3

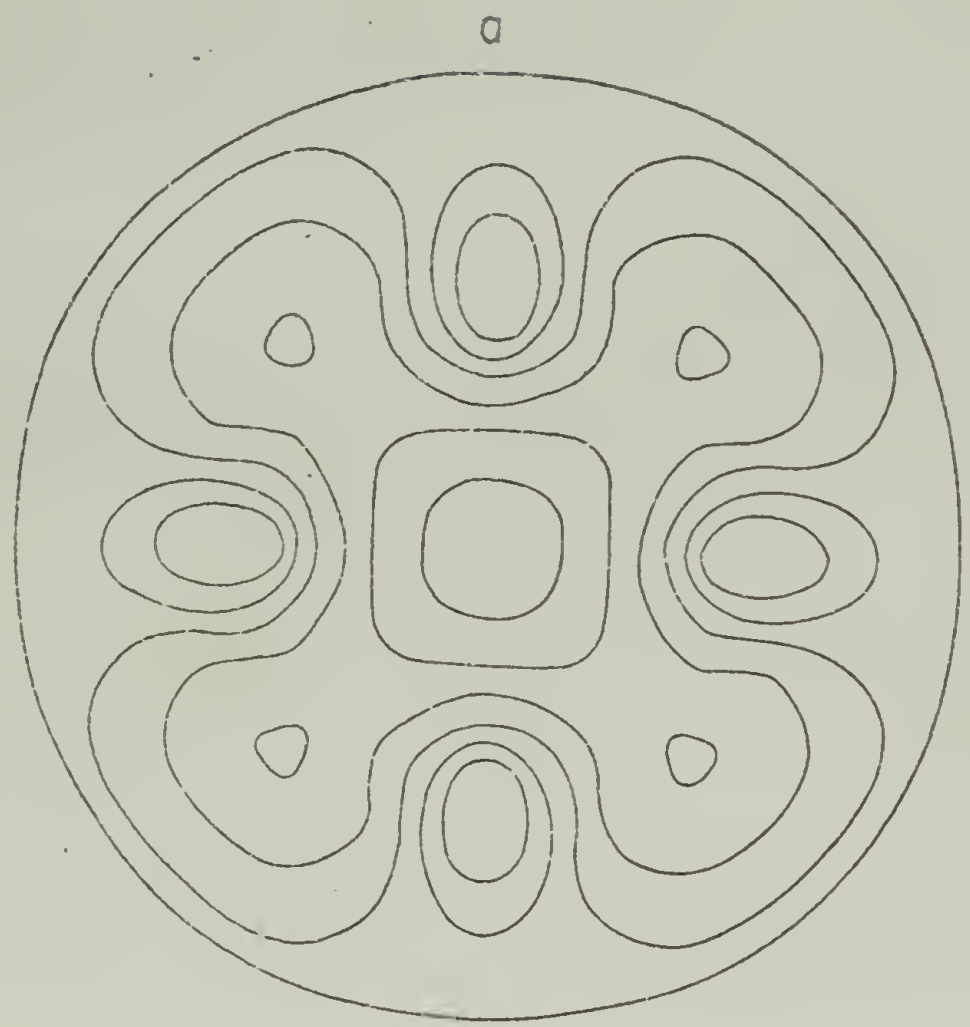

	t/t_c	R	B
a	0.4	0.73μ	36°
b	0.6	1.10	54°
c	0.8	1.46	72°
d	1.0	1.83	90°

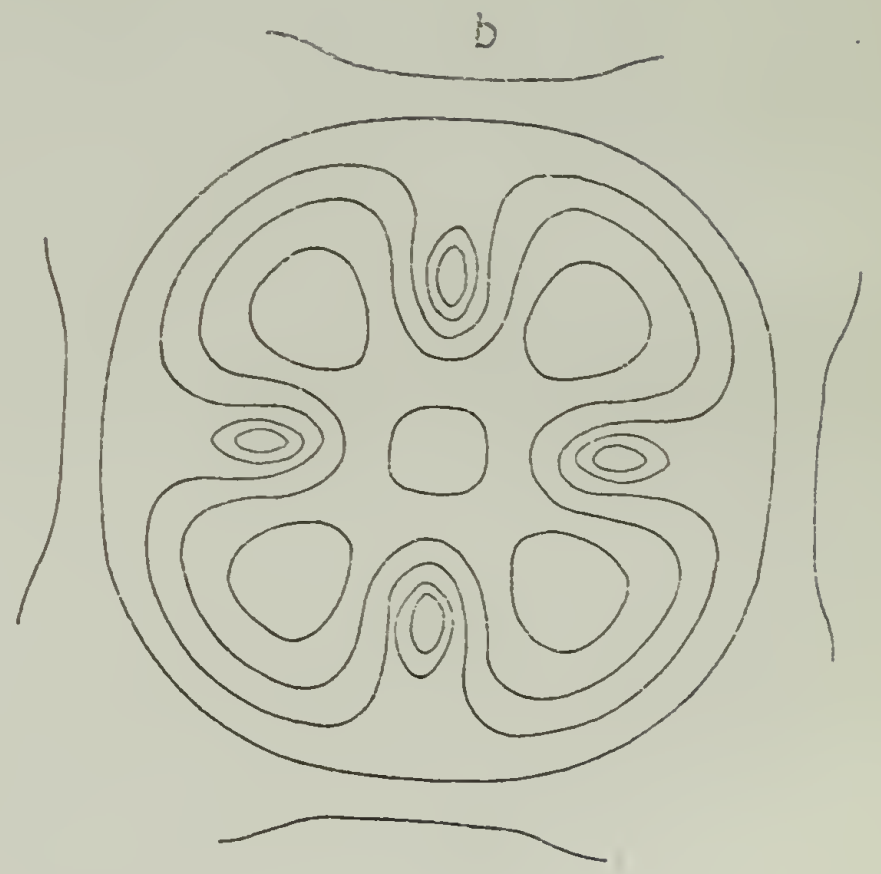

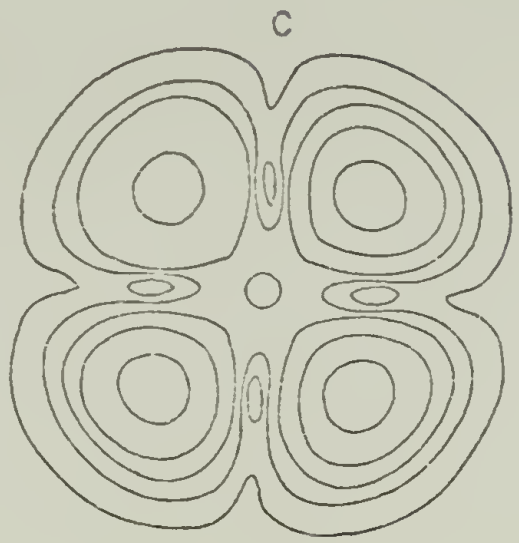

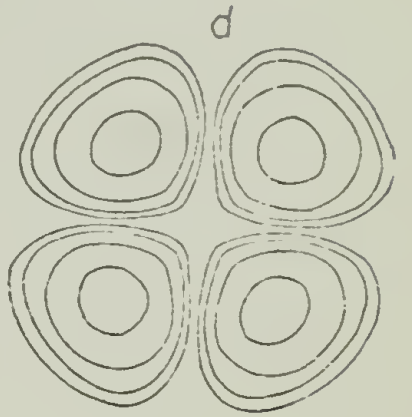

Figure 4

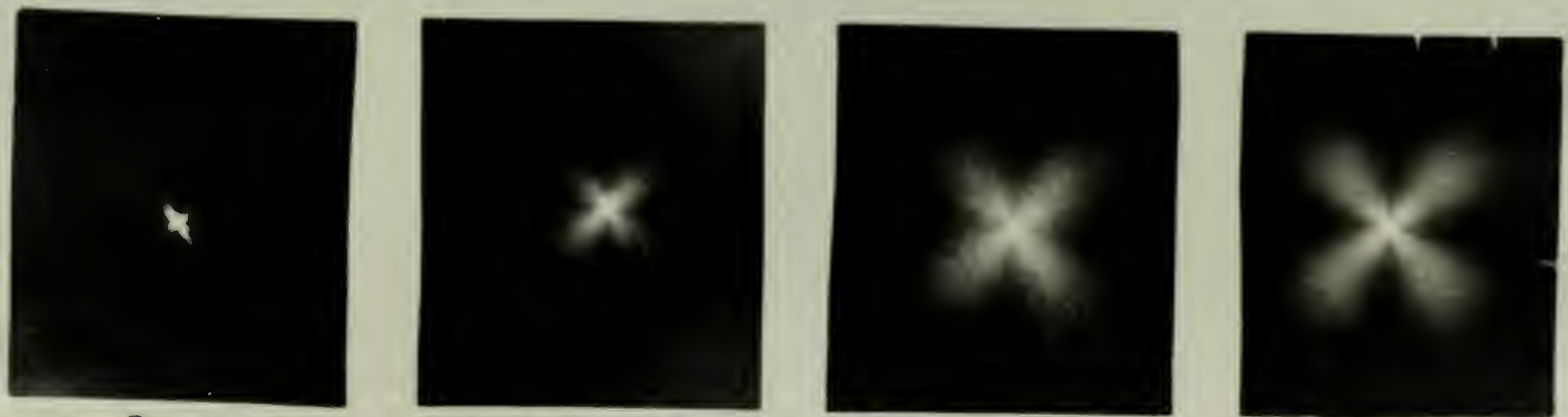
a. 0 min
b. 0·5 min
c. 1 min
d. 2 mins
5 cm
e. 2·75 mins
f. 3·5 mins
g. 5 mins
h. 45 mins

Figure 5

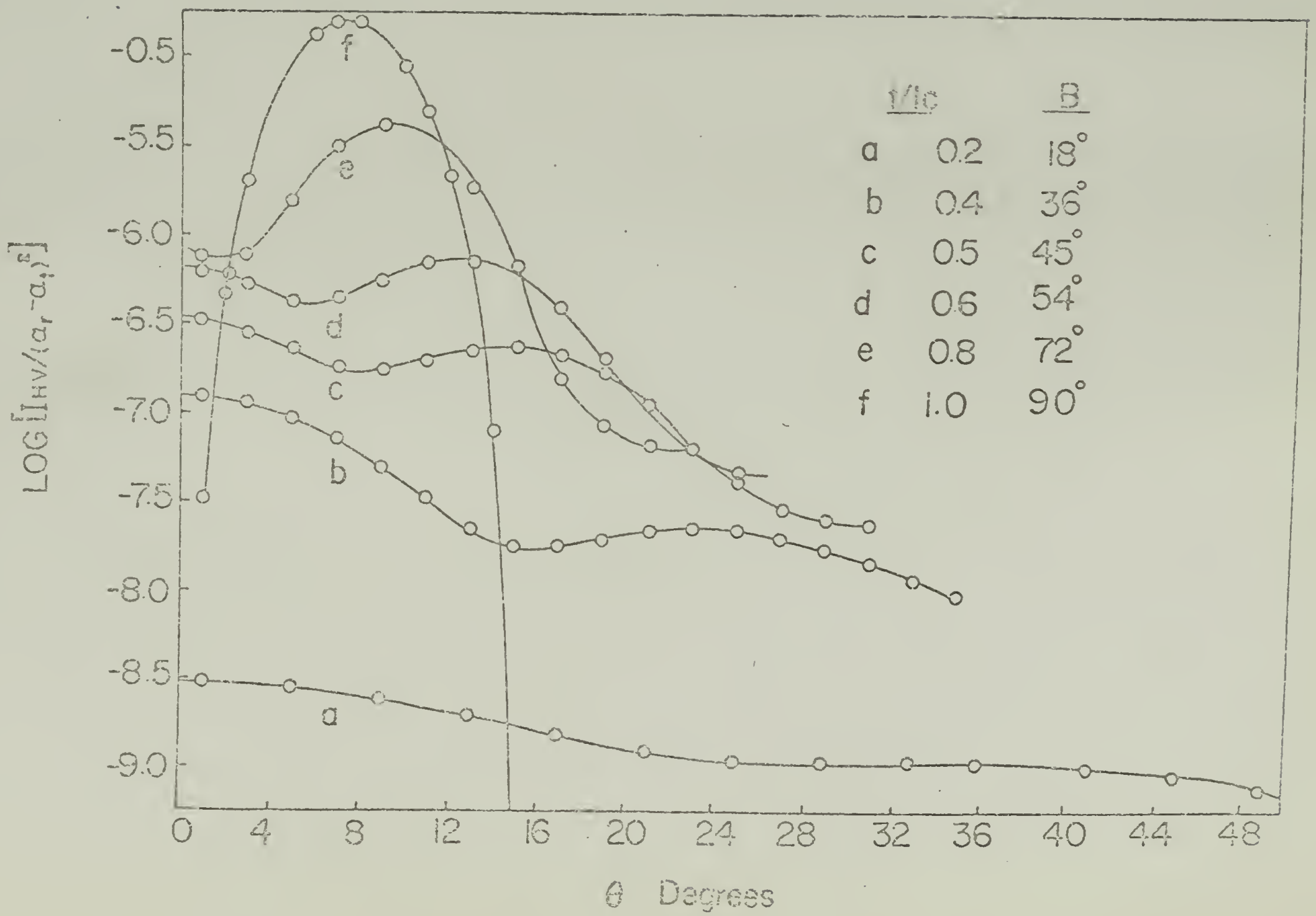
LOG [IHV/(ar-a1)²]
-0.5
-5.5
-6.0
-6.5
-7.0
-7.5
-8.0
-8.5
-9.0
0
4
8
12
16
20
24
28
32
36
40
44
48
θ Degrees
a
b
c
d
e
f
1/lc
B
a 0.2 18°
b 0.4 36°
c 0.5 45°
d 0.6 54°
e 0.8 72°
f 1.0 90°

Figure 6

CHAPTER III

THE DISTRIBUTION OF SPHERULITES IN A POLYETHYLENE SAMPLE*

Introduction

For spherulitic polymers in which the spherulites are volume filling, it is usually assumed that each spherulite arises from a primary nucleus and the resulting spherulite size will be dependent upon the concentration of such nuclei. For heterogeneous nucleation, when all nuclei are activated simultaneously, the spherulite size distribution is narrower than for homogeneous or sporadic nucleation when nucleus activation occurs during the entire time of crystallization. With heterogeneous nucleation, the truncation boundary between spherulites will be midway between two adjacent spherulite centers if the growth rate from both is equal. However, for homogeneous or sporadic nucleation, the boundary will be closest to the nucleus which is activated last.

It is usually assumed that the positions of nuclei are random, leading to a characteristic breadth of spherulite size distribution since some adjacent pairs of nuclei will be close together and some will be more separated. If heterogeneous nucleation is assumed, this size distribution may be calculated and compared with experiment. It is conceivable that deviations from this random distribution may occur resulting from some interaction among growing spherulites. Consequently, an analysis of the distribution of spherulite sizes or truncation positions can provide information about crystallization mechanisms. These statistics

---

*Portions accepted for publication, A. Misra, R. E. Prud'homme and R. S. Stein, J. Polymer Sci., Part B.

are also of interest because it is necessary to consider the distribution in truncation positions for calculating the light scattering patterns from volume filling assemblies of spherulites.

Experimental

A photomicrograph of a Marlex 50 (Phillips Petroleum Company) linear polyethylene sample, M_w = 10,000, density = 0.98 g/m^3, melted at 150°C for 15 minutes in a laboratory press, then pressed at 15,000 psi for another 15 minutes after which it was quenched to room temperature is shown in Figure 1. The resulting film was 2 mils thick. As is seen, the sample forms truncated spherulites which can be easily resolved under a polarizing microscope (crossed polars).

Calculations

Distribution of nuclei

A computer program to simulate the growth of truncated spherulites from specified locations of nuclei in a given area was developed. Assuming simultaneous activation of nuclei and a linear radial growth rate, the spherulitic boundaries were determined in a two dimensional matrix. Three to eight sided polygons were observed from this procedure. As an example, an array of 20 computer simulated "spherulites" is shown in Figure 2. In addition, for each spherulite j, its average size $\bar{a}_j$ (average distance from the center to the bounderies), variance in size $\bar{a}_j$, and a "truncation parameter" $(\sigma^2/\bar{a}^2)_j^{-1}$ were calculated. Using these results for a sample of N spherulites, an arithmetic average and an average weighted to the

sixth power of size were calculated for the spherulitic radius and the truncations parameter. These averages have been previously defined as:[1]

$$\bar{a} = \sum \bar{a}_j / N \tag{1}$$

$$\langle a \rangle = \frac{\sum \bar{a}_j \cdot \bar{a}_j^{\,6}}{\sum \bar{a}_j^{\,6}} \tag{2}$$

$$\frac{\sigma^2}{\bar{a}^2} = \frac{\sum (\sigma^2/\bar{a}^2)_j}{N} \tag{3}$$

$$\left\langle \frac{\sigma^2}{\bar{a}^2} \right\rangle = \frac{\sum (\sigma^2/\bar{a}^2)_j \cdot \bar{a}_j^{\,6}}{\sum \bar{a}_j^{\,6}} \tag{4}$$

In the present work a total of 808 spherulitic centers were specified in a circle of 225 μm radius. Care was taken to neglect centers near the circumference of the circle since their surrounding neighbors were not completely known. Numerical values obtained for the parameters in equations 1 through 4 were found to be constant for samples of about 300 spherulites or more. To illustrate this the values of these parameters obtained with a different number of spherulites simulated by a random distribution of nuclei are listed in Table I.

The center coordinates of all the 808 spherulites in an arbitrarily chosen circle of 225 μm radius were determined from the photomicrograph of a polyethylene sample shown in Figure 1. The values calculated for

$\bar{a}$, $\langle a \rangle$, $\sigma^2/\bar{a}^2$ and $\langle \sigma^2/\bar{a}^2 \rangle$ are listed in Table II.

In order to interpret these experimental parameters, 808 spherulites were generated on the computer in a circle of 225 μm, thus attempting to duplicate the situation of Figure 1. In the first case, the nuclei were generated completely at random. Three additional cases were considered in which the nuclei were again generated at random but with the restriction that any two nuclei could not be closer than a specified distance d. The values chosen for d were 3, 4 and 5 μm respectively. By following the previously described procedure, the parameters $\bar{a}$, $\langle a \rangle$, $\sigma^2/\bar{a}^2$, and $\langle \sigma^2/\bar{a}^2 \rangle$ were calculated for these four cases and are also reported in Table II.

An analysis of Table II indicates that the different parameters obtained for the experimental sample agree best with the non-random generation calculation having a restriction of 4 μm. It is seen that the effect of imposing a restriction on the location of the nuclei increases the value of $\bar{a}$ and decreases the values of $\langle a \rangle$, $\sigma^2/\bar{a}^2$, and $\langle \sigma^2/\bar{a}^2 \rangle$. This is understandable since such a restriction produces a more regular array of spherulites. Their different average sizes then become closer to each other as the restriction becomes more severe. At the same time, since the spherulites become more regular, their truncation parameters become smaller, as indicated by the smaller values of $\sigma^2/\bar{a}^2$ and $\langle \sigma^2/\bar{a}^2 \rangle$ which were obtained. The limiting case would be the one where all spherulites were regular. One such case is that of hexagonal spherulites where the $\bar{a}$ and $\langle a \rangle$ values would be equal and where $\sigma^2/\bar{a}^2$ and $\langle \sigma^2/\bar{a}^2 \rangle$ would have a value of 0.0019.[1] This calculation thus indicates that the nuclei of the spherulites are not randomly located, but that they are separated

by an average minimum distance of approximately 4 μm. Of course, in practice, this 4 μm restriction is not a step-function as used in our calculation, but is a continuous function which we do not know. It may be reasonable to say that the "probability" of two nuclei being closer that 4 μm is low. Furthermore, the analysis of the experimental picture is limited by the resolution of the microscope which is of the order of 1 μm.

This result is also apparent in Figure 3 where the number of nuclei pairs contributing to mutual boundaries and separated by a distance "d" is plotted as a function of distance "d". This number was computed for 1 μm intervals. The three curves correspond to (a) the experimental situation, (b) to the non-random generation with a 4 μm restriction and (c) to the completely random generation case. Again it is seen that the 4 μm restriction case matches up better with the experimental situation while the random case gives a broader curve and higher values at small distances.

By analyzing the photomicrographs of PE in Figure 1 and in those of a previous publication,[1] it is observed that the spherulitic boundaries are midway between adjacent spherulitic centers. Thus the assumption made in the calculations presented here, that the nucleation is heterogeneous with simultaneously activating nuclei, seems to be valid. This conclusion is in general agreement with the data available in the literature for isothermal crystallization of PE.[2-5] The explanation of the observed minimum distance of separation of spherulites is not apparent. There are several possible explanations for a decreasing tendency for spherulites to grow in the vicinity of one which is already growing. One is that

during spherulitic crystallization, impurities (especially the low molecular weight ones) are rejected in the melt outside the crystallizing region.[6,7] Consequently, there may very well be regions surrounding a given nucleus where the probability of forming a second nucleus is low.

Another possibility is that heat is given out during crystallization since it is an exothermic process. Once a nucleus is formed, its surrounding regions would sense an increase in temperature, thus reducing the possibility of forming another nuclei in its vicinity.

Both of these mechanisms, however, presume successive growth of nuclei where the formation of one diminishes the probability of the next forming in its vicinity. It is difficult to see how they completely apply to the present case where nucleation appears to be simultaneous and it seems that some mechanism leading to an initial non-random distribution of nuclei must be employed.

Once a non-random distribution of spherulite centers is generated, one may explain how it is preserved during subsequent crystallizations. The formation of nuclei upon crystallization from the melt may be affected by the previous thermal history of the sample. This can be termed as the "memory effect" and is likely to occur if polymer chains or potential sites for potential heterogeneous nucleation are not completely dispersed during the sample preparation described earlier. In such a case, the new nuclei are more likely to form at either the locations of previous nuclei[8] or at previous spherulitic boundaries. The latter is possible because the impurity concentration is usually higher at the boundaries and provides nucleation sites. Therefore, a result of the memory effect is that the nucleation is not completely random.

Light Scattering

Theories for light scattering from circular[9] as well as truncated disks[10] have been reported previously. Prud'homme and Stein[1] have used these to calculate H_V (vertical polarizer and horizontal analyser) scattering patterns from two-dimensional truncated spherulites (disks) with various degrees of truncation as measured by the value of truncation parameters. Using a similar approach, H_V scattering intensities at $\mu = 45°$ and varying scattering angle (θ) were calculated here for the 20 truncated spherulites in Figure 2 (simulated by a random distribution of nuclei) and for 20 circular spherulites with radii equal to the corresponding $\bar{a}$ values of the truncated spherulites. Average H_V intensities for the two cases are plotted as a function of θ in Figures 4 and 5. Figure 4 shows that the value of θ_{max} for truncated spherulites is less than that for perfect spherulites by a factor of 1.155 which is close to the value obtained by Prud'homme.[11] In Figure 5 the scattering curves from these two cases are compared with each other and with that calculated by Prud'homme for 17 truncated spherulites of a polyethylene sample. The truncated cases have higher scattering values at small θ than the perfect spherulitic case while there is no significant trend at high values of θ. This is expected for low values of truncation parameter (.087 for random case and .065 for polyethylene.)

It may be pointed out that the above results are for a relatively small number of spherulites which do not represent a true value for the truncation parameter (Table II). However, too much time would be required for calculations from 300 or so spherulites and is not considered necessary at the present time.

TABLE I

Calculated values for $\bar{a}$, $\langle a \rangle$, $\sigma^2/\bar{a}^2$ and $\langle \sigma^2/\bar{a}^2 \rangle$ for different number of spherulites simulated by a random distribution of nuclei

Number of Spherulites Considered	$\bar{a}$	$\langle a \rangle$	$\sigma^2/\bar{a}^2$	$\langle \sigma^2/\bar{a}^2 \rangle$
20	7.07	9.37	.085	.087
50	6.38	8.98	.221	.101
177	6.56	10.10	.225	.103
335	6.73	10.34	.228	.134
519	6.91	10.76	.226	.133
569	6.94	10.68	.228	.132

TABLE II

Average size $\bar{a}$ and $\langle a \rangle$ and truncation parameters $\sigma^2/\bar{a}^{-2}$ and $\langle \sigma^2/\bar{a}^{-2} \rangle$ for an experimental sample and various computer simulated experiments

System	Number of Spherulites Considered	$\bar{a}$ μm	$\langle a \rangle$ μm	$\sigma^2/\bar{a}^{-2}$	$\langle \sigma^2/\bar{a}^{-2} \rangle$
Marlex 50	581	7.20	10.16	.145	.108
Completely Random Generation: with restriction	569	6.94	10.68	.228	.132
Restriction: 3 μm	571	7.12	10.24	.162	.128
4 μm	564	7.24	10.12	.141	.118
5 μm	565	7.35	9.85	.120	.102

REFERENCES

1. R. E. Prud'homme and R. S. Stein, J. Polymer Sci., A-2, 11, 1683 (1973).
2. L. Mandelkern, Crystallization of Polymers, McGraw Hill (1964).
3. W. Banks, M. Gordon, R. J. Roe, and A. Sharples, Polymer (London) 4, 61 (1963).
4. W. Banks, I. J. Hay, A. Sharples, and G. Thomson, Polymer (London) 5, 163 (1964).
5. A. Booth and J. N. Hay, Polymer (London) 12, 365 (1971).
6. H. D. Keith and F. J. Padden Jr., J. Appl. Phys., 34, 2409 (1963).
7. H. D. Keith and F. J. Padden Jr., J. Appl. Phys., 35, 1270, 1286 (1964).
8. F. P. Price, J. Am. Chem. Soc., 74, 311 (1952).
9. C. Picot, R. S. Stein, M. Motegi and H. Kawai, J. Polymer Sci., A-2, 8, 2125 (1970).
10. R. S. Stein and C. Picot, J. Polymer Sci., A-2, 8, 2127 (1970).
11. R. E. Prud'homme, private communications.

CAPTIONS FOR FIGURES

Figure 1: Photomicrograph of a Marlex 50 linear polyethylene sample between crossed polars.

Figure 2: An array of 20 truncated "spherulites" simulated on the computer for randomly located nuclei.

Figure 3: Number of nuclei pairs per 1 μm intervals contributing to mutual boundaries and separated by a distance d as a function of the distance d.

Figure 4: Logarithm of H_V scattering intensity at $\mu = 45°$ as a function of scattering angle (θ = .6 to 2.8) for:

a) 20 truncated spherulites simulated by a random distribution of nuclei.

b) 20 perfect spherulites with radii equal to corresponding $\bar{a}$ values of truncated spherulites in (a).

Figure 5: Logarithm of H_V scattering intensity at $\mu = 45°$ as a function of scattering angle (θ = .6 to 2.8) for:

a) 20 truncated spherulites simulated by a random distribution of nuclei.

b) 20 perfect spherulites with radii equal to corresponding $\bar{a}$ values of truncated spherulites in (a).

c) 17 truncated spherulites of polyethylene.

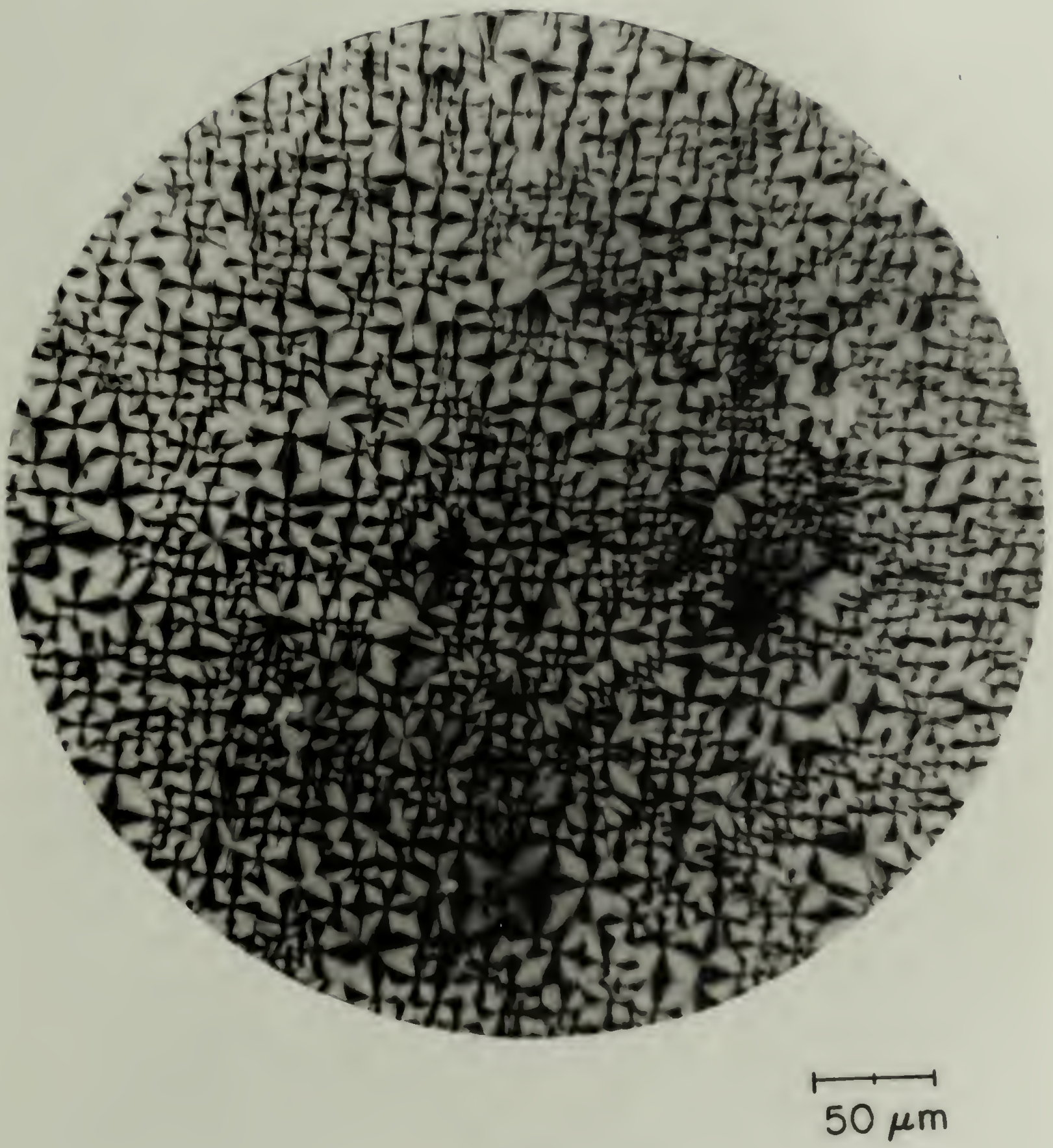

Figure 1

Figure 1

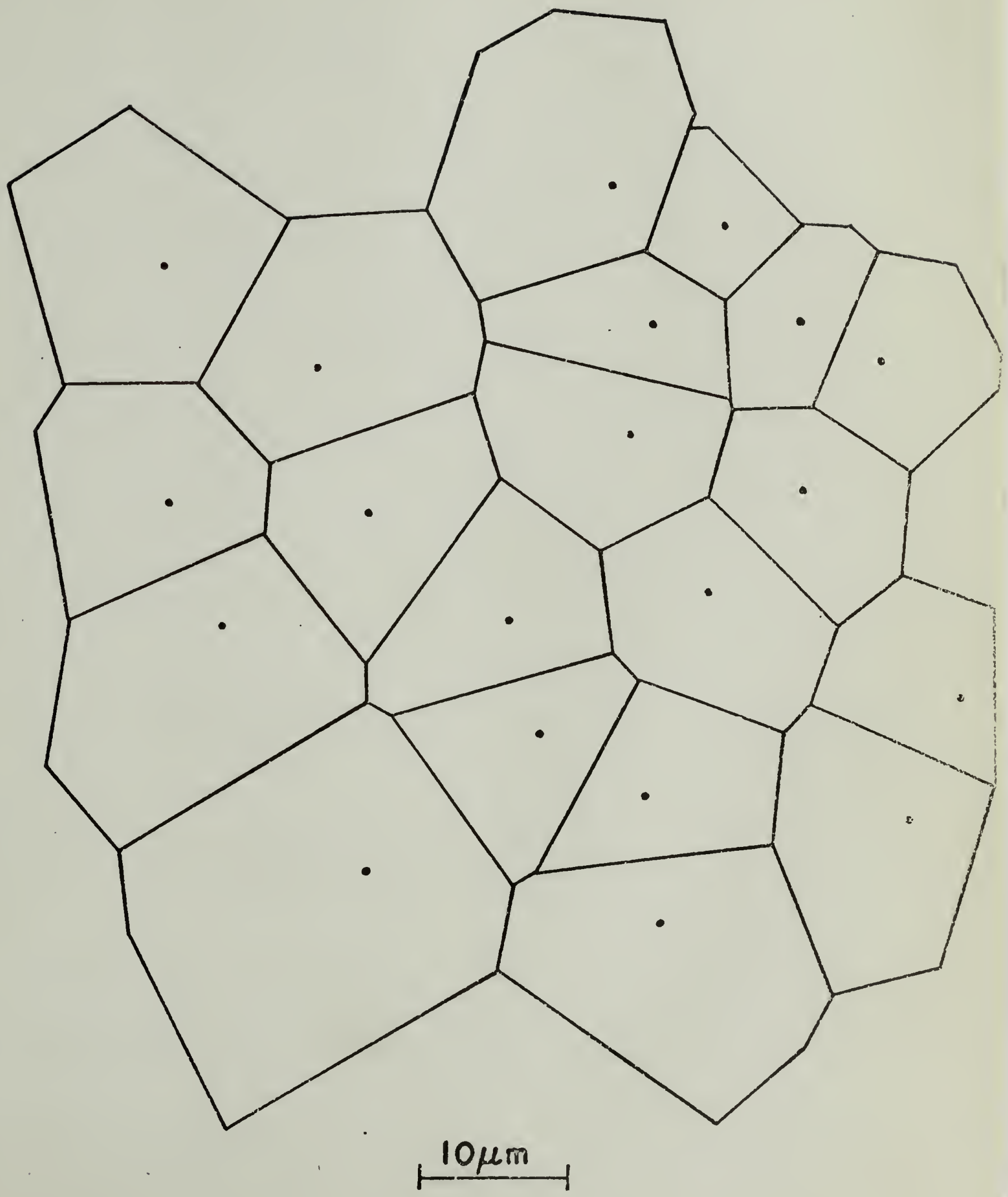

Figure 2

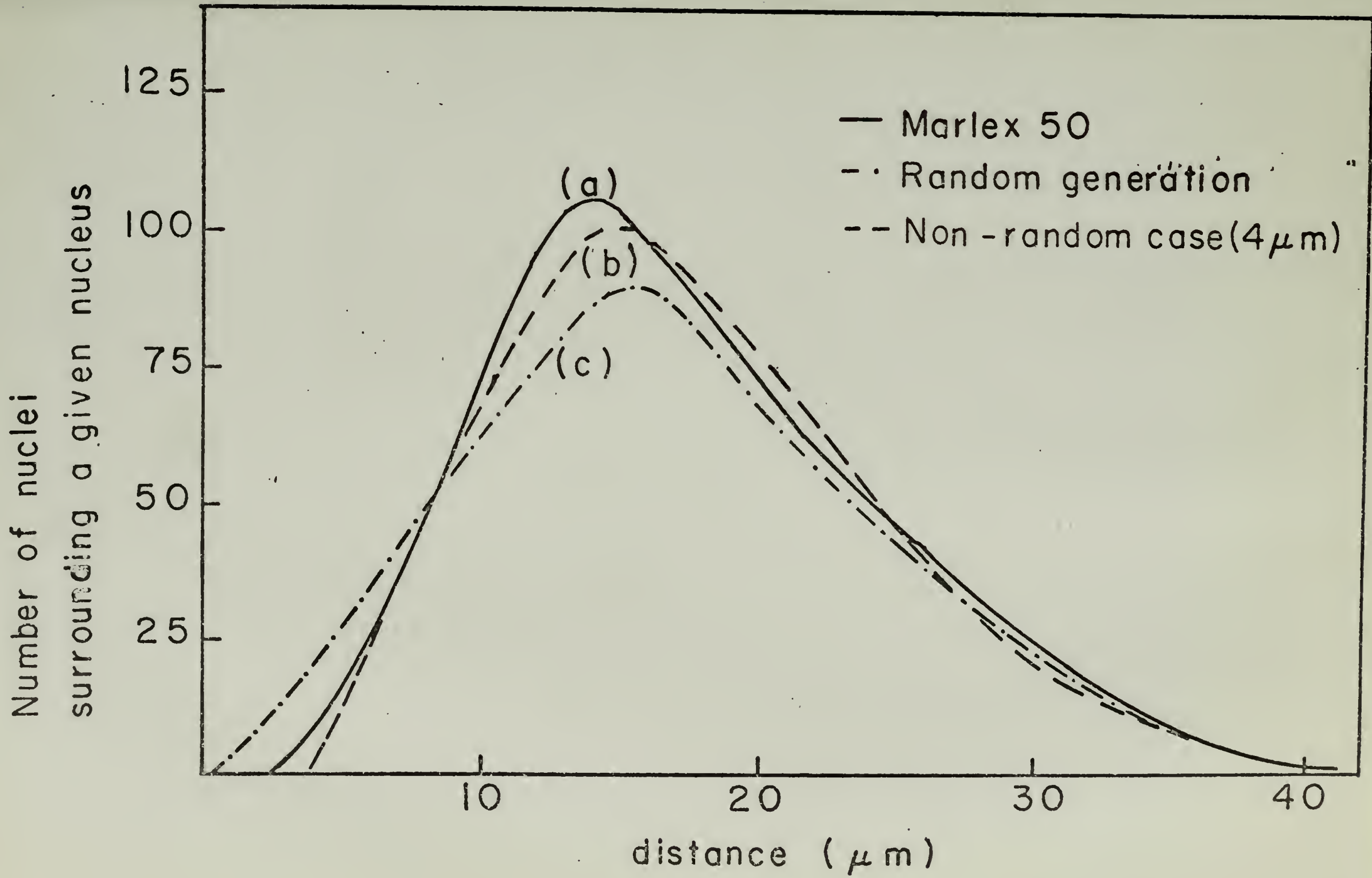
Marlex 50
Random generation
Non-random case(4μm)
(a)
(b)
(c)
125
100
75
50
25
Number of nuclei surrounding a given nucleus
10
20
30
40
distance (μm)

Figure 3

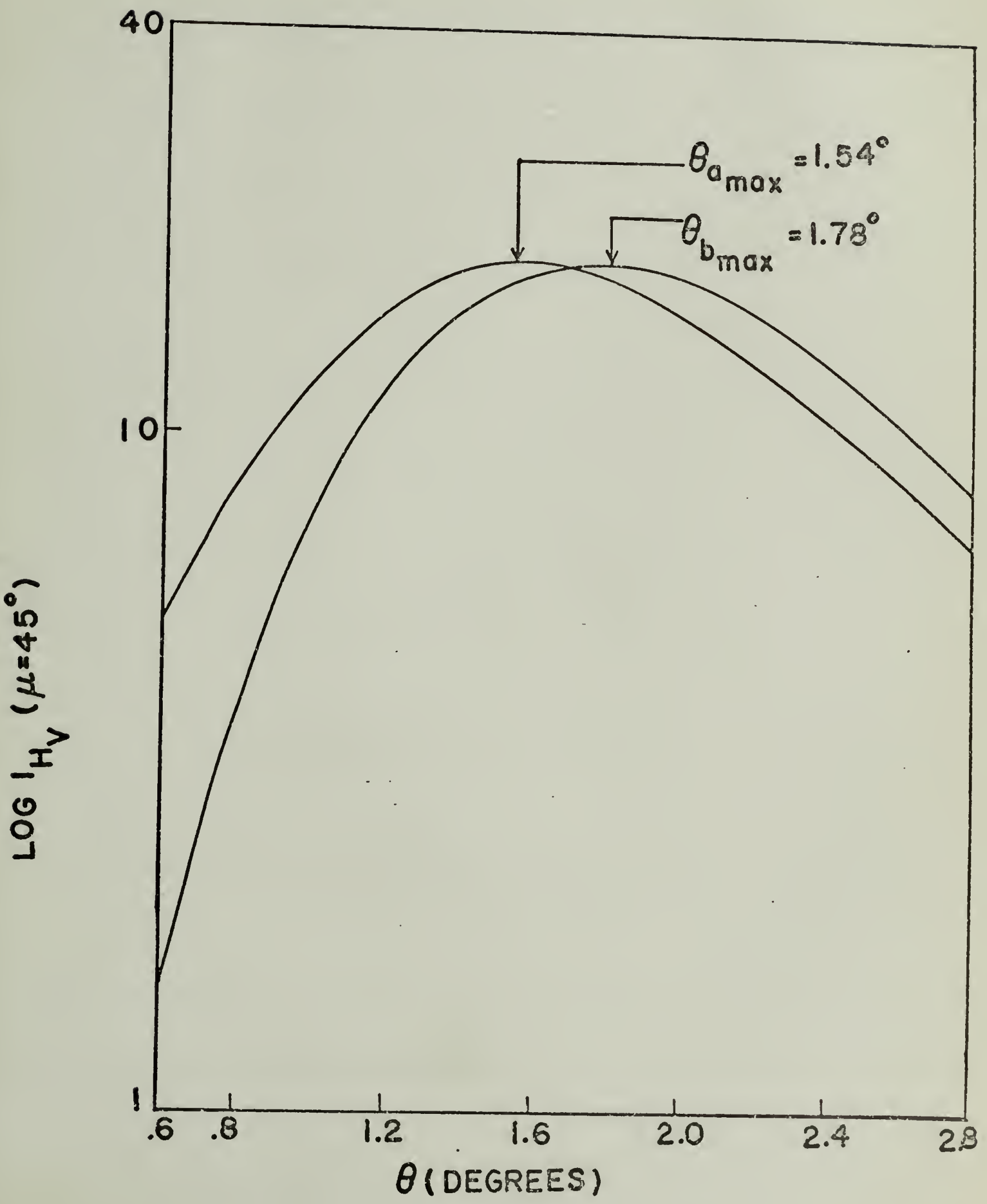
40
10
1
$\theta_{a_{max}}$ = 1.54°
$\theta_{b_{max}}$ = 1.78°
LOG I_{H_V} (μ=45°)
.6
.8
1.2
1.6
2.0
2.4
2.8
θ (DEGREES)

Figure 4

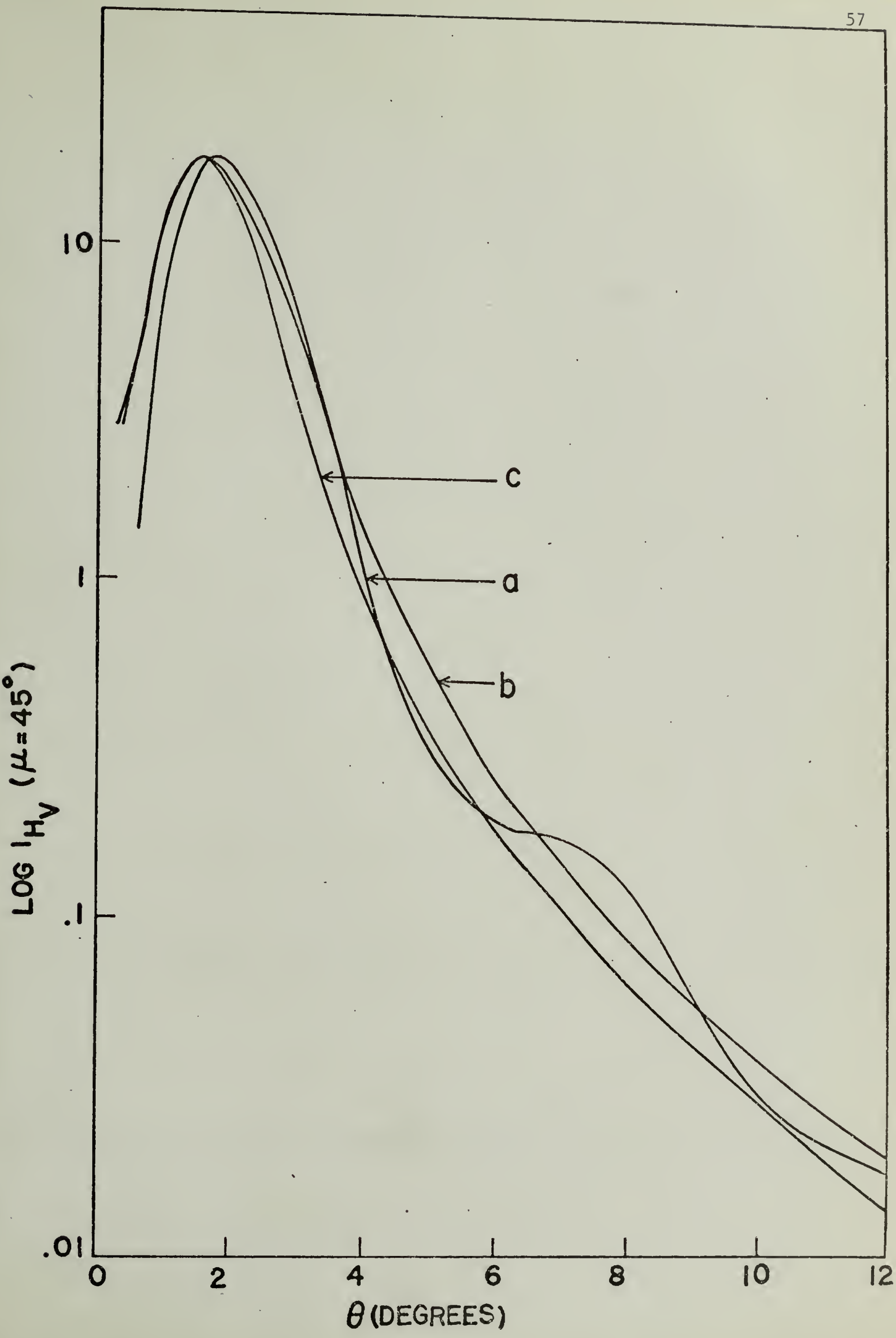

Figure 5

CHAPTER IV

DEFORMATION STUDIES OF PET

Introduction

Polyethylene terephthalate (PET) is most useful commercially in the form of fibers and films which have a high degree of orientation.[1-4] The effects of draw ratio, temperature and strain rate on the orientation and crystallinity produced upon drawing amorphous PET has been well studied and reported.[1,5-9] Relatively little work has been done to study the structure of PET drawn below its glass transition temperature.[10-12] While extensive work has been reported on the study of its structure when drawn above the glass transition temperature using several techniques.[13-36] Based on these studies several models have been proposed to explain the molecular orientation and structure of oriented PET.[15-19,23,29-34]

It has been shown that the superstructure formed under stress (or strain) is considerably different from that in unoriented systems.[13,37,38] However little work has been done to study the superstructure produced during the strain induced crystallization of PET. PET is a good polymer for such a study since it can be prepared in its amorphous state and then stretched at temperatures at which isothermal crystallization is negligible.

The purpose of the present investigation was to study the superstructure in PET films drawn both below and above the glass transition temperature using low angle light scattering[39,40] and optical microscopy. The crystalline structure was studied by wide angle X-ray diffraction.

In addition birefringence and crystallinity measurements were made.

A brief description of the industrial fiber spinning process along with a literature review of the work done on studying the structure of oriented PET films and fibers is presented in the section following.

Literature Review

Commercially available PET fiber yarns are produced by a two-stage process.[1-4] The polymer is first melt spun and the resultant spun yarn is later drawn on a separate machine. During the melt spinning of PET, it is extruded as amorphous molten polymer, followed immediately by simultaneous stretching and cooling. After it has had time to cool to a solid filament, it is wound up on a bobbin at a high speed so as to stretch the filament somewhere between extrusion and collection. The cooling is generally done by forced air. At this stage the filaments have a very small degree of orientation along the fiber axis as measured by birefringence. Moreover, these filaments are still amorphous when examined by density and X-ray methods. This is because the rate of cooling is considerably faster compared to the rate of crystallization so that there is insufficient time for any measurable crystallization to occur. The above is true for normally used wind-up speeds. It may be noted that at very high wind up speeds, a high degree of orientation as well as crystallinity is achieved.

In the second stage, the amorphous filaments produced at normal wind-up speed are drawn in a separate subsequent operation to produce highly

oriented crystalline fibers. The degree to which changes occur upon drawing depends on the temperature, rate of stretching and the draw ratio.[6-8] A detailed analysis of the melt spinning and subsequent drawing has been discussed by Thompson[1] and Ziabicki.[4] A brief description of industrial operation along with typical operating conditions is given in Reference 3.

Thompson and Marshall[5-7] worked on the continuous drawing of PET and studied the effects of operating conditions on drawing. They used a drawing machine with two rolls, the second of which was made to revolve faster than the first. The fiber was wrapped around each of these rollers a sufficient number of times to prevent its slipping. Under these conditions the fiber was stretched by a ratio equal to that of the roller speeds. The draw ratio, therefore, can be simply controlled by changing roller speeds. A heater capable of maintaining constant temperature was interposed between the rolls. Various sets of experiments were carried out in which the tension required to stretch the polymer was measured at different sets of draw-ratios. From the experimental data, Thompson and Marshall drew tension-temperature-draw ratio characteristic curves for the drawing of amorphous PET.[6,7]

Drawing below the glass transition temperature, termed "cold drawing", is accompanied by necking. The ratio of initial and drawn specific lengths is called the "natural draw ratio r",[5,6] which can be expressed as:

$$r = \frac{a_1}{a_2} \cdot \frac{d_1}{d_2}$$

where a_1 and d_1 are the area and density respectively before drawing and a_2 and d_2 are the corresponding quantities after drawing. If the

draw ratio, R, is equal to the natural draw ratio, r, then stable cold drawing occurs with a stationary neck. However if R is greater than or less than r, the shoulder at which the neck occurs moves forward or backwards between the rolls. It should also be noted that the natural draw ratio is a function of both draw ratio, temperature and the rate of stretching.

The effect of cold drawing (drawing below T_g) upon the structure of PET has been studied.[5,9-11] Newman[10] concluded that the cold drawing occurs at stresses near the fracture stress of the material which is indicated by the craze marks or microvoids forming in the undrawn region. The shoulder separating the unnecked and necked regions is known to be at a temperature higher than the ambient temperature.[5,10] Blakey and Sheldon[11] found diffused equatorial lobes on the wide angle X-ray diffraction photographs upon cold drawing amorphous and heat crystallized PET. They suggested that molecular orientation occurred for the amorphous case while disruption of crystalline region occurred for the heat crystallized sample. Annealing produced disorientation for the amorphous drawn film but an improved resolution (the diffuse lobes in the equatorial direction changing to arcs) for the heat crystallized film.

Recently Asano and Sato[12a] have reported detailed morphological studies on cold drawn PET by wide angle X-ray diffraction. They followed the changes in crystal structure upon annealing of cold drawn PET at various temperatures.

Wilkes and Chu[12] studied the morphology of cold drawn PET by scanning electron microscopy following chemical etching with n-propyl amine. They show the existance of a structure described as a network of ribbon-like

elements. The thickness of the ribbons was designated as the characteristic dimension of the network. The size and orientation of the ribbons depended on the processing conditions.

Drawing above the glass transition temperature can be divided into two basic regions:

1. Flow and hot drawing where uniform drawing takes place as seen by the uniform reduction of cross-sectional area. In flow drawing low orientations and crystallization occur while in hot drawing higher orientations and crystallization occur to give useful drawn filament. The transition from flow drawing to hot drawing is smooth except in a narrow range of draw ratio.[7]

2. Self-induced drawing which occurs at relatively higher draw ratios and higher strain rates. Drawing occurs at a neck and is accompanied by the formation of a high degree of crystallinity and molecular orientation. This region can also be termed as the "strain induced crystallization" region.

Thompson[7] was one of the earlier workers who noted that the crystallization of PET under high stress was about a 1000 times faster than under zero stress and suggested that the stress has a large effect on nucleation. Thompson,[7] and Spruiell, McCord and Benerlein[8] studied the effect of strain (or stress), rate of strain and temperature on strain (or stress) induced crystallization. They conclude that strain induced crystallization in PET is accompanied by necking and that at a given temperature it occurs when the strain rate is sufficient to generate a critical stress level within the material. Spruiell et al. also studied the crystallization occurring during the annealing of previsouly oriented PET samples and have suggested that this crystallization was nucleated by the crystallites formed during

deformations. They have proposed models for cases when PET is deformed above and below its glass transition temperature. Sheldon[9] found that extrusion conditions influenced the rate of crystallization but not the equilibrium crystallinity value.

Many investigators have studied the structure of PET films and fibers drawn above their glass transition temperatures using both wide and low angle X-ray,[8,13-23] birefringence,[14,23-25] crystallinity,[8,22,26-28] infrared absorption,[29-31] electron microscopy,[32-34] fluorescence polarization[35] and NMR[36]. A brief review of the work done and results obtained in the above studies is presented here.

Keller[13] stretched PET slowly at 140°, 180° and 200°C, conditions at which crystallization and stretching take place simultaneously. He explained the orientation of crystals formed by wide angle X-ray diffraction pattern. He also observed rows of spherulites under microscopic examination but only in isolated instances and over small localities. Such rows of spherulites were clearly seen in oriented polyamides and polyethylene. Most other workers strained PET above the glass transition temperature but at temperatures where isothermal crystallization is negligible. This means a temperature range from about 70°C to 100°C. Dalmage and Geddes[14] strained PET films at 90°C and at 100% per minute then heat crystallized them. They followed the birefringence as a function of extension and found a steady increase for uncrystallized samples. Upon annealing the birefringence decreased, becoming negative in some cases, for low extensions and increased for high extensions. From their work on wide angle X-ray they suggested that the preferred fiber axis direction of the crystallites is perpendicular to the stretching direction at low elongations and is parallel to the

stretching direction at high elongations. They also showed that at high elongations, the (100) plane and consequently the molecular plane tends to be parallel to the plane of the film.

The work of Heffelfinger and Schmidt[15] support the above conclusions and show that uniaxial stretching extends the molecular chains along the direction of stretch in such a manner that some of the gauche isomer is transformed into trans. The trans isomer is the extended form relative to the gauche and occurs both in crystalline and amorphous regions of the polymer while the gauche isomer occurs only in amorphous regions. At high elongations, the amount of amorphous trans increases at a faster rate than the amount of "crystalline trans" thus producing some kind of order in the amorphous region which is measured by the amount of trans at a given level of crystallinity. They also measured the size of crystallites and the amorphous regions in stretched and heat set PET as a function of draw ratio using both wide angle X-ray and low angle X-ray techniques. They reported that the crystallite length increased slowly with draw ratio while the amorphous length decreased. The small angle long period remained almost unchanged. Similar work was done by Statton and Godard.[16] Lindner[18] has proposed a three-phase model for PET fibers comprised of crystalline, intermediate and amorphous regions. He discussed an X-ray method for the characterization of these three phases with limited success.

Several workers[9,20,26-28] have attempted to measure the crystallinity of oriented PET by X-ray, density and infrared techniques. Farrow and Preston[26] and Farrow and Ward[27] have compared the crystallinity values obtained by these three different techniques and found no correlation in the results.

Dumbleton[24] has done some interesting work on the "slow" drawing of PET at 80°C from its amorphous state. He measured the birefringence as a function of draw ratio. The birefringence of an oriented fiber or film can be expressed as:[41]

$$\Delta = X_c f_c \Delta_c^\circ + (1 - X_c) f_{am} \Delta_{am}^\circ$$

where:

Δ is the measured birefringence

Δ_c° is the intrinsic crystalline birefringence

Δ_{am}° is the intrinsic amorphous birefringence

X_c is the fractional crystallinity

f_c is the crystalline orientation function

f_{am} is the amorphous orientation function

Crystallinity and the crystalline orientation function were calculated by wide angle X-ray diffraction using the procedure developed by Dumbleton and Bowles.[22] They defined X-ray crystallinity as:

$$X_c = 1 - (A/A_{100})$$

where A is the ratio of intensities at 14° and 28.5° for any given samples and A_{100} is this ratio for the amorphous sample. The samples were rotated to eliminate orientation effects. The crystalline orientation function was determined by azimuthal scans on the $(\bar{1}\bar{0}\bar{5})$ plane. The orientation function is defined as:[42]

$$f_c = \frac{1}{2} (c \overline{\cos^2} \phi - 1)$$

where ϕ is the angle between the chain axis in the crystal and the fiber axis. The amorphous orientation was determined by sonic modulus measurements. A plot of $\frac{\Delta}{Xcfc}$ versus $\frac{1-Xc}{Xc} \cdot \frac{f_{am}}{fc}$ was a straight line, the slope of which gave a value of 0.275 for Δ°_{am} and the intercept gave a value of 0.22 for Δ°_{c}. Δ°_{am} and Δ°_{c} can be related by a constant factor K as:

$$\Delta^{\circ}_{am} = K\Delta^{\circ}_{c}, \quad K = 1.2 \text{ in this case.}$$

Dumbleton[24] found that upon drawing amorphous PET, the amorphous orientation function rises linearly up to a point at which crystallization can occur. The threshold of crystalline formation was found at $f_{am} = 0.75$ and a draw ratio of about 2.5X. Upon further drawing, f_{am} remains almost constant since any material which orients beyond the threshold will crystallize. The orientation of crystalline regions was not much greater than that of amorphous regions since the crystals originate from highly oriented amorphous material.

McGraw[35] has used fluorescence polarization to study the molecular orientation in PET. He found that the amorphous orientation increased with draw ratio up to a draw ratio of about 2-3X and then remained almost constant. This is in fair agreement with the results of Dumbleton[24] where the amorphous orientation increased with draw ratio to about 2.5X and then remained constant.

Dumbleton[23] further studied the effect of annealing drawn PET by low angle X-ray in addition to the techniques he used previously. Upon annealing drawn samples he found, 1) a decrease in the width of wide-angle scans along the equator which is indicative of an increase in crystal perfection; 2) an increase of about 50-fold in the integrated intensity

of the low angle X-ray maxima which is indicative of an increase in folds; 3) shrinkage of the drawn film while the crystalline orientation was preserved to a great extent. On the basis of his results he suggested that drawn PET consists of highly extended molecules essentially parallel to one another with few folds present. Annealing causes chain folding to occur on the folds present which act as nuclei. This model also explains why drawn PET showed very little intensity in the low angle X-ray maxima while exhibiting a fairly high crystallinity. His model is similar to that of Statton and Dismore[43] for the drawing of Nylon 6,6.

Several investigators[29-31] have studied the chain folding in oriented PET by infrared absorption. Koenig and Hannon[29] have proposed that strain induced crystallization does not produce regular folds but produces long-loop type folds. Subsequent annealing of the drawn film generates additional mobility to allow these random length folds to become regular. Recent studies of Mocherla and Bell[31] show that at low draw ratio regular folds in addition to irregular folds are present and the amount of regular folds decreases with increasing draw ratio. The results of IR studies are in general agreement with the model of Statton and Dismore[43] and the results of Dumbleton.[23]

Yeh and Geil,[32] and Klement and Geil[33,34] have conducted electron microscopic studies on unoriented and oriented films. They found the existence of a 75-100Å nodular structure and a 250-500Å super-nodular structure. They propose that upon uniaxial stretching the action of internodular links tends to rotate the nodules so that the chain axis orients parallel to the draw direction. They also observed lamellar fibrils oriented perpendicular to the stretching direction for uniaxial drawn and annealed samples.[34]

Thus it is seen that the study of oriented PET has attracted considerable attention by a large number of investigators. It is known that PET can be crystallized by the application of strain under suitable conditions.[5-7] Below the glass transition temperature crystallization is produced by relatively low strain rates provided they are not so rapid as to cause failure. Above the glass transition the amount of orientation and crystallinity produced are a function of strain rate, temperature and draw ratio.[7-9] Morphology produced by strain induced crystallization is different than that produced by isothermal crystallization. Most of the work done has been on the study of molecular orientation and crystalline structure of PET drawn above the glass transition temperature. Several models have been proposed to explain experimental observations.[8,15-18,23,29,33]

It is generally agreed that in drawn PET the polymer molecules are extended and preferentially oriented along the stretching direction[8,14-17, 23,33,34]. There are relatively few folds present in these samples, however annealing causes chain folding to occur as shown by low angle X-ray[23] and infrared.[29-31] Relatively imperfect crystals are formed upon drawing which become more perfect upon subsequent annealing.[23] Very little has been reported on the superstructure in oriented PET and forms the basis for the present work.

It may be pointed out that PET is suitable for studying the superstructure produced during strain induced crystallinity since it can be prepared in its amorphous state and can then be drawn at temperatures at which thermal crystallization does not occur. In this work PET was drawn both below and above its glass transition and was characterized by

low angle light scattering, polarizing microscope, wide angle X-ray birefringence and density measurements. Of special interest was the study and understanding of the superstructure which forms during stress induced crystallization.

Experimental

Sample preparation. Samples were prepared from 2 mil thick amorphous film of PET obtained through the courtest of the Film Division of E. I. duPont de Nemours and Co. The film was characterized as:

Weight average molecular weight,

Mw (light scattering) = 41,000

Number average molecular weight,

Mn (osmometry) = 27,800

Mark-Houwink relations:

$$[\eta]_{TFA} = 4.33 \times 10^{-4} M_w^{0.68}$$

$$[\eta]_{TCE/Phenol} = 2.29 \times 10^{-4} M_w^{0.73}$$

Pieces of the film were cut into thin strips and stretched below or above the glass transition of temperature as described below. The length of the strips was at least two times their width.

Stretching below glass transition. Strips of amorphous PET, with an initial length to width ratio of about 4, were stretched at room

temperature on an Instron model TM. The rate of stretching used was 10%/ minute. Stretching PET under the above conditions caused the formation of a neck at 5% strain, which propagated with further strain till the sample broke. Such a break occurred at a total strain of about 270% or a draw ratio of about 3.7X. For purposes of uniformity, all samples were stretched to 200% thus not allowing breakage. The effective draw ratio, r, in the necked region would be equal to the "natural draw ratio" of the polymer and is defined as:[5,6]

$$r = \frac{a_1}{a_2} \cdot \frac{d_1}{d_2}$$

where a_1 and d_1 are the area and density respectively before drawing and a_2 and d_2 are the corresponding quantities after drawing. The unnecked portions were of little interest and were discarded. Necked regions were characterized. Some of the necked samples were annealed in a constant temperature silicone oil bath (140°C) for a predetermined period of time. This was done both with samples held freely thus allowing for shrinkage and with samples held at constant length.

A few necked samples were stretched further at 90°C. This was done by immersing the sample fixed on a stretcher in a silicone oil bath at 90°C and then stretching it. It was found that the samples could be stretched only an additional 20% after which they broke.

Stretching above glass transition. Strips of amrophous PET, with a length to width ratio of about 2 were stretched on a small stretcher, which was operated manually, at temperatures between 80° - 100°C. In this temperature range the rate of isothermal crystallization of PET is known

to be negligible.[44,45] The glass transition temperature for amorphous PET is known to be 69°C.[45,46] The procedure followed for preparing samples is described below. The stretcher with the sample in place was immersed in a constant temperature silicone oil bath for one minute and stretched rapidly by hand for a predetermined amount of strain. The exact amount of strain was determined from the ratio of final length to initial length. The rate of strain, as determined by several experiments, was about 300%/minute. Immediately following the end of stretching, the stretcher with the sample was quenched in a 0°C silicone oil bath. The quenching of strained samples prevents the relaxation of the strain, and the effect of strain on the structure and properties can be studied at room temperature.

A disadvantage of making samples by the procedure described is that human element is involved in the rate of stretching and the rate of quenching. In the present work reproducible samples could be made with relative ease. Any mechanical set-up for stretching is usually too bulky and the problem of quenching the sample fast enough arises. The possiblity of making a small mechanical stretcher is being investigated for any future work in this area.

The samples that were stretched below and above the glass transition were characterized by birefringence measurements, crystallinity measurements, low angle light scattering, microscopy and wide angle X-ray diffraction. A brief description of these techniques is given below.

Birefringence measurements. For the measurement of birefringence, a Babinet Compensator with a mercury lamp source was used. Babinet Compensator is an optical device which contains a wedge of birefringent

material such as quartz. Using a non-monochromatic light source such as mercury results in one black fringe along with several others as seen through the eyepiece of the compensator. The black line is brought to a reference line with no sample in the path of the light beam. With a sample in the beam, the black fringe is shifted and is brought back to the reference line by the compensating effect of the quartz wedge. The displacement is measured by the scale on the Babinet and the birefringence calculated by the relation:

$$\Delta = 4.05 \times 10^{-3} \frac{R}{t}$$

where R = retardation as measured by the displacement of the black fringe.

t = thickness of the sample in mils.

For some cases the birefringence was measured during the stretching and subsequent relaxation using transmitted light technique. The experimental set-up consists of a laser light source, analyser, sample holder, polarizer, photomultiplier, and oscillioscope. The sample is kept vertical while the analyser and the polarizer have their polarizing axes inclined at 45° to the vertical and are at 90° to each other.

The transmitted intensity is detected by the photomultiplier tube and recorded on the oscilloscope. The stretcher with the sample is immersed in a preheated silicone oil bath for one minute and then stretched by the desired amount. Care should be taken to insure that the silicone oil is free of suspended particles and the surface of the bath is clean. The speed of scanning on the oscilloscope is adjusted to follow the build up of total birefringence in one sweep.

The relationship between transmitted intensity and birefringence is: $$\text{Transmittance} = \sin^2 \frac{\pi d \Delta}{\lambda_o}$$

where d = thickness of the sample

λ_o = valve length of the light source

Δ = birefringence

A plot of birefringence versus time can be made using the transmitted light values from the oscilloscope scan.

Density measurements. The density of the samples was measured at room temperature using a density gradient column made by mixing two solutions with different concentrations of potassium iodide. The column was calibrated by standard density floats (glass beads) in the range of 1.33 to 1.41 gm/ml in steps of 0.01. Density of completely amorphous PET is 1.333 and that of completely crystalline PET is 1.455.[47] Percent crystallinity, X, from density measurements is calculated as:

$$X = \frac{1/d_a - 1/d}{1/d_a - 1/d_c} \times 100$$

where d_a = density of completely amorphous polymer

d_c = density of completely crystalline polymer

Low angle light scattering. A photographic low angle light scattering apparatus[48] was used to study the superstructure in oriented PET films. Scattering patterns were obtained with the analyser and polarizer parallel to one another (V_V and H_H) and perpendicular to each other (H_V and V_H). The stretching direction of the film is considered as the vertical

direction. For example, V_V scattering results when the polars are parallel to the stretching direction and H_H scattering results when the polars are at 90° to the stretching direction. A schematic diagram of the photographic light scattering apparatus is shown in Figure 1.

Optical microscopy. A Zeiss Standard GFL polarizing light microscope was used to study the superstructure in oriented PET films. Photomicrographs were obtained with a Zeiss Ikon 35 mm focal plane camera mounted on a Zeiss beam splitting system (basic body II). The samples were placed with the polars crossed and the stretching direction along either the polarizer or the analyser. This was achieved by rotating the sample till maximum extinction was obtained. Magnification was calculated by using a standard scale. A Zeiss 50X objective and an 8X ocular were used.

Wide angle X-ray diffraction. A Phillips X-ray unit equipped with a pinhole camera arrangement was used to record wide angle X-ray diffraction patterns. The patterns were recorded on a 4" x 5" flat photographic film. Sample-to-film distance could be adjusted to a desired value. The wide angle X-ray pattern provided information about the crystalline structure and its preferred orientation. The crystal structure for PET has been determined by Daubney, Bunn and Brown.[47] The unit cell contains one monomer unit and is triclinic with a = 4.56 Å, b = 4.94 Å, c = 10.75 Å, α = 98 1/2°, β = 118°, and γ = 112°.

The X-ray set-up is being modified to enable quantitative measurements of diffracted intensities by the help of a counter and a recorder. The operation is planned to be automatically controlled by a PDP-8 computer. With the help of intensity measurements, crystallinity and crystalline orientation function could be determined.

Uniaxial Stretching of PET Below its Tg

Results. Stretching a polymer below its glass transition is generally termed as "cold drawing". For the purpose of characterizing cold drawn PET, samples were strained at room temperature by 200% with a strain rate of 10% per minute. All the results that follow are for the necked position of the sample which was retained for its characterization. The effective strain in the necked region was calculated by taking the ratio of undrawn and drawn areas.

Initial width = 1 cm

Initial thickness = 2 mil

Final width = .65 cm

Final thickness = .7 mil

Initial density = 1.337 gm/ml

Final density = 1.3565 gm/ml

Effective Draw ratio = 4.32X

Upon annealing this sample at 140°C, a shrinkage of 20% was observed. The results reported in this section on cold drawn samples are for the necked region unless specified otherwise.

Birefringence. The birefringence was measured during stretching in both the necked and unnecked regions. Up to 5% strain, no necking was observed and the birefringence increased to a value of .006. At this point necking starts and the birefringence of the unnecked portion remained constant irrespective of strain. Upon release of strain the birefringence of this unnecked portion went to zero. The effect of strain upon the

birefringence of the necked region could not be determined in the early stages of the development of the neck for it was not in the path of the light beam. However, beyond 100% strain the birefringence of the necked region was constant at a value of .19 and was not affected by the release of strain. When the necked samples were annealed, both without constraint and at constant length, there was no detectable change in the birefringence.

Crystallinity. Crystallinity was measured by the Density Column method. The results are listed below.

Initial crystallinity of 2 mil thick amorphous PET = 4%

Crystallinity of necked region after 200% strain = 18%

Crystallinity of unnecked region after 200% strain = 3%

Necked portion annealed at 110°C for 1 hour = 32%

Amorphous PET annealed at 110°C for 1 hour = 31%

Necked portion annealed at 140°C for 10 minutes = 40%

Amorphous PET annealed at 140°C for 10 minutes = 39%

It is seen that upon cold drawing PET, the necked portion developes significant crystallinity. The crystallinity values reported for the annealed samples are the maximum values that were attained at the respective temperatures and do not change with an increase in annealing times. It was found that the crystallization rates of the cold drawn samples were much higher than those for undrawn samples. For this reason crystallization kinetic studies could not be carried out for the strained samples.

Low angle light scattering. Low angle light scattering is a very useful technique for studying the superstructure and its preferred orientation in a cyrstalline polymer sample. In the present work this technique

has been used to study 1) the superstructure that forms upon cold drawing amorphous PET samples; 2) the superstructure that forms upon annealing the cold-drawn samples. For this purpose V_H, H_V, H_H and V_V light scattering patterns were obtained.

Figure 2 shows a set of light scattering patterns obtained from the necked region of the cold drawn samples. The H_V and V_H patterns in Figure 2a and 2b have four lobes which show no indication of an intensity maxima along the scattering angle. The intensity is maximum in the center and decreases monotonically with increasing scattering angle. This is indicative of the presence of a rodlike superstructure as has been previously shown by Rhodes,[49] Stein and Rhodes,[50] and Samuels.[51] The azimuthal dependence of patterns arising from rods is determined by the value of ω, the angle between optic axis and the long axis of the rod.[50,52] When $\omega = 0°$ or $90°$, the H_V pattern is of the (X) type with minimum intensity along the polarizer and analyser directions. Figures 2a and 2b show similar characteristics, therefore it is inferred that the optic axis direction in the rods is either along or perpendicular to the long axis of the rod.

These patterns show considerable amount of secondary scattering which is believed to be arising from the disorder in the internal structure of the rods. Hashimoto et al[53] have shown that the internal disorder in rods leads to a decrease in the azimuthal dependence of the pattern. Similar effects of disorder have been studied for a spherulite by Stein and Yoon.[54]

A closer examination of these patterns show that the four lobes are inclined toward the equatorial direction, i.e., in the direction perpendicular to stretch. This means that the rodlike superstructure has a preferred orientation in the direction of stretch.[50,51,55]

The H_H and V_V patterns shown in Figures 2c and 2d are approximately 1500 times more intense than the V_H and H_V patterns as seen by the exposure time required to take the photographs. This shows that there is a great amount of density fluctuation in the polymer sample.[39,56] In unstretched samples, the V_V and H_H patterns arising merely due to density fluctuation are circularly symmetric[40,56] as observed for polyethylene by Stein and Rhodes[39] and for PET in Chapter II of this dissertation. It is seen that the H_H and V_V patterns in Figures 2c and 2d are symmetric but elongated in the direction perpendicular to stretch. Thus it can be inferred that superstructure giving rise to these patterns is preferentially oriented along the stretching direction. Rhodes and Stein,[57] Samuels,[58] Adams and Stein,[59] and Chien and Chang[60] have observed similar effects of orientation on the light scattering patterns between parallel polars. A comparison of 2c and 2d shows that the V_V pattern is more intense than the H_H pattern. This would be the case if the superstructure contributing to scattering was preferentially oriented in the stretching direction. This observation supports the previous inferences. The effect of orientation seems to be greater on the H_H and V_V patterns than on the V_H and H_V patterns. This is to be expected since the V_V and H_H patterns are more sensitive to orientation as pointed out by Samuels.[58] On the basis of light scattering results it can be said that cold drawing of PET results in the formation of a rod-like, non-volume filling superstructure which is preferentially oriented in the stretching direction. Dumbleton[23] has shown that drawing of PET results in the alignment of molecules in the direction of stretch and that they essentially are parallel to one another with relatively few folds present. If this is so, the optic axis would be parallel to the long axis of the

rods ($\omega = 0°$) and extended chain morphology would result.

Figure 3 shows light scattering patterns obtained from the annealing of the necked portion at 140°C held at constant length. These patterns are very similar to those in Figure 2 for drawn but unannealed sample. The only noticeable difference is that the H_V and V_H patterns for the annealed sample show a slight increase in the azimuthal dependence when compared with the corresponding patterns for the unannealed sample. This may be due to a decrease in the internal disorder.[53] Thus it can be said that the annealing of cold drawn PET at constant length does not change the rod-like superstructure but does decrease the internal disorder within the rods.

Figure 4 shows a set of light scattering patterns obtained from the necked portion of a cold drawn sample that was annealed at 140°C for 10 minutes without constraint. In Figure 4a and 4b the V_H and H_V patterns show four lobes that are oriented in the direction of stretching. Upon visual scanning in the θ direction along the azimuthal angle of highest intensity, a maxima can be seen. This is indicative of the presence of a spherulitic type superstructure in the polymer sample. The orientation of the pattern is similar to those obtained from ellipsoidal spherulites as reported by several workers.[39, 57-59,61-64] Stein and co-workers[65-67] and Samuels[58] have developed light scattering theories to predict patterns from ellipsoidal spherulites. Most of the above work was done to explain the deformation of spherulites upon drawing a polymer film with spherulitic morphology. Such a procedure results in the elongation of the spherulites such that the long axis of these ellipsoidal spherulites is along the stretching direction. Thus the light scattering pattern is elongated in

the direction perpendicular to the direction of stretch.

In the present case the pattern is elongated in the stretching direction suggesting that the ellipsoidal spherulites have their long axis oriented preferentially perpendicular to the direction of stretch. Barnov, Volkov, Farshyan and Frenkal[68] have obtained similar H_V light scattering patterns in their study of crystallizing polypropylene from drawn melts. They also conclude that the polymer contains ellipsoidal spherulites elongated perpendicular to the direction of stretching of the crystallizing melt. Samuels,[58] and Pakula and Kryszewski[69] have presented procedures for the calculation of the aspect ratio of the "ellipsoid" and their size from H_V and V_H scattering patterns. An estimation of size of ellipsoids is made for the patterns in Figures 4a and 4b. For an accurate value, however, photometric measurements should be made. It should also be noted that the V_H and H_V scattering intensity increased considerably upon annealing, as seen by the exposure time required. This suggests an increase in the concentration of anisotropic entities or an increase in the anisotropy of existing superstructure.

Estimation of size of ellipsoids by Samuels' method[58]

Let a = major axis of the ellipsoid

b = minor axis of the ellipsoid

r = a/b

Using Samuels method for calculating ellipsoidal ratio r and stretching ratio λ

$$r = \lambda^{3/2}$$

$$\lambda = 1 + \left(\frac{4[\sin^2(\frac{\theta max,1}{2}) - \sin(\frac{\theta max,2}{2})]}{\sin^2\theta max,_2\cos^2\mu_2 - \sin^2\theta max,_1\cos^2\mu_1} \right)^{1/3}$$

where $\theta max,1$ and $\theta max,2$ are scattering angles for maximum intensity at azimuthal angles μ_1 and μ_2 respectively.

From Figure 2a or 2b:

1. $\mu_1 = 45°$, $\theta_{max,1} = \tan^{-1} 0.1$

$$\sin^2\theta_{max,1} = 0.01$$

$$\sin^2 (\frac{\theta_{max,1}}{2}) = 0.0025$$

2. $\mu_2 = 60°$, $\theta_{max,2} = \tan^{-1} 0.133$

$$\sin^2\theta_{max,2} = 0.0172$$

$$\sin^2 (\frac{\theta_{max,2}}{2}) = 0.00435$$

$$\lambda = [1 + \frac{4(.0025 - .00435)}{(.00435- .005)}]^{1/3}$$

$$= (12.4)^{1/3} = 2.31$$

$$r = \lambda^{3/2} = 3.4$$

To determine a and b:

$$\frac{4\pi b}{\lambda'} \sin (\frac{\theta_{max,1}}{2})[1+(\lambda_s^3 - 1) \cos^2 (\frac{\theta_{max,1}}{2}) \cos^2 \mu_1]^{1/2}=4.09$$

where λ' = wavelength of laser = .6328μ

b = 1.55μ

a = 5.3μ

These results were obtained by an estimation of values for $\theta_{max,1}$, $\theta_{max,2}$, $\mu_{max,1}$, and $\mu_{max,2}$ from a photographic pattern. For more accurate results, photometric scans should be made to obtain the above patameters.

Figures 4c and 4d show the V_V and H_H scattering patterns for the cold drawn and annealed samples. These patterns are approximately 250 times more intense than the V_H and H_V patterns as seen by the exposure time required to take the photographs. Similar to the case of drawn and unannealed samples, these samples also show a high degree of density fluctuation.[39,56] The H_H and V_V patterns of Figure 4 have four lobes, with two large lobes oriented normal to the stretching direction and two small ones along it. Thus it can be inferred that the orientation of the superstructure is affecting these patterns. By comparison with the H_H and V_V patterns of Figure 2, it can be seen that the large lobes in the patterns for annealed samples are similar to those in the patterns for unannealed samples. It is, therefore, believed that similar superstructure may be giving rise to the patterns in both the cases. From the V_H and H_V patterns it has been inferred that the polymer contains ellipsoidal spherulites, thus the two small lobes that appear in the H_H and V_V patterns are believed to be from these ellipsoids. This conclusion is consistant in that the ellipsoids are elongated normal to the stretching direction while the scattering arising from them are in the direction of stretch as is expected by theoretical considerations.[58,65]

At this time it is suggested that the superstructure consists of rows of ellipsoids where these "rows" are oriented along the stretching direction and give rise to the two lobes oriented normal to stretching

direction. The ellipsoids by themselves can be considered as the sub-superstructure which are oriented preferentially in the direction normal to stretching and give rise to the two small lobes along it. If the above model is true, then the intensity of the large lobes would be less in the V_V case than in the H_H case as can be observed by comparing Figures 4c and 4d.

It may further be pointed out that neither the ellipsoidal spherulites nor the rows of these ellipsoids are volume filling, as is seen later in microscopic studies, therefore both the superstructure and the sub-superstructure contribute greatly to the scattering arising from density fluctuations. This accounts for the higher intensity of the V_V and H_H patterns compared to the H_V and V_H patterns.

The light scattering patterns from necked samples that were stretched another 20% at 90°C are shown in Figure 5. The H_V and V_H patterns are characteristic of a rod-like superstructure highly oriented in the stretching direction since there is no maxima in the scattering intensity and the lobes are inclined in the direction normal to stretching.[49,50] This is similar to the case of necked samples, Figure 2, except that the pattern is more oriented in the equatorial direction for the samples that were further drawn, thus suggesting that additional drawing increases the orientation of the rods in the stretching direction.

The V_V and H_H patterns in Figure 5 are similar to those in Figures 2 and 3 and the same explanations would apply here.

Microscopic studies. Microscopic examination of the cold drawn PET samples provided a confirmation of some of the interpretations and conclusions made on the basis of light scattering result.

The unnecked portion of the cold drawn samples showed the existance of craze marks[10] but was not considered necessary to be presented here. A photomicrograph of the necked region is shown in Figure 6a and it shows an ill-defined superstructure, the size nor the shape of which could be determined.

However, there is a tendency for the superstructure to be aligned parallel to the stretching direction. Some spherulitic type entities seem to be present but cannot be distinguished readily. The existence of streaks perpendicular to the stretching direction can be seen in Figure 6a. These are believed to be craze marks which initially form in the necked region and continue to exist when the unnecked portion gets drawn into the necked region.

Annealing of necked regions without constraint at 140°C results in the formation of spherulitic superstructure as shown in Figure 6b. These spherulites are ellipsoidal in nature and have their long axes oriented perpendicular to the stretching direction. Moreover these ellipsoids appear in rows along the stretching direction with about 4-10 spherulites in a row. The size of these ellipsoids has been estimated to be:

long axis, a = 2.7 - 3 μm

short axis, b = .9-1.1 μm

aspect ratio $\tilde{}$ 3

It is further observed that this ellipsoidal superstructure is not volume filling. These results are in general agreement with the light scattering results. In Figure 6b, there is also the presence of a few rows of spherulites that oriented normal to the stretching direction. These rows appear similar in nature to the craze marks observed in the unannealed

samples, Figure 6a. This may be due to a greater tendency of spherulites to grow along the craze marks than elsewhere. The number of such rows is small compared to the rows in the stretching direction therefore their effect on light scattering was not observed.

A necked sample annealed at 140°C and at constant length show a superstructure similar to that in Figure 6a for the unannealed sample and is not presented. Thus it is seen that the superstructure of a cold drawn sample occurs only upon annealing without any constraint. This is also in agreement with light scattering results.

Wide Angle X-ray Diffraction. Wide angle X-ray patterns were obtained for undrawn and drawn PET films and are shown in Figure 7. The sample-to-film distance used was 5 cm. The samples were relatively thin which required a relatively long exposure time (approximately 18 hours) to record a pattern. Such long exposure times resulted in a very bright central spot as can be seen in the patterns. Figure 7a shows a characteristic amorphous halo obtained from an undrawn amorphous sample of PET. Figure 7b is a diffraction pattern from the necked region of a cold drawn sample and shows two diffused lobes oriented in the equatorial direction. This indicates the existance of crystalline or semi-crystalline material in the sample. It is suggested that the crystals are very imperfect which causes the diffraction lines to broaden to an extent that they are indistinguishable. The orientation of the lobes suggest a preferred orientation of crystals. Since no diffraction lines are observed, no judgment can be made of the preferred orientation of the crystals. Such patterns have been previously observed for cold drawn PET.[11,12a] Asano and Sato

have recently reported a detailed wide angle X-ray studies on cold drawn PET.[12a]

Annealing of the necked sample results in sharp diffraction patterns which are characteristic of oriented crystalline polymers. Figure 7c shows a diffraction pattern obtained from a sample annealed without constraint while 7d is one obtained from a sample annealed at constant length. Both these show that the lobes of 7b change to arcs upon annealing. The azimuthal dependence of arcs is less in 7d than 7c suggesting a higher orientation attained in samples annealed at constant length. Diffraction patterns similar to the ones observed here have been reported by other workers.[11,12a,13,14,21a,70,71]

It may now be suggested that the equatorial lobes of Figure 7b arise due to a preferred c axis orientation of the imperfect crystals in the direction of stretching. The imperfect crystals that form upon cold drawing become more perfect upon annealing while retaining their orientation. Similar observations have been made by Dumbleton[18] and Dalmage and Geddes.[14]

The crystal structure of PET is well known,[47,72-75] thus the diffraction lines can be identified and preferred orientation of the crystals determined. Daubney, Bunn and Brown[47] found that the unit cell of PET contained one monomer unit and was triclinic with a = 4.56 Å, b = 4.94 Å, c = 10.75 Å, α = 98 1/2°, β = 118° and γ = 112°.

The values for 2θ were measured from Figures 7c and 7d and compared with those listed by Krigbaum and Vasek.[73] The crystallographic planes giving rise to the diffraction lines were identified and are presented in the form of a scale drawing in Figure 8a. Planes (010) and (100) give diffraction lines in the equatorial region which indicates their preferred

orientation parallel to the direction of stretch. Thus the "c" axis of the crystal and hence the molecular chain axis are preferentially oriented in the direction of stretch.

Upon further stretching the cold drawn sample at 90°C, the X-ray diffraction pattern changes to a fiber pattern,[70,71] shown in Figure 7d, which is characteristic of highly oriented PET. The respective reflections have been identified by comparing the 2θ values obtained to those listed by Krigbaum and Vasek[73] and shown on a scalar drawing in Figure 8b. As deduced previously, the 010 and 100 reflections show that the crystals are highly oriented in the stretching direction. The orientation is greater than in the case of cold drawn and annealed samples as judged by the more localized reflections in the former case. Thus the redrawing of the cold drawn sample results in the formation of fairly perfect and highly oriented crystals.

The X-ray diffraction work presented here is merely qualitative and helps in the understanding of results from other techniques. A quantitative X-ray study could be carried out to determine the crystallinity and the orientation as has been done by several investigators in the past.[15-18, 20,25-28]

Discussion for stretching below Tg. It is shown that cold drawing of PET produces a necked region with a high amount of crystallinity and birefringence, and an unnecked region with no significant crystallinity or birefringence. As proposed by Spruiell et al.[8] stretching below the glass transition forces the polymer chains to extend as they pass through the neck and produces regions of crystalline and paracrystalline order with

relatively few folds present. A high degree of internal stress is present in the sample which cannot be relieved below Tg due to low molecular mobility. When annealed at temperatures above Tg, the molecules rapidly rearrange to relieve the internal stress. Dumbleton[18] has shown that chain folding occurs when drawn PET is annealed and has explained his results using the model of Statton and Dismore,[29] who proposed that a drawn fiber consisted of highly extended molecules that are essentially parallel to one another with only a few fold chains present. Annealing causes chain folding to occur on the few folds already present that act as oriented nuclei. Spruiell et al further suggest that the removal of stress upon annealing is accompanied by melting of very imperfect crystals and is followed immediately by rapid recrystallization.

In the present work, low angle light scattering and microscopic observations show that cold drawing produces a rod-like superstructure in which the rods are preferentially oriented in the stretching direction. Moreover, these rods are not volume filling. This leads to the suggestion that the polymer sample consists of oriented rods dispersed in an oriented amorphous matrix. The crystal structure is presumed to be formed of extended chain crystallites in accordance to the model of Spruiell et al,[9] and Statton and Dismore.[43]

Annealing at constant length has little effect on the superstructure however it does make the crystal structure more perfect. It is believed that the few chain folds that might be present according to the model of Statton and Dismore,[43] rearrange to improve the crystal structure in a manner similar to the model of Fisher for polyethylene.[77] On the other hand, annealing without any constraint results in the change from a rod-like

morphology to a spherulitic one. The superstructure consists of rows of ellipsoids where the rows are parallel to the stretching direction while the long axis of the ellipsoids is normal to it. As before, annealing without constraint also makes the crystals more perfect. It is suggested at this point that the ellipsoids nucleate at sites along the length of rods thus resulting in rows. Dumbleton[23] proposed that chain folding occurs upon free annealing without loss of molecular orientation. Assuming that his model is correct, the growth of crystals formed by chain folding would be higher in the direction normal to stretching. It may also be pointed out that since the chains are aligned in the stretching direction prior to annealing, steric hinderance effects would restrict the growth of folded chain crystals in directions other than normal to it. This explains the formation of ellipsoids with their long axis perpendicular to the stretching direction.

The rapid increase in crystallinity upon annealing is in agreement with the observations of Spruiell et al. The ultimate crystallinity for undrawn and drawn annealed samples was the same, however, the superstructure is volume filling in the undrawn case while it is non-volume filling in the drawn case. This suggests that in the drawn samples either a) the superstructure is more crystalline than in undrawn samples or b) the amorphous regions are actually paracrystalline and contribute to crystallinity. Apriori the latter is more likely to be correct.

Based on the results and discussion presented it is proposed that cold drawing of PET results in formation of a rod-like superstructure consisting of imperfect extended chain crystals. External constraints affect the changes that occur on annealing. Annealing at constant length does not change the rod-like superstructure and extended chain crystal structure while during

free annealing ellipsoidal spherulites nucleate along the long axis of each rod and produce rows of ellipsoids.

Based on the conclusions of Dumbleton[23] and Spruiell[9] et al, it is believed the chain folded crystals are formed upon free annealing. Such a model helps explain the experimental observations.

Uniaxial Stretching of PET Above its Glass Transition

Results. Most of the results reported in this section are on samples that were stretched at elevated temperatures and quenched to 0°C. The measurements were made at room temperature except for a few birefringence experiments,where the birefringence was measured as a function of time as the samples were being stretched. Such experiments also provided an estimation of the time taken for quenching the strained samples. The Tg of amorphous PET is known to be 67-69°C.[44,46] The samples were drawn at temperatures at which thermal crystallization is negligible so that the effect of strain on the morphology of PET could be studied. The strain rate was approximately 300%/min for all experiments.

Birefringence measurements. Birefringence was measured both as a function of temperature for a fixed strain and as a function of strain at fixed temperatures. Samples were stretched to 80% strain at 300%/min and at 80°, 90° and 100°C respectively. Birefringence, measured at room temperature, is plotted as a function of temperature of stretching in Figure 9 and is seen to decrease in an exponential manner with increasing temperature. This would be expected because the mobility of polymer chains is

higher at higher temperatures and therefore the strain relaxes out faster.[7,8] However, higher orientation and consequently higher birefringence can be produced at the higher temperatures by increasing the strain rate.[6] At the strain rate used here (300%), the temperatures chosen for further work were 80°C and 90°C.

For the next set of experiments, samples were stretched by fixed amounts ranging from 40% to 175% at 90°C and at a strain rate of 300%/min. Their birefringence was measured at room temperature and plotted as a function of strain in Figure 10. It can be seen that the birefringence increases in a non-linear fashion at low values of strain and then increases linearly from about 80% to 175%. The elongations occuring in this set are believed to be in the flow region as described by Thompson[1] where the orientation and crystallinity are low. If the samples are allowed to stay at 90°C after the completion of stretching, instead of their being quenched, the strain was seen to relax out almost entirely in about 20-30 minutes as measured by the decrease in birefringence. Consequently the rate of quenching becomes an important factor at temperatures where the relaxation rates are relatively high.

A birefringence relaxation experiment was done by following the intensity of light transmitted between cross polars for a sample stretched to 45% at 90°C and at 300%/min. Oscilloscope scans were obtained for changes in intensity during the stretching and subsequent relaxation at 90°C. Two such scans for different time scales are shown in Figure 11. From the scan "a" it is seen that the birefringence increases for about 9 seconds, the time taken to stretch, and then begins to decrease. Birefringence was calculated from this scan and plotted as a function of

time in Figure 12. Separate samples were prepared in the same manner but were quenched immediately after the end of stretching. Their birefringence, as measured on the Babinet Compensator, was found to be between 7.8×10^{-3} and 8.2×10^{-3}. This presents a drop of about 3×10^{-3} during quenching when compared to the maximum value of 11×10^{-3} attained at the completion of stretching (Figure 12). The values of 7.8×10^{-3} and 8.2×10^{-3} correspond to 13 and 14 seconds respectively, on the time scale of Figure 12. Subtracting the time taken for stretching, it is noted that quenching to prevent relaxation of stretched sample effectively takes 3.5 to 4.5 seconds.

Samples strained to 40% and 80% at 300%/minute and at 90°C were annealed without constraint at 140°C and the birefringence followed as a function of time. The annealing caused the samples to shrink almost to their original length. The birefringence decreased with time of annealing and attained a negative value as shown in Figure 13. Dalmage and Geddes[14] had also observed negative birefringence upon annealing of samples with low initial elongations. On the basis of their wide angle X-ray work they suggested that for the above case the crystallites have their fiber axis perpendicular to the stretching direction resulting in a negative birefringence value.

Another set of experiments was done for samples stretched by fixed amounts from 40% to 175% at 80°C and at 300%/minute. To obtain higher elongations, quenched samples with 175% strain were heated at 80°C for 15 seconds and stretched an additional 40 to 175%. Birefringence values measured at room temperature are plotted in Figure 13. The plot shows a gradual increase in birefringence at smaller strain followed by a sharp

linear increase between 120% and 175%. The change in slope at about 120% is believed to be due to the effect of strain induced crystallization. Beyond 175% the slope of the curve decreases but the birefringence between about 200% and 350% increases linearly. This second change of slope may be because samples in this range were stretched in two steps as has been mentioned earlier. It may be pointed out that the absolute values of birefringence for corresponding strains are higher at 80°C than at 90°C.

Crystallinity. Crystallinity measurements were made by measuring densities using a density gradient column. Samples stretched at 90°C up to 175% and those stretched to 75% at 80°C, 90°C and 100°C showed no measurable crystallinity. These samples can be classified as amorphous oriented samples. Maximum crystallinity in these samples was 5% compared to 4% of unstretched amorphous sample.

An increase in crystallinity was observed for samples stretched at 80°C and at 300%/min beyond 80% strain. The crystallinity rises with strain tending to level off at high strains. Only strain (or stress) induced crystallization is taking place at this temperature and strain rate since no thermal crystallization is known to occur at 80°C. A plot of crystallinity versus percent strain is shown in Figure 15.

Light Scattering. Low angle light scattering was used to observe the superstructure that might develop by straining amorphous PET samples above its glass transition temperature. V_H, V_V and H_H scattering patterns were obtained and analyzed. It was possible to obtain light scattering patterns from samples that showed little or no crystallinity and for which no superstructure could be observed under the microscope.

Figure 16 shows a series of V_H scattering patterns for samples stretched at 80% at 80°, 90° and 100°C. All three patterns have four scattering lobes with no maxima in intensity along the scattering angle direction. Moreover, the lobes are inclined towards the stretching direction. Such patterns are characteristic of scattering from a rod-like superstructure with the rods oriented preferentially in the direction normal to stretching.[49,50,52]

With increasing temperatures, the intensity of the pattern was found to decrease while there was little change in the shape. This suggests that with an increase in temperature there is a decrease in either a) the number of rods; b) their size; c) their anisotropy or a combination of these.

Figure 17 shows V_H patterns for samples stretched at 90°C by amounts from 40% to 175%. Patterns in a, b and c are similar to those of Figure 16 and show the presence of a rod-like superstructure oriented normal to the stretching direction. At 175%, in d, there is evidence of a maxima in scattering while the lobes have moved away from the stretching direction although they are still inclined in that direction. The pattern is characteristic of a sheaf-like superstructure[80] where the sheaves are oriented preferentially normal to stretching. It is suggested at this time that rod-like nuclei form at low strains which tend to form spherulitic superstructure a higher elongations. The rods are preferentially oriented normal to stretching direction but this is reduced during spherulitic growth from these rods. This point will be discussed later. An increase in intensity was observed with elongation suggesting either an increase in a) number of scattering entities; b) their size;

c) their anisotropy or a combination of the above.

Figure 18 shows a series of V_H scattering patterns for samples stretched at 80°C. At low elongations the V_H patterns are similar to those of Figures 16 and 17 (a, b, c) and are characteristic of rod-like superstructure with the rods oriented normal to the stretching direction. At higher elongations, the V_H patterns still have four lobes that are oriented in the stretching direction but show a minima and a maxima in intensity along the scattering angle direction at the azimuthal angle of highest intensity. This is indicative of the presence of "spherulitic" type superstructures. The orientation of the pattern indicates that the "spherulites" are ellipsoidal in nature and have their long axis preferentially oriented normal to the direction to stretch. It can also be observed that the angle the lobes make with the stretching direction increases as the patterns change from a rod-like to a sheaf-like, i.e., from c to d. This can be best explained by considering a special case where spherulites grow from oriented rods as nuclei. The scattering from rods would show an orientation while the spherulites would not show any orientation and would give a pattern with lobes at 45°. Similar situation may be imagined for present case except that ellipsoidal spherulites are formed. The angle of the lobes in d is dependent upon the aspect ratio of these ellipsoids. Since the ellipsoids in d have their long axis normal to the stretching direction it is suggested that the rate of growth of crystals is higher in this direction.

Patterns in Figure 18 (d-f) are similar to those obtained from ellipsoidal spherulites by several workers.[39,57-59,61-64] Stein and co-workers,[65-66] and Samuels[42] have developed light scattering theories

to predict patterns from deformed spherulites that are ellipsoidal in nature.

It should be pointed out that the patterns at intermediate elongations may be arising from a sheaf-like superstructure rather than ellipsoidal spherulites. This is reasonable since the rods produced at low elongations would be expected to change into sheaves before taking the form of ellipsoids in a manner similar to crystallizing in an unoriented state.[80] The presence of ellipsoidal spherulites in polymers, that are elongated in the direction normal to the direction of strain, have also been observed by Barnov et al.[68] and Rhodes and Stein.[39] Barnov et al.[68] have studied the crystallization of polyolefins from drawn melts. They obtained H_V patterns with the four lobes tilted in the direction of stretching, and concluded that the spherulites were elongated transverse to the direction of stretching of the crystallizing melt. Rhodes and Stein observed the development of four lobe patterns with the lobes oriented along the stretching direction in polyethylene that was drawn and then annealed. Samuels[58] and Pakula and Kryszewski[69] have presented procedures for calculating the size of ellipsoidal spherulites.

An estimation of size of ellipsoids formed at 175% elongation is made using Samuels' method[58] as has been described in the case of stretching below Tg.

The stretching ratio, λ is given as:

$$\lambda = 1 + \left[\frac{4\left[\sin^2\left(\frac{\theta_{max,1}}{2}\right) - \sin\left(\frac{\theta_{max,2}}{2}\right)\right]}{\sin^2\theta_{max,2}\cos^2\mu_2 - \sin^2\theta_{max,1}\cos^2\mu_1} \right]^{1/3}$$

From Figure 18 g:

$$\mu_1 = 45°, \quad \theta_{max,1} = \tan^{-1} 0.12$$

$$\sin^2 \theta_{max,1} = 0.0144$$

$$\sin^2 \frac{\theta_{max,2}}{2} = 0.0036$$

$$\mu_2 = 50°, \quad \theta_{max,2} = \tan^{-1} 0.13$$

$$\sin^2 \theta_{max,2} = 0.0169$$

$$\sin^2 \frac{\theta_{max,2}}{2} = 0.00422$$

$\lambda = 1.25$

$r = 1.4$

$b = 1.5\mu$

$a = 2.1\mu$

Changes in the V_H patterns occurring upon drawing the samples beyond 175% at 80°C are presented in Figure 19. The four lobes of pattern begin to move away from the stretching direction accompanied by a decrease in intensity and a loss of maxima. Eventually the pattern changes to horizontal streaks as has been seen by the stretching of polyethylene by Rhodes and Stein.[39,57] Such a pattern is shown in Figure 19d and is related to a rod-like superstructure that is aligned in the direction of stretching. This is because the ellipsoids after they are formed, deform as the stretching of the sample continues and the ellipsoidal

morphology changes into a fibrillar morphology.

A set of V_V and H_H scattering patterns are shown in Figures 20 and 21 respectively for samples stretched at 90°C and at 300% per minute. These patterns correspond to the V_H patterns shown in Figure 18. In Figure 20 it is seen that at low elongations the V_V pattern is circular and of low intensity. However at high elongations the patterns have four lobes and are elongated in the direction normal to stretching. Similar patterns were observed for drawn polyethylene by Rhodes and Stein.[39] These patterns represent scattering from rods. On the basis of V_H patterns, it has been proposed that the superstructure consists of ellipsoids (or sheaf-like structures) with their long axis normal to the stretching direction. The ellipsoids can be considered to be formed of rods such that the rods are preferentially oriented in the direction normal to stretching. If the optic axis of these rods is at 90° to the long axis of the rods, the optic axis would be aligned parallel to the stretching direction.[50] Such a rod would give a V_V pattern of the type shown in Figure 20d through 20f. If the above model is correct, a decrease in the H_H intensity would be observed. Comparing Figures 20 and 21, the intensity of H_H patterns is seen to be less than corresponding V_V patterns. The difference in the pattern e compared to d and f cannot be explained.

Microscopic studies. Strained samples were examined under a polarizing microscope to confirm some of the conclusions made about the superstructure by low angle light scattering. Most samples for which light scattering patterns are shown in Figures 16 and 17 showed no superstructure under the microscope. However for samples of Figure 18, stretched at 80°C, significant results were obtained. At 80% strain the

presence of a few ellipsoidal spherulites was observed as shown in Figure 22a. As the strain increased, the number as well as size of these "spherulites" was found to increase as can be seen in Figures 22b and 22c. In all of these photomicrographs the ellipsoids are oriented with their long axis normal to the stretching direction as was observed by the light scattering results. The size of the ellipsoids was found to be:

$a = 1.7 - 2.2\mu$

$b = 1.4 - 1.8\mu$

aspect ratio $\simeq 1.5$

For samples stretched beyond 175%, there is evidence of deformation of the ellipsoidal spherulites. They tend to be deformed and become elongated in the direction and finally attain a fibrillar morphology. Very clear photomicrographs could not be obtained for the above samples and only one of these for 350% is presented in Figure 22d.

Wide angle x-ray diffraction. Wide angle X-ray diffraction patterns were obtained for samples stretched at 80°C and at 300% per minute. A series of such patterns is shown in Figure 23. Pattern "a" is from an amorphous unoriented sample and is included for reference. Pattern "b" is from a sample with 80% elongation and shows an amorphous halo characteristic of amorphous polymers. At 175% strain the pattern shows diffused lobes in the equatorial direction, Figure 23c, which is indicative of the presence of imperfect crystals. Further stretching shows the transition of the diffused lobes to a fiber pattern as seen in "d" and

"e". The pattern in 23e is similar to the pattern of Figure 7e, the scale drawing for which is shown in Figure 8b. The procedure for identifying the diffractions has been discussed in the section on drawing below glass transition.

Using the scale drawing of Figure 8b for the pattern in 23e, it is found that planes (010) and (100) are oriented preferentially parallel to the stretching direction. Thus the "c" axis of the crystal and hence the molecular chain axis are also oriented along the stretching direction. By comparison similar deductions can be made for the patterns in Figure 23c and d.

Discussion. Straining of amorphous PET above its glass -ransition but at temperatures at which thermal crystallization does not occur provides information about the superstructure that forms due to strain induced crystallization. In this study the strain rate was not changed while the temperature and the amount of strain were varied. Most information about the superstructure was obtained for PET strained at 80°C. Results indicate that at low elongations a rod-like superstructure exists which does not contribute to crystallinity and is oriented in the direction normal to stretching. Such observations were also made by Ulrich[81] for polyethylene oxide crystallized from the melt under shear. Barnov and his co-workers[68,82,83] have done work on the development of superstructure by crystallizing from oriented melt. They came to conclusions similar to those in this study, that the superstructure is oriented in the direction perpendicular to stretching.

At higher elongations the rods change into ellipsoidal spherulites which are elongated normal to stretching. Rhodes and Stein[57] observed

similar behavior when stretched polyethylene was annealed. Barnov[84] et al. have proposed models for the development of superstructure when polymers are crystallized under molecular orientation. The results of this work seem to agree with one of their regions where they predict the formation of ellipsoids elongated transversely to the direction of stretching.

Based on the light scattering results the ellipsoids can be considered to be compased of rods such that the rods are oriented preferentially in the direction normal to stretching. Such a model helps explain the V_H, V_V and H_H scattering results and is consistent with the wide angle X-ray and microscopic observations.

References

1. A. B. Thompson in Fibres Structure, J. W. S. Hearle and R. H. Peters, Ed, Butterworth & Co., 1963.
2. Fibres from Synthetic High Polymers, R. Hill, Ed., Elsevier, 1953.
3. Encyclopedia of Polymer Science and Technology, Volume 11, Pages 1-41.
4. A. Ziabicki in Man Made Fibers, H. F. Mark, S. M. Atlas, E. Cernia, Volume I, Interscience, 1967.
5. A. B. Thompson and I. Marshall, Proc. Roy. Soc. (London), A211, 541 (1954).
6. A. B. Thompson and I. Marshall, J. App. Chem. 4, 145 (1954).
7. A. B. Thompson, J. Polymer Sci., 34, 741 (1959).
8. J. E. Spruiell, D. E. McCord and R. A. Benerlein, Tran. of the Soc. of Rheology, 16, (3), 535 (1972).
9. R. P. Sheldon, Polymer, 4, 213 (1963).
10. S. Newman, J. Polymer Sci., 27, 563 (1963).
11. P. R. Blakey and R. P. Sheldon, J. Polymer Sci. A, 2, 1043 (1964).
12. G. E. Wilkes and C. M. Chu, Polymer Preprints, 14 (2), 1282 (1973).

12a. T. Asano and T. Seto, Polymer Journal, 5, 72 (1973).

13. A. Keller, J. Polymer Sci., 21, 363 (1958).
14. W. J. Dalmage and A. L. Geddes, J. Polymer Sci., 31, 499 (1958).
15. C. J. Heffelfinger and P. G. Schmidt, J. Appl. Polymer Sci., 9, 2661 (1965).
16. W. O. Statton and P. G. Godard, J. Appl. Phys., 28, 1111 (1957).
17. R. Bonart, Kolloid Z. Z. Polym, 199, 136 (1964).

18. W. L. Lindner, Polymer, 14, 9 (1973).

19. C. J. Heffelfinger and R. L. Burton, J. Polymer Sci., 47, 289 (1960).

20. C. J. Heffelfinger and E. L. Lippert, J. Appl. Polymer Sci., 15, 2699 (1971).

21. L. G. Kazaryan and D. Ya Tsvankin, Vysokomol Soyed, A9 (2), 377 (1967).

22. J. M. Dumbleton and B. B. Bowles, J. Polymer Sci., A-2, 4, 951 (1966).

23. J. H. Dumbleton, J. Polymer Sci., A-2, 7, 667 (1969).

24. J. H. Dumbleton, J. Polymer Sci., A-2, 6, 796 (1968).

25. P. R. Pinnock and I. M. Ward, Brit. J. Appl. Phys., 15, 1559 (1964).

26. G. Farrow and D. Preston, Brit. J. Appl. Phys., 11, 353 (1960).

27. G. Farrow and I. M. Ward, Polymer, 1, 330 (1960).

28. P. F. Statton, J. Appl. Polymer Sci., 7, 803 (1963).

29. J. L. Koenig and M. J. Hannon, J. Macromol. Sci., (Phys.), B 1, 119 (1967).

30. D. C. Prevorsek and J. P. Sibila, J. Macromol. Sci., (Phys.), B 5, 617 (1971).

31. K. K. Mocherla and J. P. Bell, J. Polymer Sci., A-2, 11, 1779 (1973).

32. G. S. Y. Yeh and P. H. Geil, J. Macromol. Sci., (Phys.), B 1, 251 (1967).

33. J. J. Klement and P. H. Geil, J. Macromol. Sci., (Phys.), B 5, 505 1971.

34. J. J. Klement and P. H. Geil, J. Macromol. Sci., (Phys.), B 5, 535 (1971).

35. G. E. McGraw, J. Polymer Sci., A-2, 8, 1323 (1970).

36. M. Kashiwagi, A. Cunnigham, A. J. Manual and I. M. Ward, Polymer, 14, 111 (1973).

37. A. Keller and M. J. Machin, J. Macromol. Sci., B 1, 41 (1967).

38. C. Gieniewski and R. S. Moore, Macromolecules, 2, 385 (1969).

39. M. B. Rhodes and R. S. Stein, J. Appl. Phys., 31, 1873 (1960).

40. R. J. Samuels, J. Polymer Sci., A-2, 9, 2165 (1971).

41. R. J. Samuels, J. Polymer Sci., A-2, 3, 1741 (1965).

42. R. S. Stein and F. H. Norris, J. Polymer Sci., 21, 381 (1958).

43. P. F. Dismore and W. O. Statton, J. Polymer Sci., C, 13, 133 (1966).

44. W. H. Cobbs and R. L. Burton, J. Polymer Sci., 10, 275 (1953).

45. K. G. Mahyan, W. J. James and W. Bosch, J. Appl. Polymer Sci., 9, 3605 (1965).

46. M. J. Kolb and E. F. Izad, J. Appl. Physics, 20, 571 (1949).

47. R. de P. Daubeny, C. W. Bunn, and C. J. Brown, Proc. Royal Soc. (London), A 226, 531 (1955).

48. G. C. Adams, J. Polymer Sci., A-2, 6, 31 (1968).

49. M. B. Rhodes, Ph.D. Thesis, University of Massachusetts (1962).

50. M. B. Rhodes and R. S. Stein, J. Polymer Sci., A-2, 7, 1539 (1969).

51. R. J. Samuels, J. Polymer Sci., A-2, 7, 1197 (1969).

52. T. Hashimoto, Y. Murakami and Hiromichi Kawai, Polymer J., 4, 452 (1973).

53. T. Hashimoto, N. Hayashi, Y. Murakami and H. Kawai, submitted for publication to Polymer J.

54. R. S. Stein and D. Yoon, submitted for publication, J. Polymer Sci., A-2.

55. M. Hayashi, Y. Murakami, M. Moritani, T. Hashimoto and H. Kawai, Polymer Journal, 4, 560 (1973).

56. R. S. Stein and D. Yoon, submitted for publication J. Polymer Sci., A-2.

57. M. B. Rhodes, R. S. Stein, J. Appl. Phys., 32, 2344 (1961).

58. R. J. Samuels, J. Polymer Sci., C, 13, 37 (1966).

59. G. Adams and R. S. Stein, J. Polymer Sci., B, 541 (1967).

60. J. C. W. Chien and E. P. Chang, Macromolecules, 5, 610 (1972).

61. M. J. Wallach, J. Polymer Sci., C, 13, 69 (1966).

62. V. G. Barnov and K. A. Gasparyan, J. Polymer Sci., A-2, 8, 1015 (1970).

63. C. Gieniewski and R. S. Moore, Macromolecules, 2, 385 (1969).

64. N. Yoshioko and M. Sato, Chemistry of High Polymers (Japan), 26, 846 (1970).

65. S. Clough, J. J. van Aartsen and R. S. Stein, J. Appl. Physics, 36, 3072 (1965).

66. R. S. Stein, P. Erhardt, J. J. van Aartsen, S. Clough and M. B. Rhodes, J. Polymer Sci., C, 13, 1, (1966).

67. J. J. van Aartsen and R. S. Stein, J. Polymer Sci., A-2, 9, 295 (1971).

68. V. G. Barnov, T. I. Volkov, G. S. Farshyan and S. Ya Frenkal, J. Polymer Sci., C, 30, 305 (1970).

69. T. Pakula and M. Kryszewski, J. Polymer Sci., C, 38, 87 (1972).

70. W. O. Statton, J. Polymer Sci., C, 20, 117 (1967).

71. H. Tadokaro, K. Tatsuka and S. Murahashi, J. Polymer Sci., 59, 413 (1962).

72. H. G. Killiam, M. Haboth and E. Jenckel, Kolloid Z, 172, 166 (1960).

73. Yu. Ya. Tomashpolskii and G. S. Markova, J. Polymer Sci., (U.S.S.R.) 6, 316 (1964).

74. Y. Yamashita, J. Polymer Sci., A, 3, 81 (1965).

75. A. Keller, J. Polymer Sci., 17, 351 (1955).

76. W. R. Krigbaum and A. M. H. Vasek, Texture, 1, 9 (1972).

77. E. W. Fisher and H. Goddar, J. Polymer Sci., C, 16, 4405 (1969).

78. T. Murayama, J. M. Dumbleton and M. C. Williams, J. Polymer Sci., A-2, 6, 787 (1968).

79. C. Picot, R. S. Stein, M. Motegi and H. Kawai, J. Polymer Sci., A-2, 8, 2115 (1970).

80. A. Misra and R. S. Stein, J. Polymer Sci., B, 10, 473 (1972).

81. R. E. Ulrich, Ph.D. Thesis, University of Massachusetts (1972).

82. V. G. Barnov, Faraday Discussions, 1B, 327 (1970).

83. V. G. Barnov, N. I. Bychkovsky, A. Sh. Gorkhman and M. P. Nosov, J. Polymer Sci., C, 38, 327 (1972).

84. V. G. Barnov, S. Ya Frenkel, V. I. Gromov, T. I. Volkov and R. S. Zurabian, J. Polymer Sci., C, 38, 61 (1972).

CAPTIONS FOR FIGURES

Figure 1: Schematic diagram of the photographic low angle light scattering apparatus.

Figure 2: Light scattering patterns from cold drawn PET (necked portion of PET drawn at room temperature at 10% per minute). Sample-to-film distance = 15 cm.

a) H_V, Exposure = 1 minute

b) V_H, Exposure = 1 minute

c) V_V, Exposure = 1/25 second

d) H_H, Exposure = 1/25 second

Figure 3: Light scattering patterns for cold drawn PET that was annealed at constant length at 140°C for 10 minutes. Sample-to-film distance = 15 cm.

a) H_V, Exposure = 1 minute

b) V_H, Exposure = 1 minute

c) V_V, Exposure = 1/25 second

d) H_H, Exposure = 1/25 second

Figure 4: Light Scattering patterns for cold drawn PET that was annealed without constraint at 140°C for 10 minutes. Sample-to-film distance = 15 cm.

a) H_V, Exposure = 10 seconds

b) V_H, Exposure = 10 seconds

c) V_V, Exposure = 1/25 seconds

d) H_H, Exposure = 1/25 seconds

Figure 5: Light scattering patterns for cold drawn PET that was drawn another 20% at 90°C. Sample-to-film distance - 15 cm.

a) H_V, Exposure = 1 minute

b) V_H, Exposure = 1 minute

c) V_V, Exposure = 1/25 second

d) H_H, Exposure = 1/25 second

Figure 6: Photomicrographs of cold drawn PET between cross polars.

a) Necked portion of cold drawn sample.

b) Sample (a) annealed at 140°C for 10 minutes.

Figure 7: Wide angle X-ray patterns.

a) amorphous

b) cold drawn (necked portion)

c) cold drawn sample annealed at 140°C for 10 minutes at constant length

d) cold drawn sample annealed at 140°C for 10 minutes without constraint

e) cold drawn sample stretched another 20% at 90°C

Figure 8: Scalar diagrams for the X-ray pattern.

a) cold drawn and annealed, corresponding to Figure 7c & 7d.

b) cold drawn and redrawn, corresponding to Figure 7e

Figure 9: Plot of birefringence versus temperature for PET stretched to 80% at 300% per minute.

Figure 10: Plot of birefringence versus percent elongation for PET stretched at 90°C at 300% per minute.

Figure 11: Oscilloscope scan of transmitted light as a PET sample stretched to 45% at 90°C. a) 0-50 secs., b) 0-20 secs.

Figure 12: Plot of birefringence versus time as calculated from Figure 11.

Figure 13: Change in birefringence as a function of time when annealed at 140°C for PET that was stretched at 90°C by

a) 40%

b) 80%

Figure 14: Plot of Birefringence versus percent strain for PET stretched at 80°C at 300% per minute.

Figure 15. Plot of crystallinity versus strain for PET stretched at 80°C at 300% per minute.

Figure 16: V_H light scattering patterns for PET stretched to 80% at

a) 80°

b) 90°

c) 100°C

Exposure time is the same for all patterns. Sample-to film-distance = 15 cm.

Figure 17: V_H light scattering patterns for PET stretched at 90°C by

a) 40%, Exposure = 5 minutes

b) 80%, Exposure = 2 minutes

c) 135%, Exposure = 1 minute

d) 175%, Exposure = 1 minute

Sample-to-film distance = 15 cm.

Figure 18: V_H light scattering patterns for PET stretched at 80C° at 300%/minute. Percent strains and Exposure times are listed below.

Pattern	% Strain	Exposure Time
a	40	2 min.
b	60	1 min.
c	80	11 min.
d	115	10 secs.
e	135	5 secs.
f	175	5 secs.

Sample-to-film distance = 15 cm.

Figure 19: V_H light scattering patterns for PET stretched at 80°C.

a) 175 %, Exposure = 5 secs.

b) 215%, Exposure = 10 secs.

c) 255%, Exposure = 10 secs.

d) 350%, Exposure = 1 minute

Sample-to-film distance = 15 cm.

Figure 20: V_V light scattering patterns for PET stretched at 80°C. Elongations correspond to those of Figure 18. Exposure time = 1/25 secs., same for all patterns. Sample-to-film distance = 15 cm.

Figure 21: H_H light scattering patterns for PET stretched at 80°C. Elongations correspond to those of Figure 18. Exposure time = 1/25 secs, same for all patterns. Sample-to-film distance = 15 cm.

Figure 22: Photomicrographs for PET stretched at 80°C between cross polars.

a) 80%

b) 135%

c) 175%

d) 350%

Figure 23: Wide angle X-ray diffraction patterns for PET stretched at 80°C

a) amorphous PET, 0%

b) 80%

c) 175%

d) 250%

e) 350%

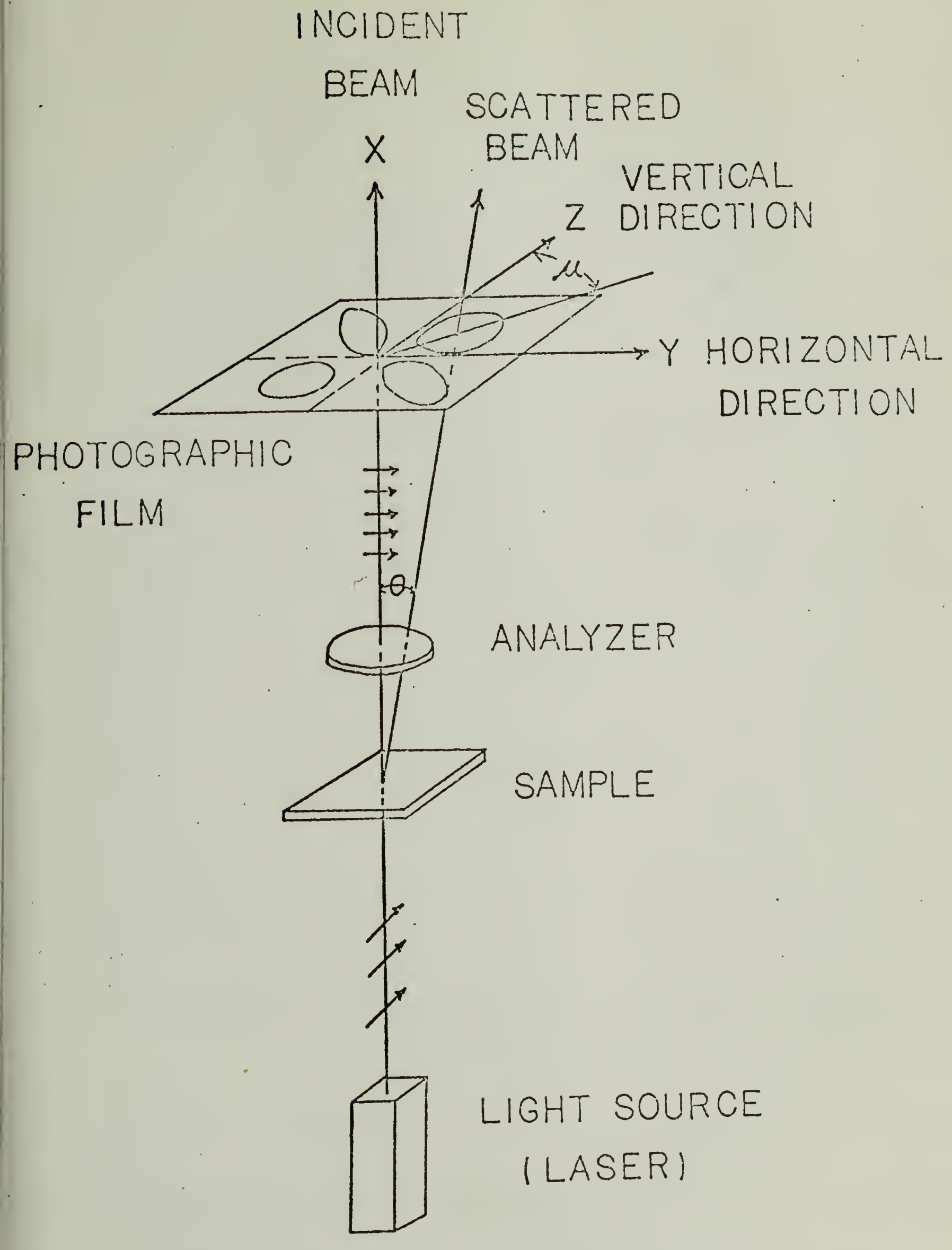
INCIDENT
BEAM
SCATTERED
BEAM
X
VERTICAL
Z DIRECTION
Y HORIZONTAL
DIRECTION
PHOTOGRAPHIC
FILM
ANALYZER
SAMPLE
LIGHT SOURCE
(LASER)

Figure 1

a. H_V

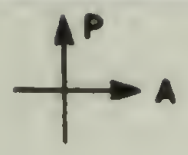

c. V_V

b. V_H

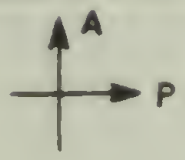

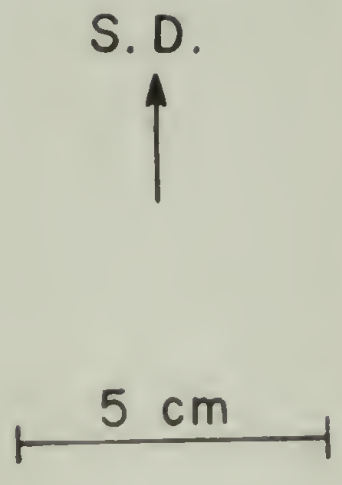

d. H_H

a. H_V

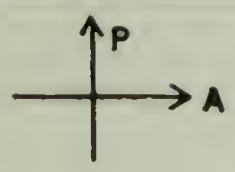

c. V_V

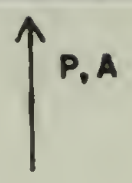

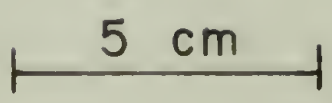

b. V_H

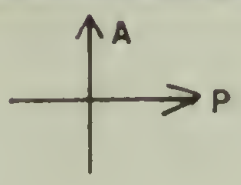

d. H_H

Figure 3

a. H_V

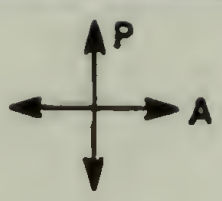

c. V_V

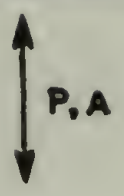

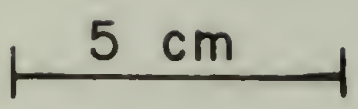

b. V_H

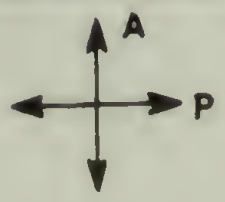

S.D.

d. H_H

Figure 4

a. H_V

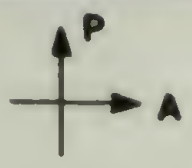

c. V_V

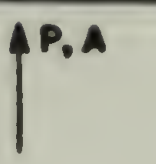

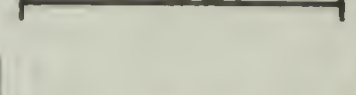

b. V_H

d. H_H

Figure 5

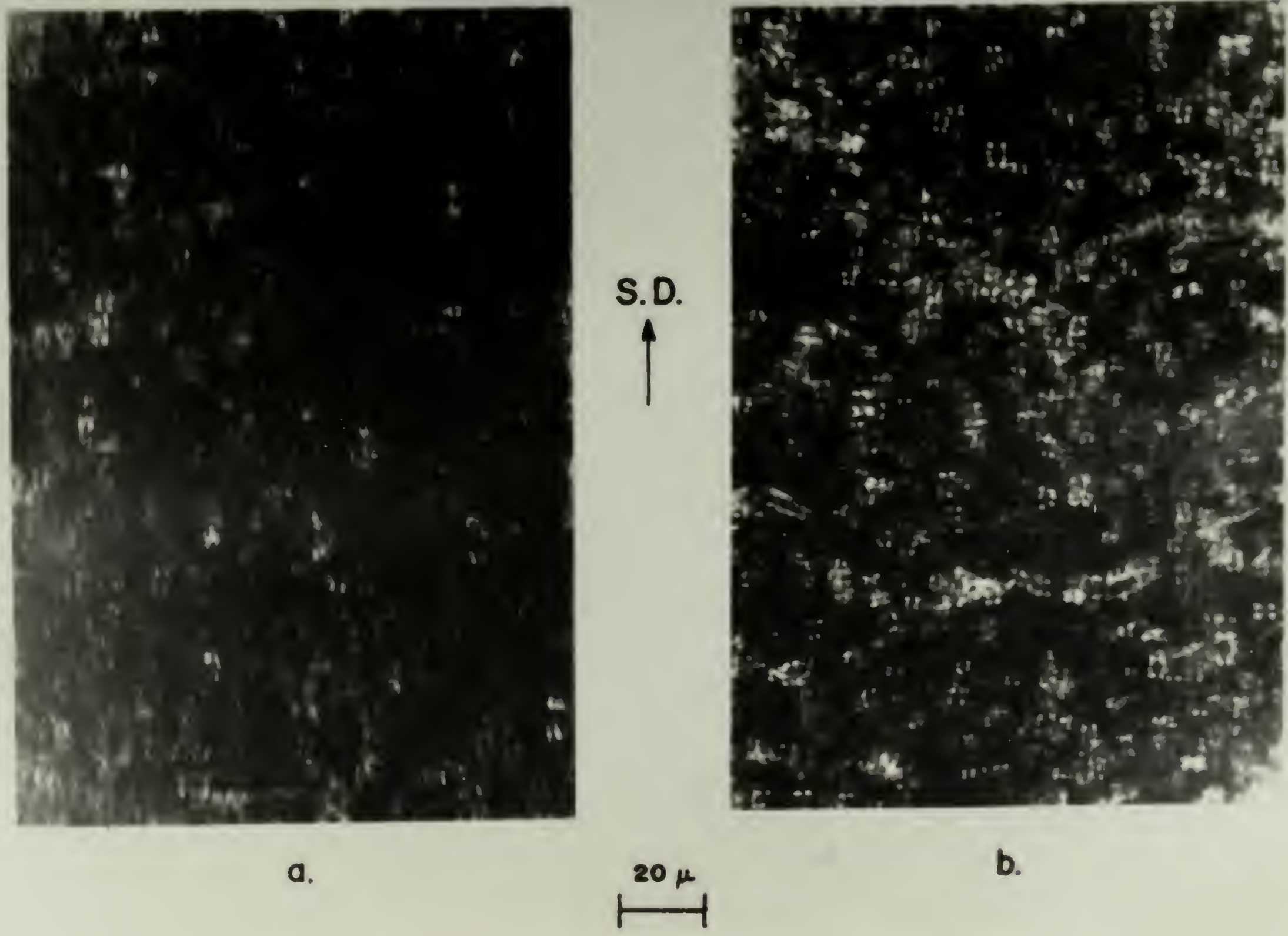

Figure 6

a.

S.D.

b.

c.

d.

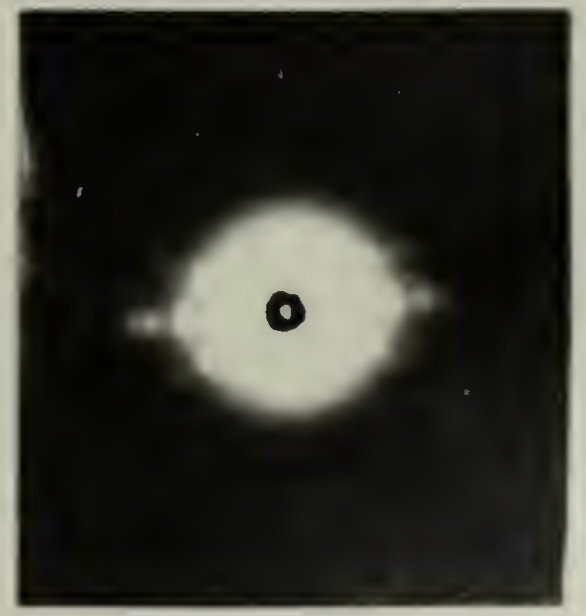

e.

Figure 7

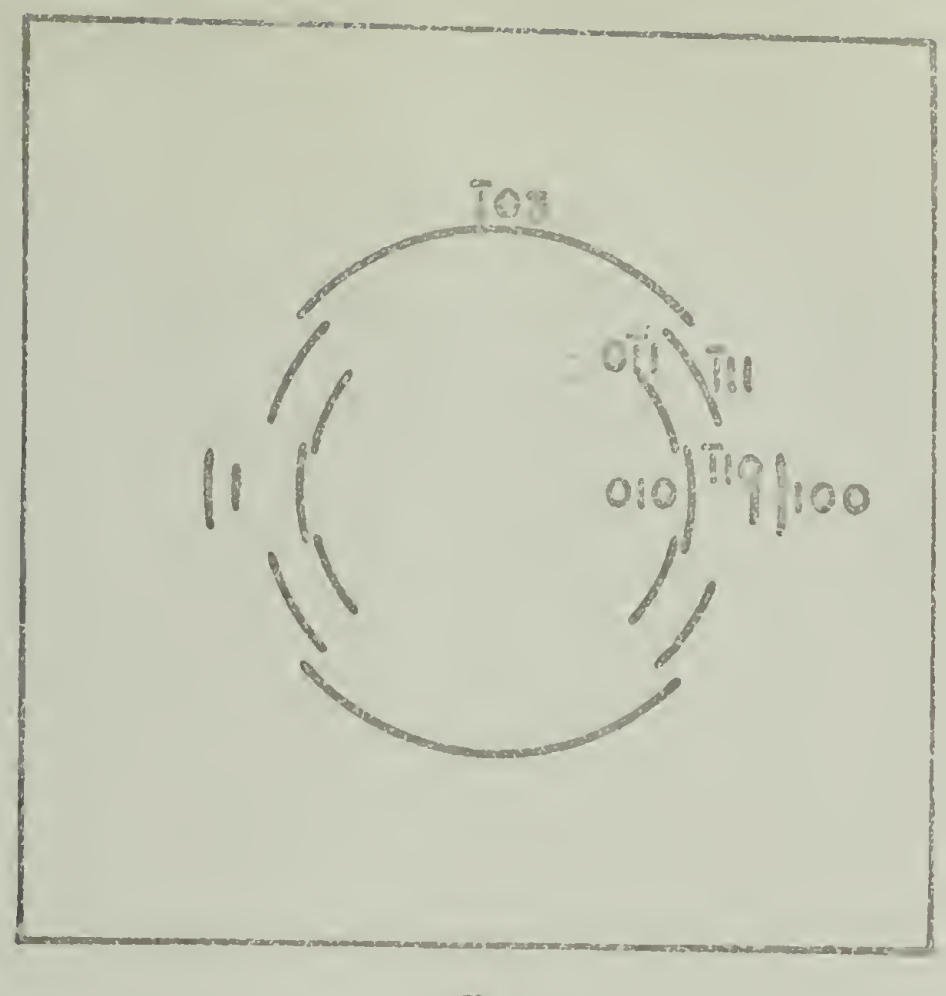

a

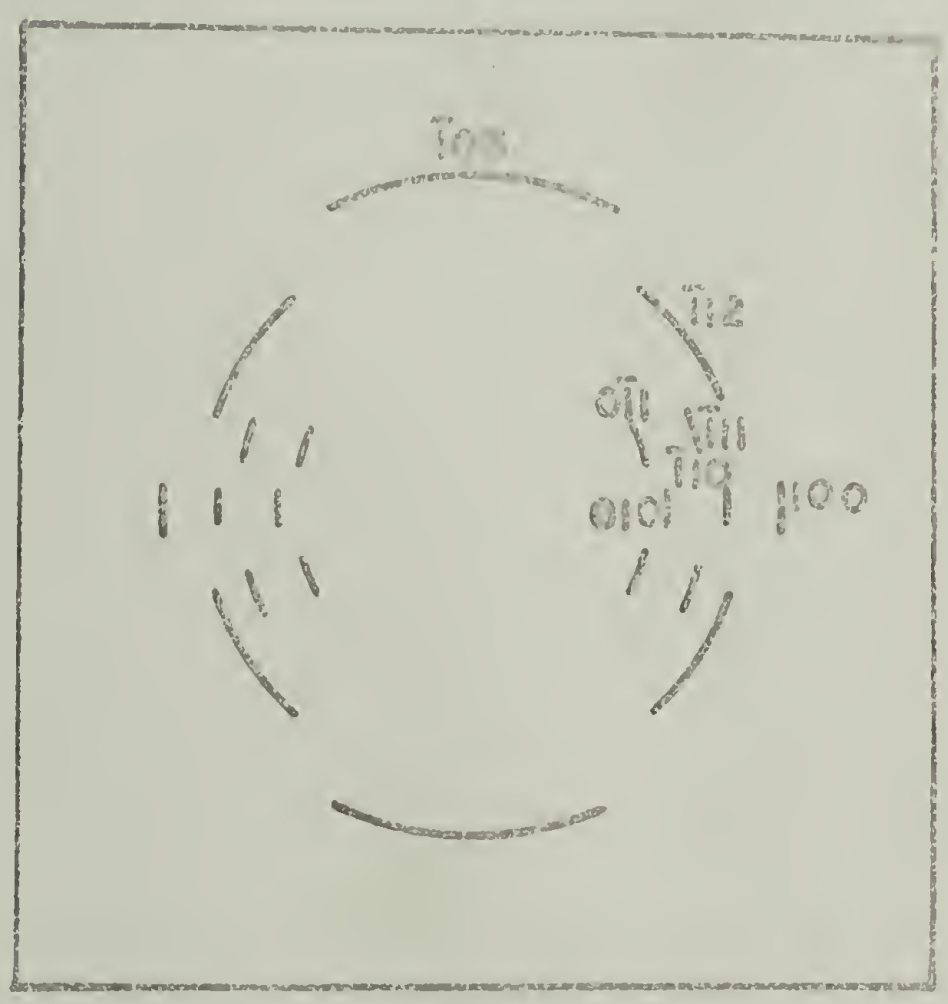

b

Figure 8

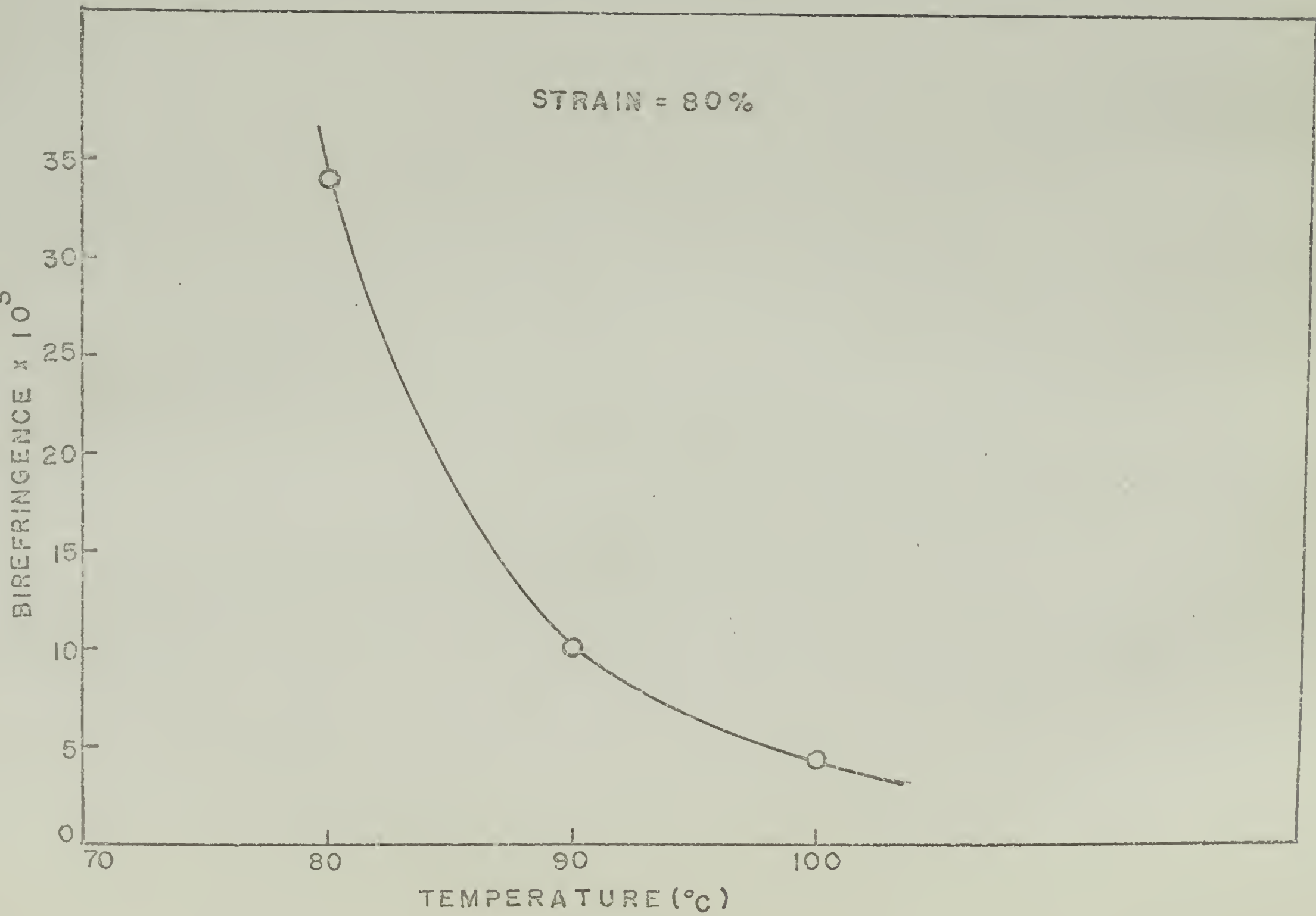
STRAIN = 80%
BIREFRINGENCE x 10^3
35
30
25
20
15
10
5
0
70
80
90
100
TEMPERATURE (°C)

Figure 9

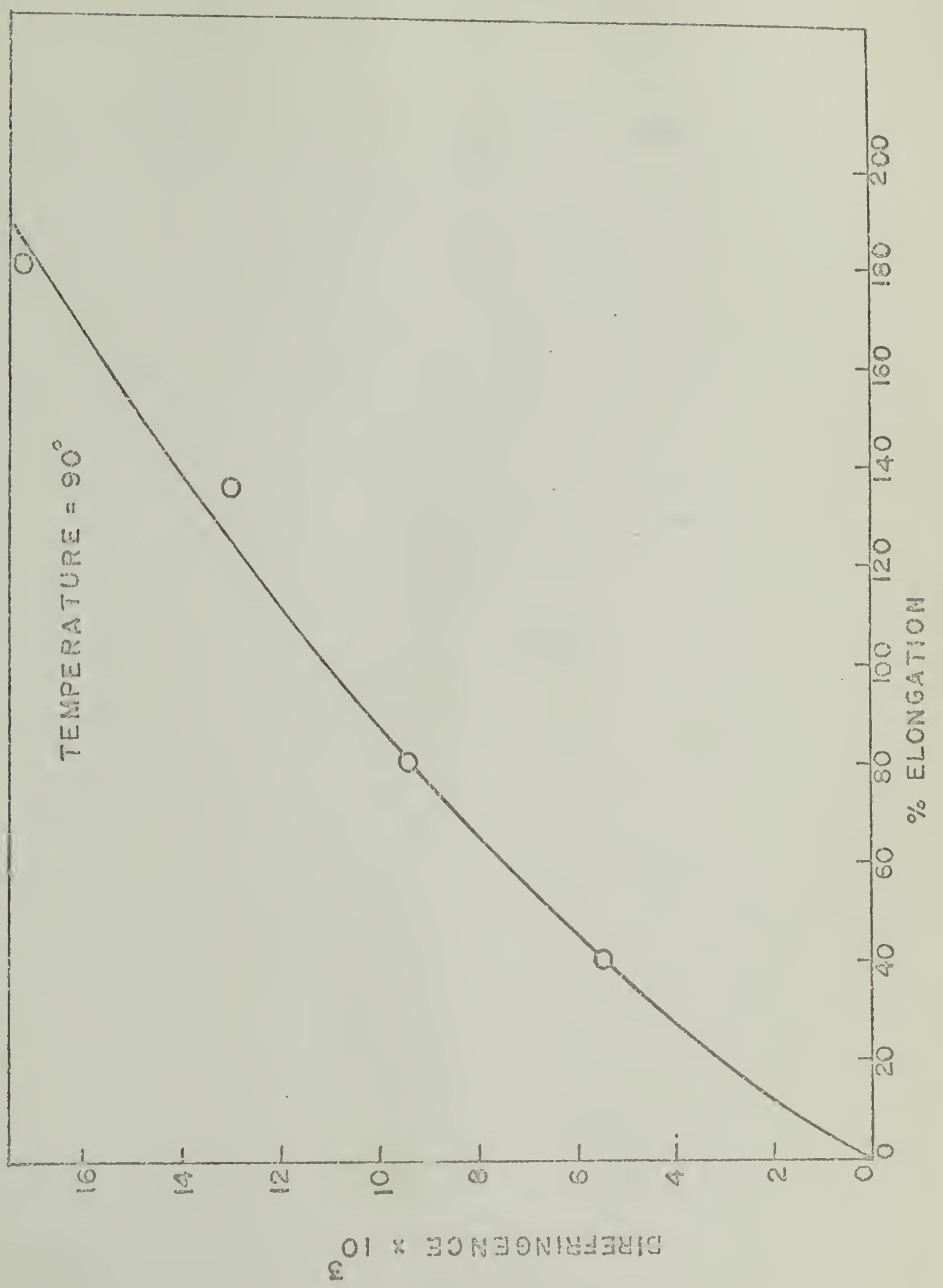
TEMPERATURE = 60°
BIREFRINGENCE x 10³
0
2
4
6
8
10
12
14
16
% ELONGATION
0
20
40
60
80
100
120
140
160
180
200

Figure 10

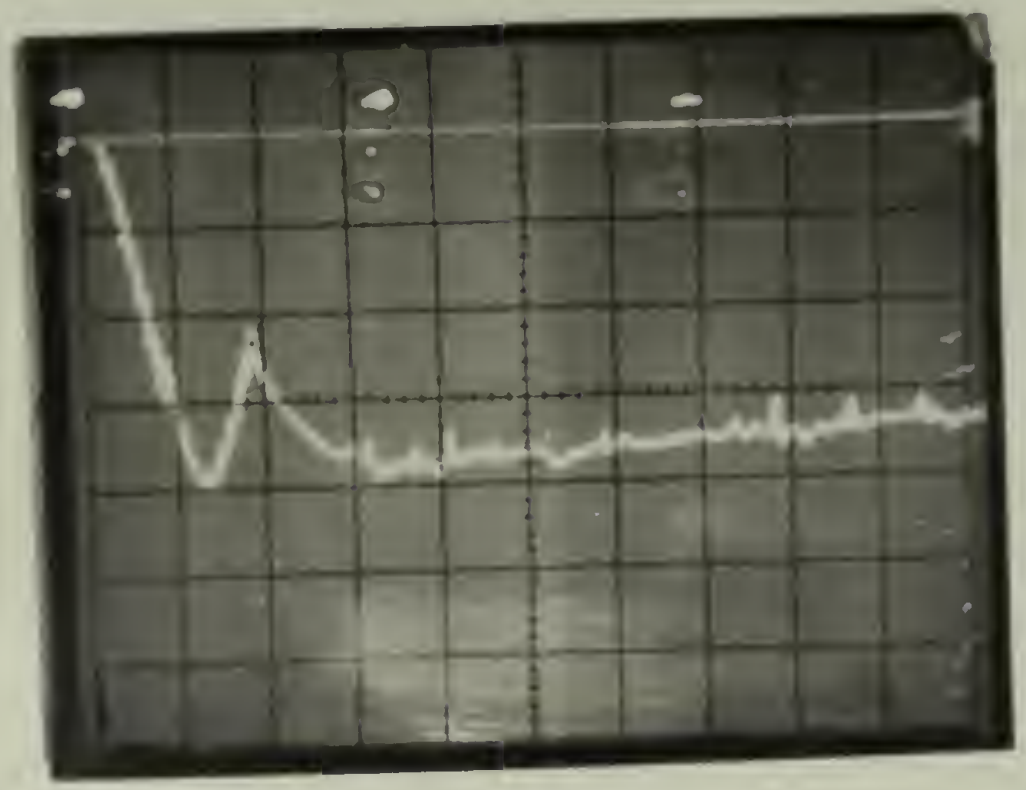

a. 0-50 secs.

b. 0-20 secs.

40% at 90°C

Figure 11

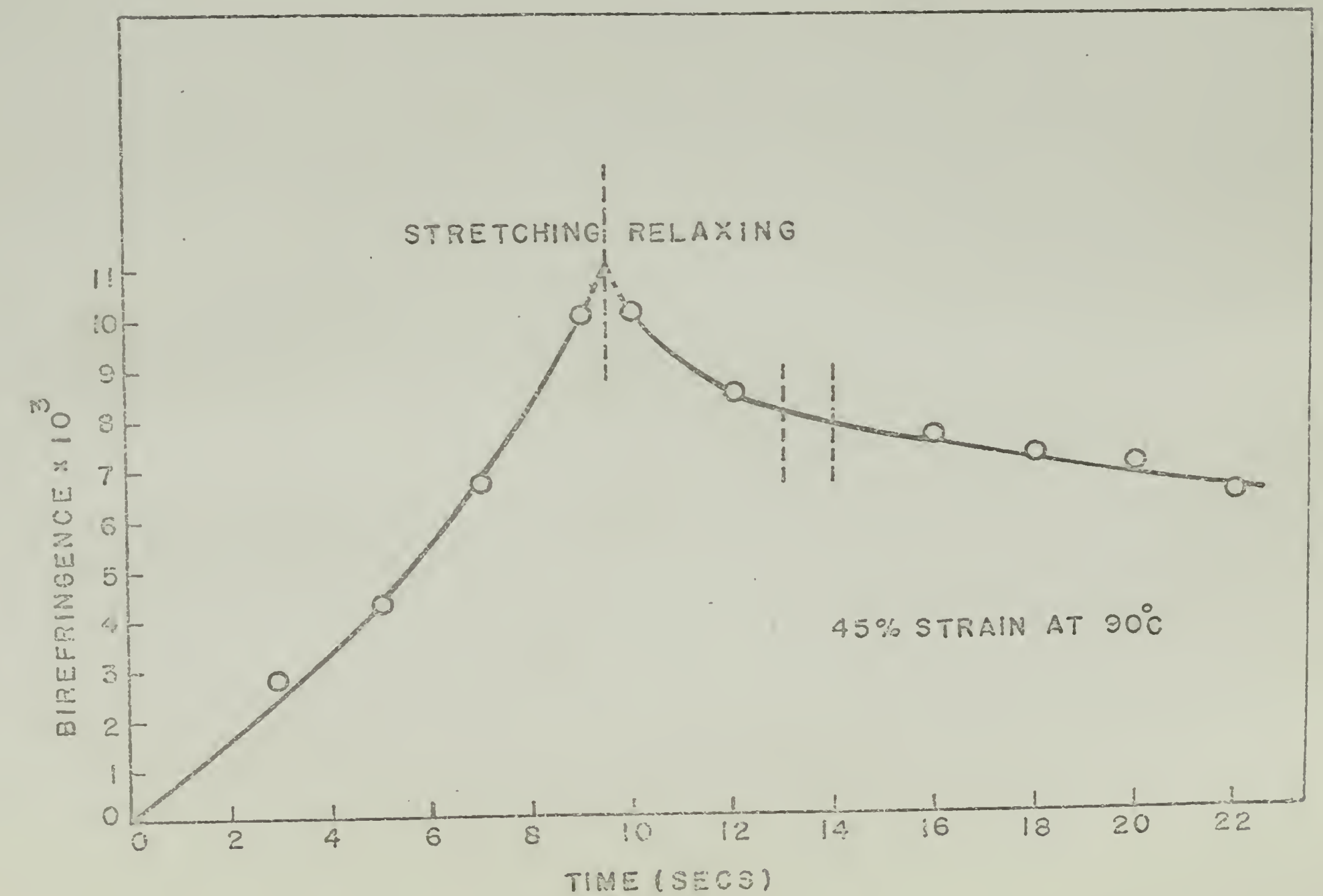
STRETCHING
RELAXING
BIREFRINGENCE × 10³
0
1
2
3
4
5
6
7
8
9
10
0
2
4
6
8
10
12
14
16
18
20
22
TIME (SECS)
45% STRAIN AT 90°C

Figure 12

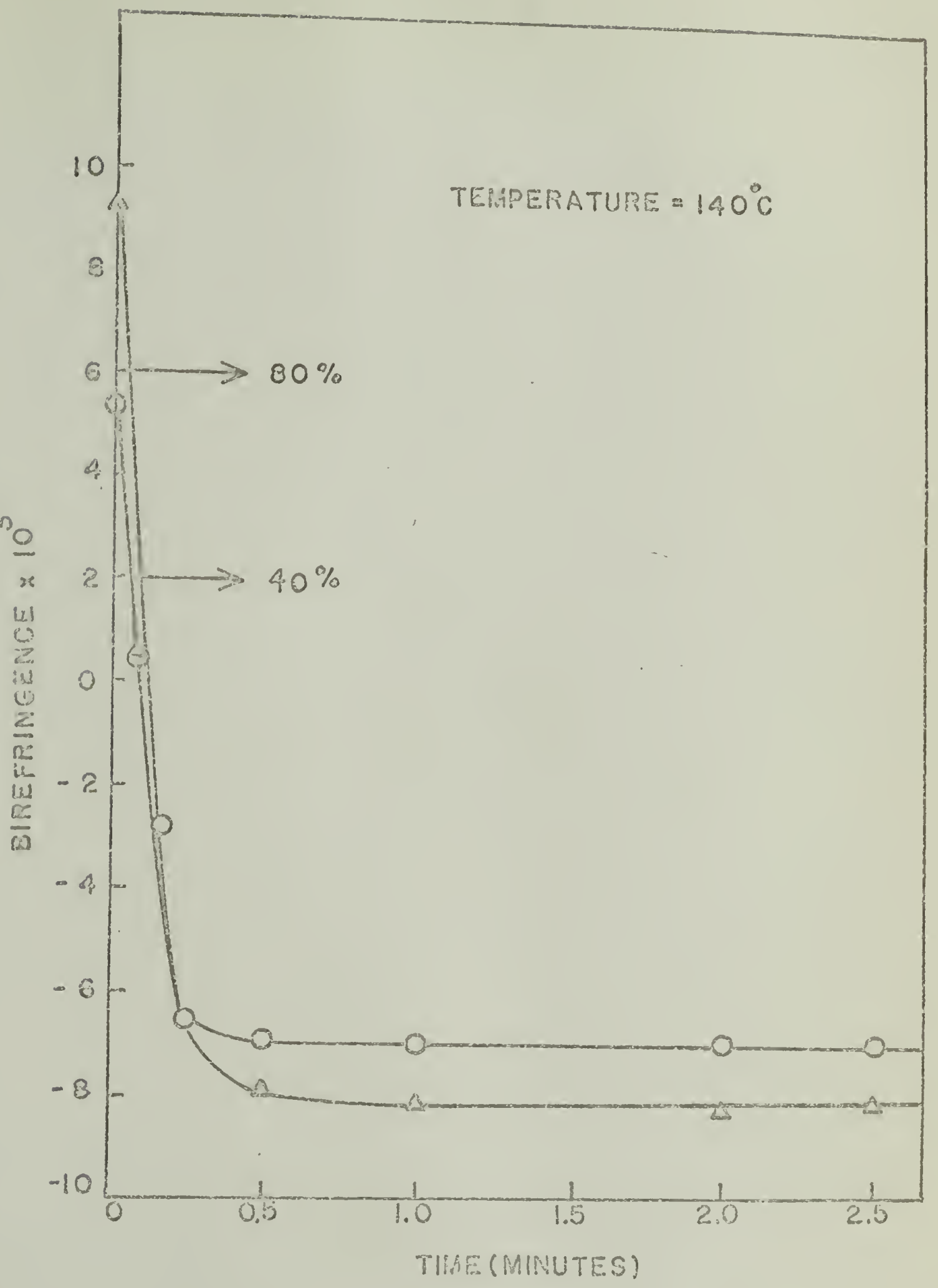
TEMPERATURE = 140°C
80%
40%
BIREFRINGENCE x 10³
10
8
6
4
2
0
-2
-4
-6
-8
-10
0
0.5
1.0
1.5
2.0
2.5
TIME (MINUTES)

Figure 13

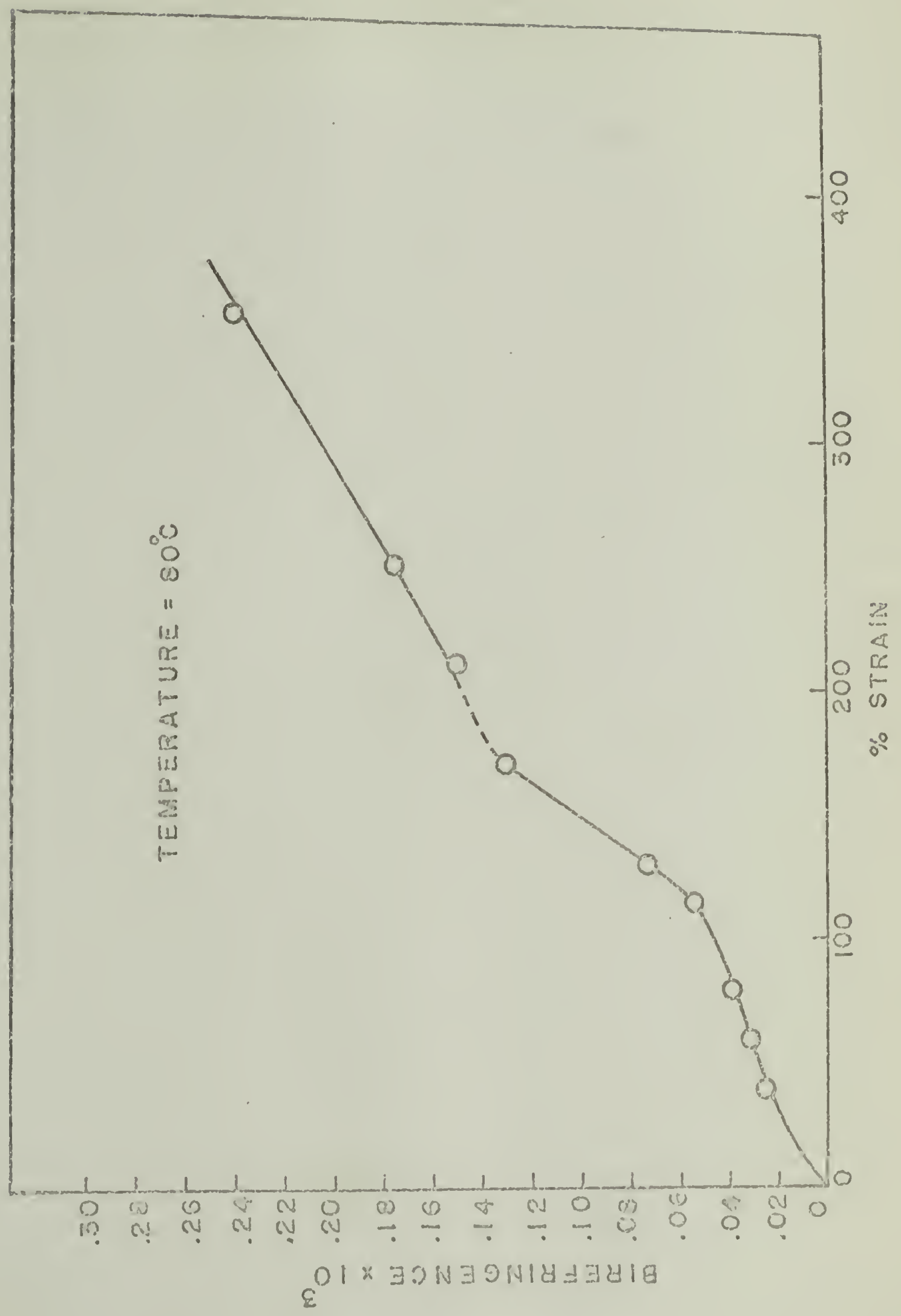
TEMPERATURE = 80°C
BIREFRINGENCE x 10³
.30
.28
.26
.24
.22
.20
.18
.16
.14
.12
.10
.08
.06
.04
.02
0
0
100
200
300
400
% STRAIN

Figure 14

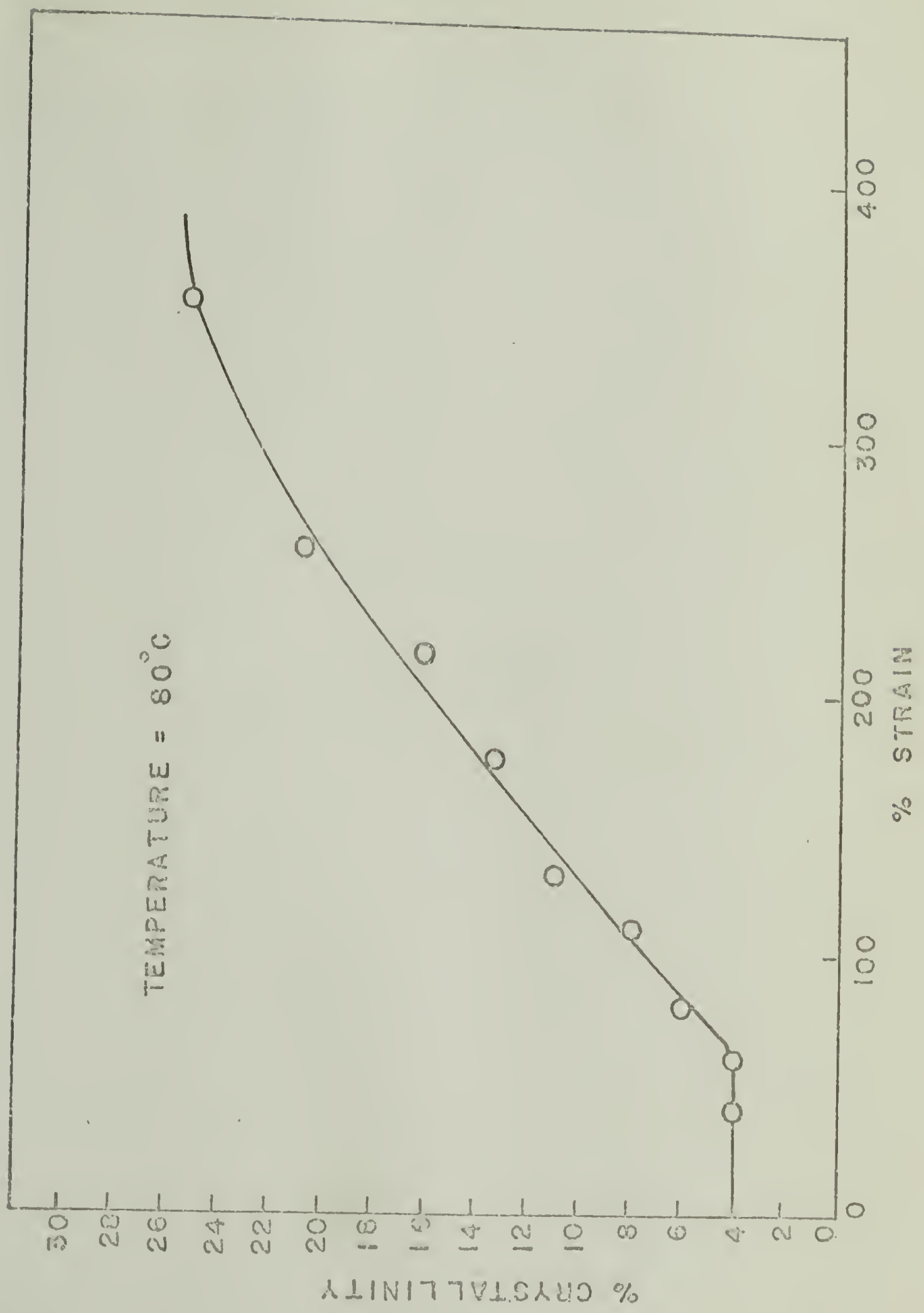
% CRYSTALLINITY
30
28
26
24
22
20
18
16
14
12
10
8
6
4
2
0
TEMPERATURE = 80°C
0
100
200
300
400
% STRAIN

Figure 15

80% STRAIN

a. 80°C

b. 90°C

c. 100°C

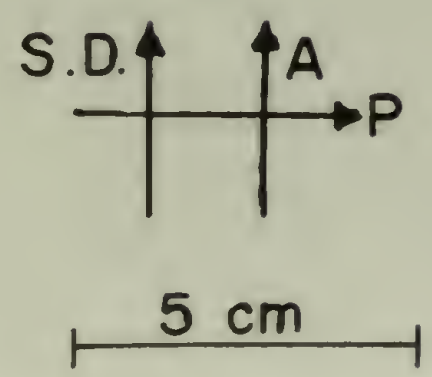

5 cm

Figure 16

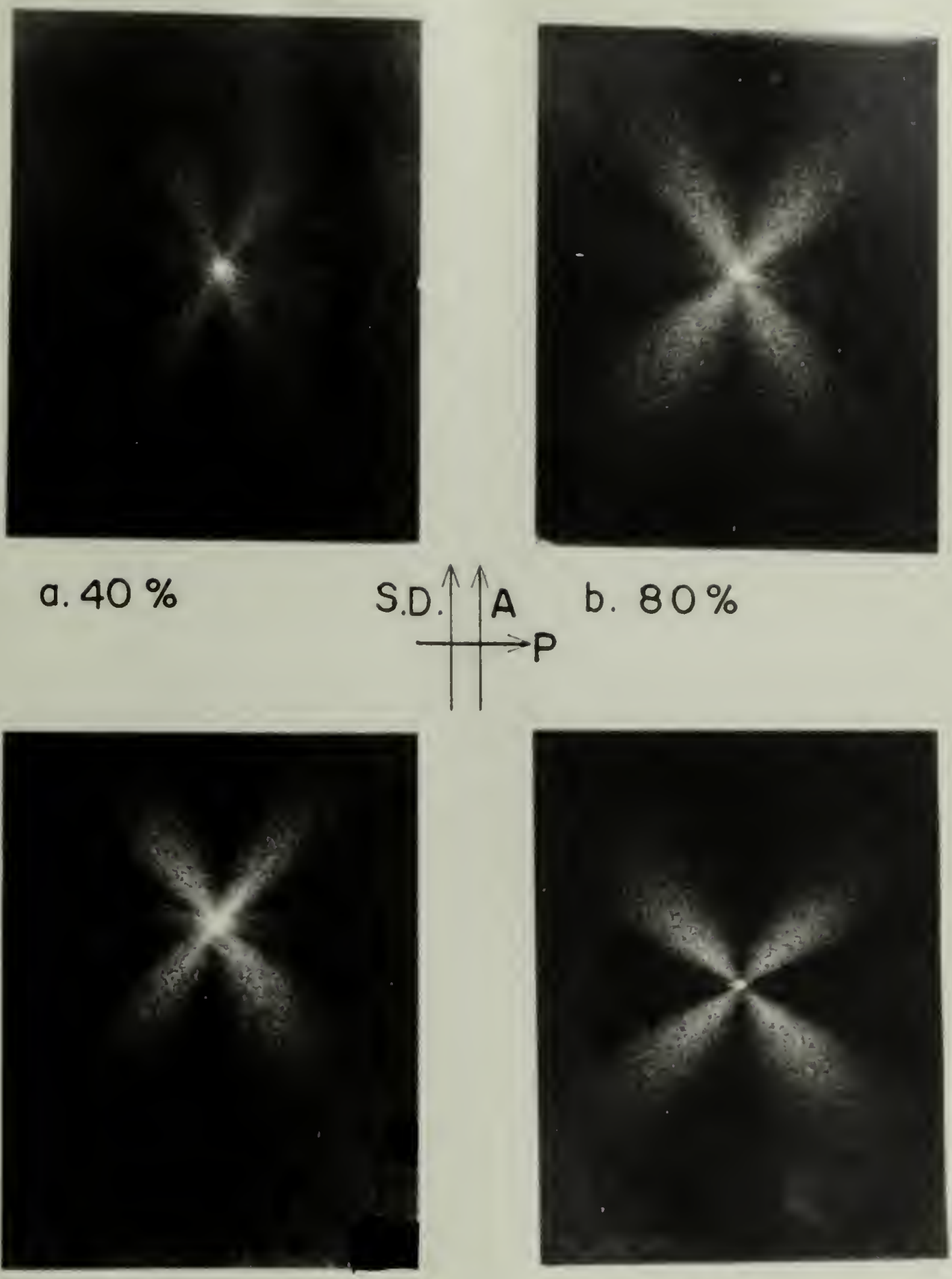

Figure 17

Figure 18

a. 175 %

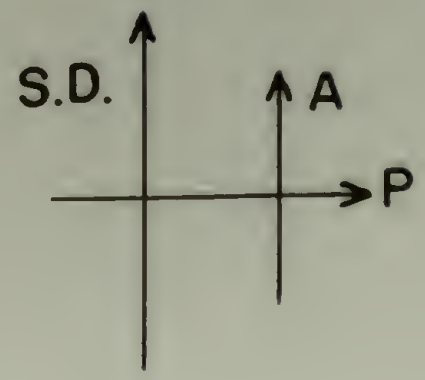

b. 215 %

5 cm

c. 255 %

d. 350%

Figure 19

Figure 20

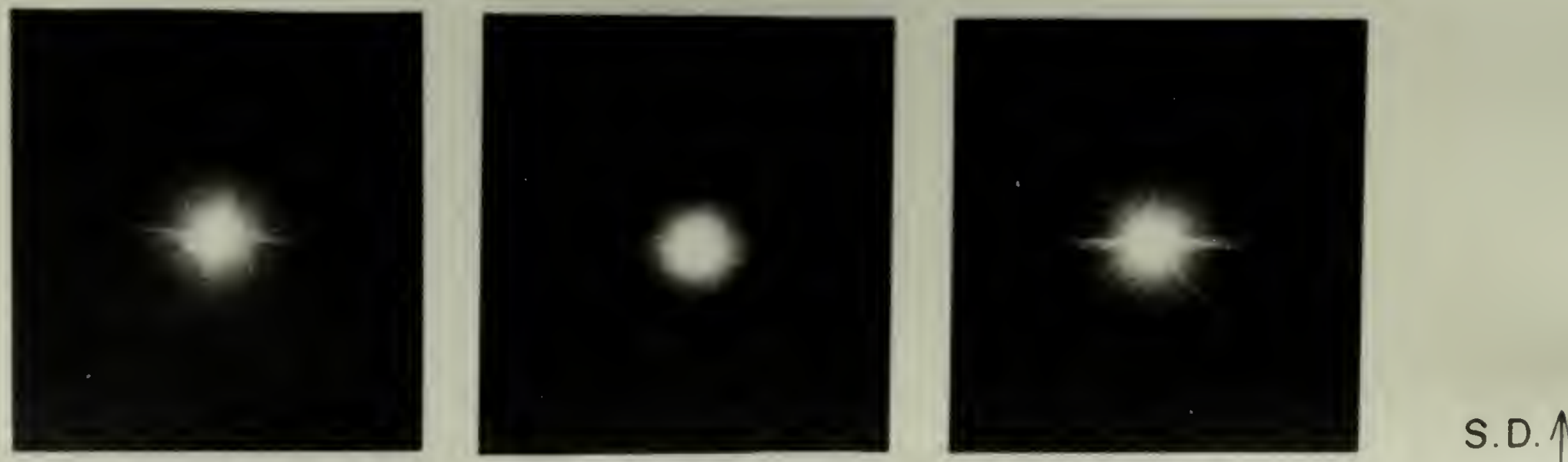

Figure 21

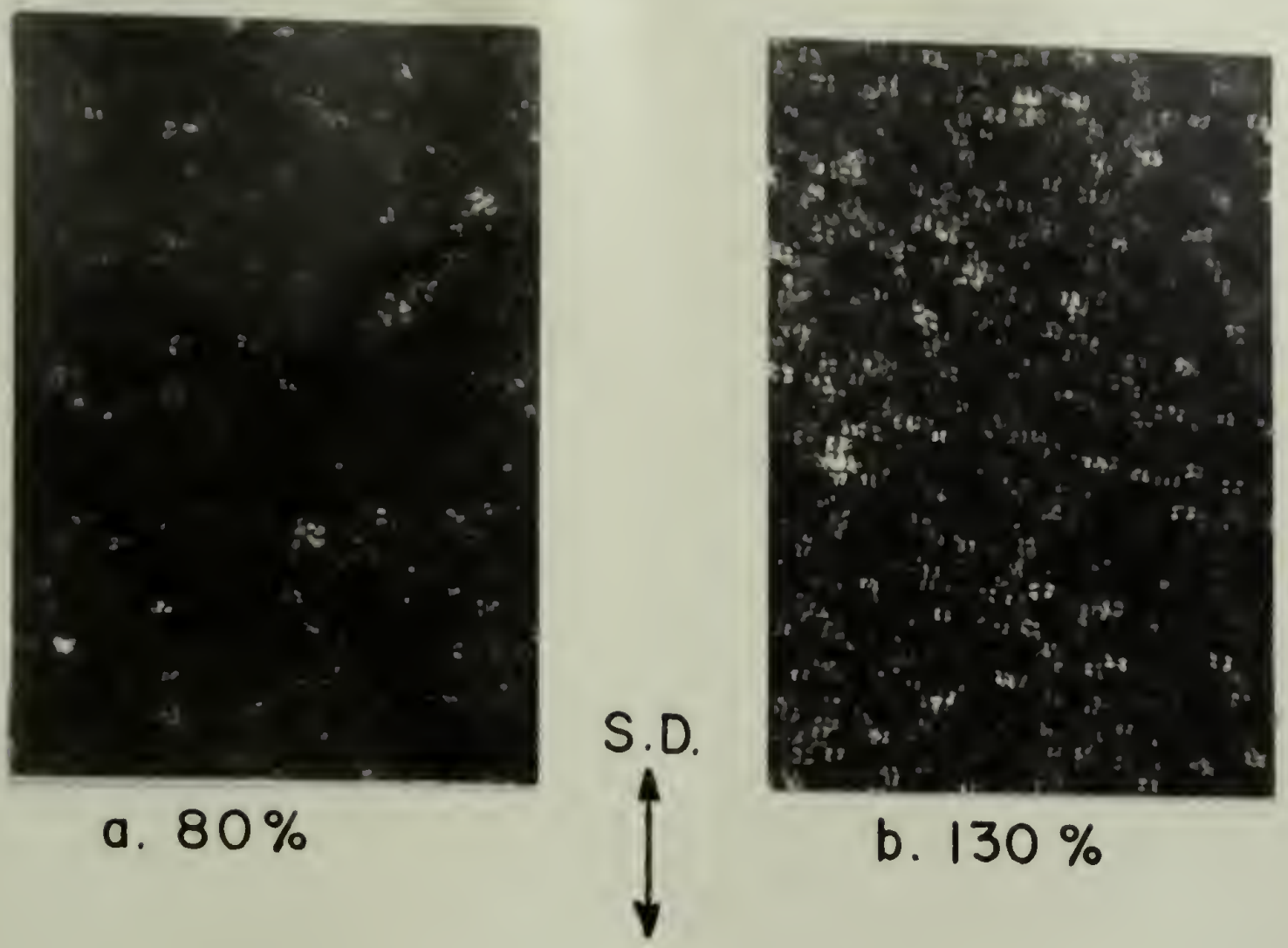

Figure 22

a. 0 %

S.D.

b. 80 %

c. 175 %

d. 255 %

e. 350 %

Figure 23

C H A P T E R V

LIGHT SCATTERING FROM "SHISH KEBABS"

Introduction

Crystallization in oriented polymers produces morphologies that are different than in unoriented polymers.[1,2] A fibrous structure has been observed by several workers[2-7] upon crystallization of polymers from stirred dilute solutions. This fibrous structure has been termed "shish kebabs" by Lindenmeyer[8] and consists of a string of platelets apparently connected by a central backbone.[1,2] The backbone fibril is postulated to be formed of highly extended polymer chains. The "kebabs" nucleate in a row along the backbone fibril (the shish) and grow in a direction perpendicular to it with a folded chain morphology. Andrews[9,10] studied the crystallization behavior of stretched natural rubber. He found that at the strains up to about 300 percent, row-like structures composed of fibrous needles oriented perpendicular to the stretching directions formed. These structures have striking similarity to the shish-kebab structure. Similar structures have been reported by Keller and Statton for polyethylene crystallized from the melt.[1,2,11]

Keller and Machin[1,2] have attempted to correlate the morphologies observed for polymers crystallized under stress ranging from stirred solutions to crosslinked rubbers. They conclude that when stress or flow is imposed on a crystallizing polymer melt or solution, some extended chain crystals or fibers are formed along lines parallel to the stress

or flow direction. These provide the nuclei from which lateral folded chain crystals grow. Due to closeness of nucleating centers along the extended chain fibrils, the growth of folded chain crystals is essentially limited to a direction normal to the former, i.e., in the direction normal to stress or flow.

In the present work a model is developed to calculate light scattering from shish kebabs. Interest for this came from the possibility of interpreting scattering patterns obtained from polyethylene terephthalate films that were stretched in their amorphous state.[12] A shish kebab is considered to be formed of preferentially oriented rods. Scattering from rod-like superstructure has been calculated previously.[13-15] Here the scattering from a shish-kebab is calculated by first summing up the scattering amplitudes from individual rods and then integrating the resultant to obtain intensities in a manner similar to that employed for scattering from a spherulite composed of preferentially oriented rods.[16]

Model for a "Shish Kebab"

A shish-kebab is known to consist of a string of platelets connected by a long central rod acting as the backbone, with an extended chain morphology in the central rod and a folded chain morphology in the kebabs.[1,2] For the purpose of the calculation of light scattering the shish kebab is represented by a simplified two-dimensional model, a schematic diagram of which is shown in Figure 1a. It consists of a central backbone rod with kebabs lying perpendicular to it. The kebabs extend equally on each side of the backbone rod. It is assumed that the kebabs are separated by an average distance equal to their width.

This means that the number of kebabs is about half of the maximum number that could fit along the backbone.

Let, Length of the backbone rod = L_1

Width of the backbone rod = H_1

Length of the kebabs = L_2

Width of the kebabs = H_2

Angle the axis of the backbone makes with the z axis = α

Angle the axes of the kebabs make with the z axis = $\alpha + 90°$

Polarizability direction of the backbone rod is along its length, $\omega_1 = 0°$

Polarizability direction of the kebabs is perpendicular to their lengths,

$\omega_2 = 90°$

Amplitude of scattering for a system made up of m rods is given as:

$$E = \sum E_m$$

$$= E_1 + \sum E_{2,n}$$

where E_1 = scattering amplitude from the backbone rod.

$\sum E_{2,n}$ = Sum of scattering amplitude from the kebabs.

H_V scattering amplitude from the backbone rod:[13]

$$E_{H_V 1} = (\alpha_1 - \alpha_2)\, \rho \sin(\alpha + \omega_1) \cos(\alpha + \omega_1) \cdot \frac{\sin(Ka_1 L_{1/2})}{Ka_1 L_{1/2}} \cdot \frac{\sin(b_1 H_{1/2})}{Kb_1 H_{1/2}} \qquad (1)$$

where $K = 2\pi/\lambda$

λ = wavelength of light in the medium

$a_1 = -\sin\theta \sin(\alpha + \Omega)$

$b_1 = -\sin\theta \cos(\alpha + \Omega)$

H_V scattering amplitude from the kebabs: Differential of scattering amplitude for a kebab "n" at a distance $\underset{\sim}{P}_n$ from the center of the shish kebab 0, as shown in Figure 1b, is given as:

$$dE_{H_V 2,n} = \rho_n e^{iK(\underset{\sim}{r} \cdot \underset{\sim}{s})} \cdot dl \cdot dh = e^{iK(\underset{\sim}{P}_n \cdot \underset{\sim}{s})} e^{iK(\underset{\sim}{r}_n \cdot \underset{\sim}{s})} \cdot dl \cdot dh \qquad (2)$$

where $\underset{\sim}{s}$ = propagation vector

$= \underset{\sim}{s}_o - \underset{\sim}{s}'$

$\underset{\sim}{s}_o$ = incident beam vector

$\underset{\sim}{s}'$ = scattered beam vector

$r = \underset{\sim}{P}_n + \underset{\sim}{r}_n$

$$\rho_n = \rho(\alpha_1 - \alpha_2) \sin\alpha' \cos\alpha'$$

$$\alpha' = (90° + \alpha + \omega_2)$$

Integrating equation (2),

$$E_{H_V 2,n} = \rho_n e^{iK(\underset{\sim}{P}_n \cdot \underset{\sim}{s})} \int_l \int_h e^{IK(\underset{\sim}{r}_n \cdot \underset{\sim}{s})} \cdot dl \cdot dh \qquad (3)$$

Limits of integration are:

$l = -L_{2/2}$ to $-H_{1/2}$, and $H_{1/2}$ to $L_{2/2}$

$h = -H_{2/2}$ to $H_{2/2}$

Let, Int = $$\int_l \int_h e^{iK(\underset{\sim}{r}_n \cdot \underset{\sim}{s})} \cdot dl \cdot dh \qquad (4)$$

Now $\underset{\sim}{s}$, $\underset{\sim}{r}$, $\underset{\sim}{l}$, and $\underset{\sim}{d}$ respectively can be written as:

$$\underset{\sim}{s} = (1 - \cos\theta)\ \underset{\sim}{i} - (\sin\theta\cos\Omega)\ \underset{\sim}{j} - (\sin\theta\sin\Omega)\ \underset{\sim}{k}$$

$$\underset{\sim}{r} = \underset{\sim}{l} + \underset{\sim}{h}$$

$$\underset{\sim}{l} = l\ (-\cos\alpha \cdot \underset{\sim}{j} + \sin\alpha \cdot \underset{\sim}{k})$$

$$\underset{\sim}{d} = h\ (\sin\alpha \cdot \underset{\sim}{j} + \cos\alpha \cdot \underset{\sim}{k})$$

$$\therefore \underset{\sim}{r} \cdot \underset{\sim}{s} = -\sin\theta \cos\Omega(-l \cos\alpha + h \sin\alpha)$$

$$-\sin\theta \cdot \sin\Omega(l \sin\alpha + h \cos\alpha)$$

$$= -\sin\theta \sin(\alpha + \Omega)\ l - \sin\theta \cos(\alpha + \Omega)\ h$$

$$= a_2\ l + b_2\ h$$

Substituting these values in Equation (4),

$$\text{Int} = \int e^{iK\,(a_2 l + b_2 h)} \cdot dl\, dh$$

$$= \int_{-H_{2/2}}^{H_{2/2}} e^{iKb_2 h} \cdot dh \left[\int_{-L_{2/2}}^{-H_{1/2}} e^{iKa_2 l} \cdot dl + \int_{-H_{1/2}}^{L_{2/2}} e^{iKa_2 l} \cdot dl \right]$$

$$= \frac{2 \sin(Kb_2 H_{2/2})}{Kb_2} \cdot \frac{2[\sin(Ka_2 L_{2/2}) - \sin(Ka_2 H_{1/2})]}{Ka_a} \qquad (5)$$

Evaluation of $e^{iK\,(\underset{\sim}{P}_n \cdot \underset{\sim}{s})}$

$$\underset{\sim}{P}_n = P_n\,(\sin\alpha\ \underset{\sim}{j} + \cos\alpha \cdot \underset{\sim}{k})$$

$$\therefore \underset{\sim}{P}_n \cdot \underset{\sim}{s} = -P_n \sin\theta \cdot \sin(\alpha + \Omega)$$

$$\text{Real}\left[e^{iK\,(\underset{\sim}{P}_n \cdot s)}\right] = \cos\left[KP_n \sin\theta \sin(\alpha + \Omega)\right] \qquad (6)$$

Substituting the results of equations (5) and (6) in equation (3):

$$E_{H_V 2,n} = \rho\ (\alpha_1 - \alpha_2) \sin(\alpha + \omega_2 + 90) \cdot \cos(\alpha + \omega_2 + 90)$$

$$\times \frac{4 \sin(Kb_2 H_{2/2})}{Kb_2} \cdot \frac{[\sin(Ka_2 L_{2/2}) - \sin(K a_2 H_{1/2})]}{Ka_2} \qquad (7)$$

$$\times \cos\left[K P_n \sin\theta \sin(\alpha + \Omega)\right]$$

$$= \rho(\alpha_1 - \alpha_2)\, F_2(\alpha) \cdot \cos [K P_n \sin\theta \sin(\alpha + \Omega) \qquad (8)$$

If the kebabs are placed randomly along the central rod then the total scattering from all kebabs is given as:

$$E_{2H_{V_2}} = \sum E_{H_V 2,n}$$

$$= \rho(\alpha_1 - \alpha_2)\, F_2(\alpha) \sum_{n=\delta} \cos [K \sin\theta \sin(\alpha + \Omega) \cdot P_n]$$

This summation is done using the computer. First the value of n is chosen, then n random numbers are generated. These correspond to the centers of kebabs. A restriction is imposed such that the centers cannot be closer than H_2, the width of the kebabs.

Now the total scattering amplitudes from the shish kebab is

$$E_{H_V} = E_{H_{V1}} + E_{H_{V2}}$$

The shish kebabs are considered to be oriented preferentially in the direction of stress, the scattering intensity from which is given as:

$$I_{H_V} = \int_0^{\pi} N(\alpha)\, E_{H_V}^2 \cdot d\alpha$$

where, $N(\alpha)$ = orientation distribution function.[13]

$$= N_o (E^2 \sin^2\alpha + E^{-2} \cos^2\alpha)^{-1/2}$$

I_{H_V} is integrated numerically on the computer by using Simpson's rule.

A special case is when the "kebabs" are evenly spaced along the central rod. The distribution of the kebabs is then approximated by the function below:

$$f(p) = f_1 \left[1 + \sin \frac{2\pi P}{d}\right]$$

where f_1 = constant

d = inter-rod distance

$E_{H_{V2}}$ can be approximated as:

$$E_{H_{V2}} = \int_{-L_{1/2}}^{L_{1/2}} E_{H_V 2,n} \cdot dp$$

$$= (\alpha_1 - \alpha_2) F_2(\alpha) \int_{-L_{1/2}}^{L_{1/2}} f(P) \cos[K\, Pn \sin\theta \sin(\alpha+\Omega)]\, dp$$

$$= (\alpha_1 - \alpha_2) F_2(\alpha) \int_{-L_{1/2}}^{L_{1/2}} f_1 \left[1 + \sin \frac{2\pi P}{d}\right] \cos (K_1 P_n)\, dp$$

where:

$$K_1 = K \sin\theta \sin(\alpha + \Omega)$$

$$\therefore E_{H_V 2} = (\alpha_1 - \alpha_2) F_2(\alpha) \quad f_1 \left(\frac{2 \sin \frac{L_1 K \sin\theta \sin(\alpha+\Omega)}{2}}{K \sin\theta \sin(\alpha+\Omega)} \right)$$

However, it is highly unlikely that the kebabs would be arranged so evenly.

RESULTS AND DISCUSSION

For calculating light scattering patterns from shish kebabs, the dimensions for the backbone and the kebabs were chosen on the basis of observations of Keller[2] and Andrews.[9,10] The backbone fibril was considered to be 2 μm (or 20,000 Å) long and .02 μm (200 Å) wide. A total of 40 kebabs of length .2 μm (2000 Å) and width .02 μm (200 Å) were considered to lie with their centers along the backbone such that 20 kebabs were on either side of the center of the fibril. The placements of the kebabs was either random with a minimum distance of .02 μm between their centers or uniform with a sinusoidal distribution function.[16]

For providing a basis for comparison, H_V patterns were first calculated from unoriented and oriented rods and are presented in Figures 2a and 2b respectively. H_V patterns from oriented shish kebabs with random and regular placements of kebabs are presented in Figures 3a and 3b respectively.

A value of E = 4.0 was used for determining the orientation distribution function, $N(\alpha)$, in the oriented cases.

Comparing patterns of Figure 3 with pattern in Figure 2b it is seen that the shape and orientation of the patterns from oriented shish kebabs and oriented rods is quite similar. The intensity for the shish kebab is higher because of larger scattering area. Thus it is concluded that H_V scattering does not distinguish between patterns from rods and shish kebabs for the dimensions chosen for the present calculation. It may be mentioned that the scattering from shish kebabs deviated from rod-like patterns if kebabs were assumed to be considerably longer (1-3 μm).

However at the present time there is no basis for considering kebabs to be that long hence no patterns from such a case are presented.

The patterns calculated here were not found helpful in explaining scattering results from oriented polyethylene terephthalate films. The calculation are presented here and may prove helpful in explaining results from some other system such as stretched natural rubber.[9,10]

REFERENCES

1. A. Keller, "Polymer Crystals", Reports on Progress in Physics, 31 (2), 623 (1968).
2. A. Keller and M. J. Machin, J. Macromol. Sci., B, 1, 41 (1967).
3. A. Keller, Kolloid Z. Polymere, 165, 15 (1959).
4. A. J. Pennings and A. M. Kiel, Kolloid-A. Polymere, 205, 160 (1965).
5. A. J. Pennings, J. M. A. A. vander Mark, and H. L. Booij, Kolloid Z. Polymere, 236, 99 (1970).
6. H. D. Keith, F. J. Padden, and R. G. Vadimsky, J. Appl. Phys., 37, 4027 (1966).
7. J. Kawai, T. Matsumoto, M. Kato and H. Maeda, Kolloid Z. Polymere, 222, 1 (1968).
8. P. H. Lindenmeyer, S. P. E. Trans., 4, 1 (1964).
9. E. H. Andrews, Proc. Roy. Soc. (London), A 277, 562 (1964).
10. E. H. Andrews, J. Polymer Sci., A-2, 4, 668 (1966).
11. W. O. Statton, J. Polymer Sci., C, 20, 117 (1967).
12. Chapter 4, this dissertation.
13. M. B. Rhodes and R. S. Stein, J. Polymer Sci., A-2, 7, 1539 (1969).
14. Y. Murakami, N. Hayashi, T. Hashimoto and H. Kawai, Polymer J., 4, 452 (1973).
15. N. Hayashi, Y. Murakami, M. Moritini, T. Hashimoto and H. Kawai, Polymer J., 4, 560 (1973).
16. R. E. Prud'homme, D. Yoon and R. S. Stein, J. Polymer Sci., A-2, 11, 1047 (1973).

CAPTIONS FOR FIGURES

Figure 1: (a) Model of a shish kebab composed of rods.

(b) Definition of vector $\underset{\sim}{P}_n$, $\underset{\sim}{r}_n$ and $\underset{\sim}{r}$ for the kebabs

Figure 2: (a) H_V scattering pattern from randomly oriented rods.

(b) H_V scattering pattern from rods oriented preferentially along the z axis with E = 4.0.

Figure 3: (a) H_V scattering pattern from shish kebab oriented preferentially along the z axis with E = 4.0. $L_1 = 2\mu$, $H_1 = .02\mu$, $L_2 = .2\mu$, $H_2 = .02\mu$, 40 kebabs randomly placed.

(b) H_V scattering pattern from shish kebabs oriented preferentially along the z axis with E = 4.0. $L_1 = 2\mu$, $H_1 = .02\mu$, $L_2 = .2\mu$, $H_2 = .02\mu$, 40 kebabs placed uniformly.

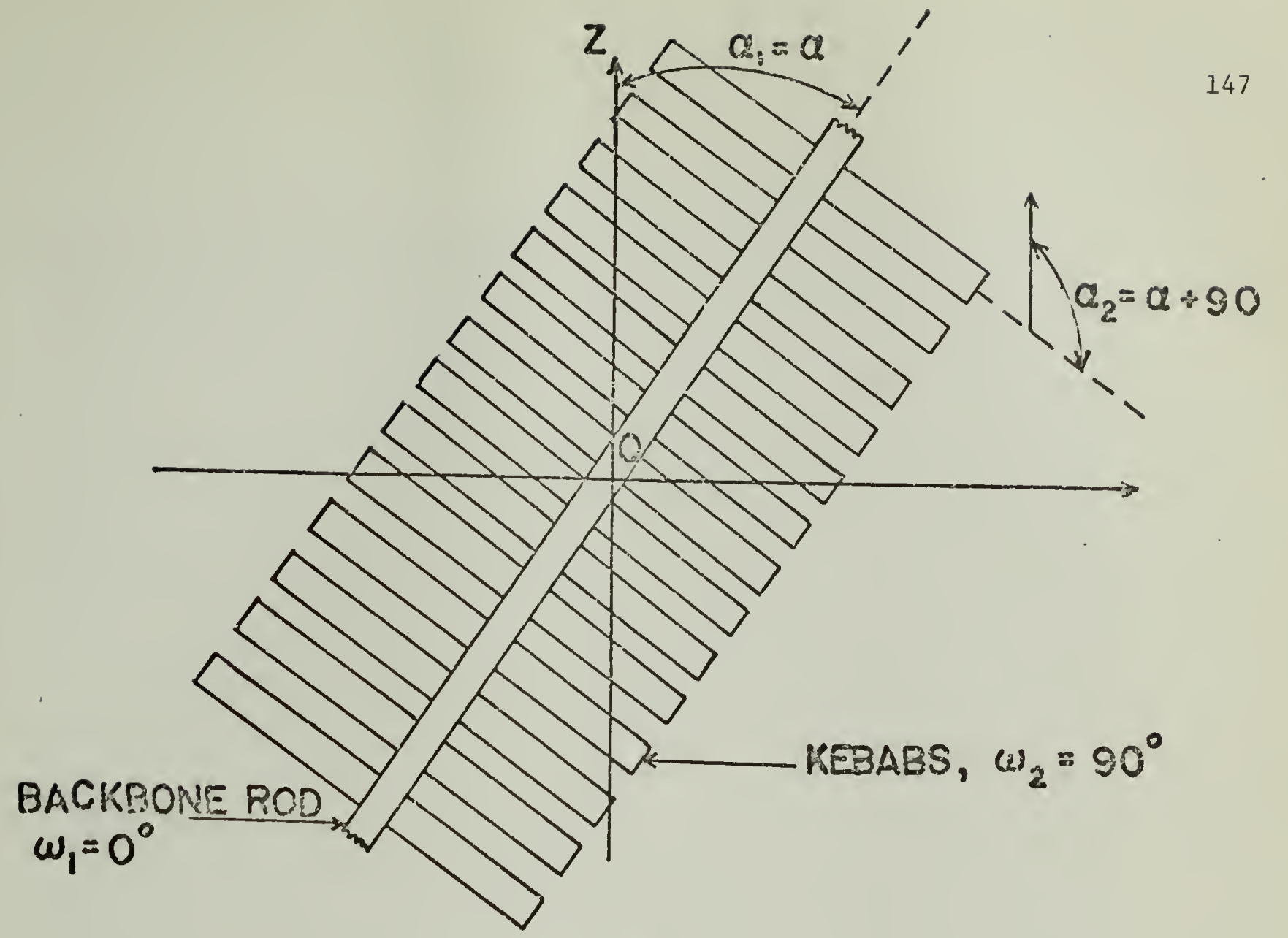
Z
$\alpha_1 = \alpha$
$\alpha_2 = \alpha + 90$
O
KEBABS, $\omega_2 = 90°$
BACKBONE ROD
$\omega_1 = 0°$

a

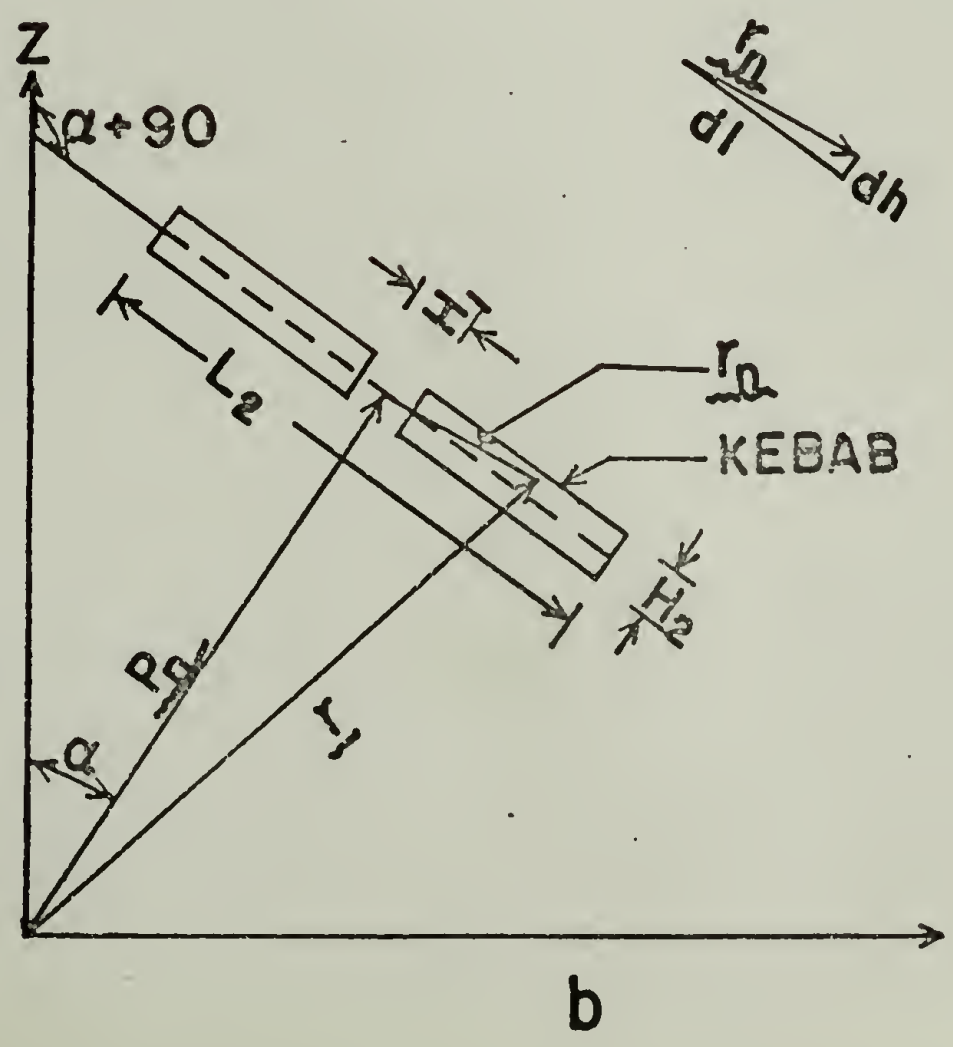
Z
$\alpha + 90$
r_n
dl
dh
L_2
H_2
r_n
KEBAB
ρ_n
r_1
α

b

Figure 1

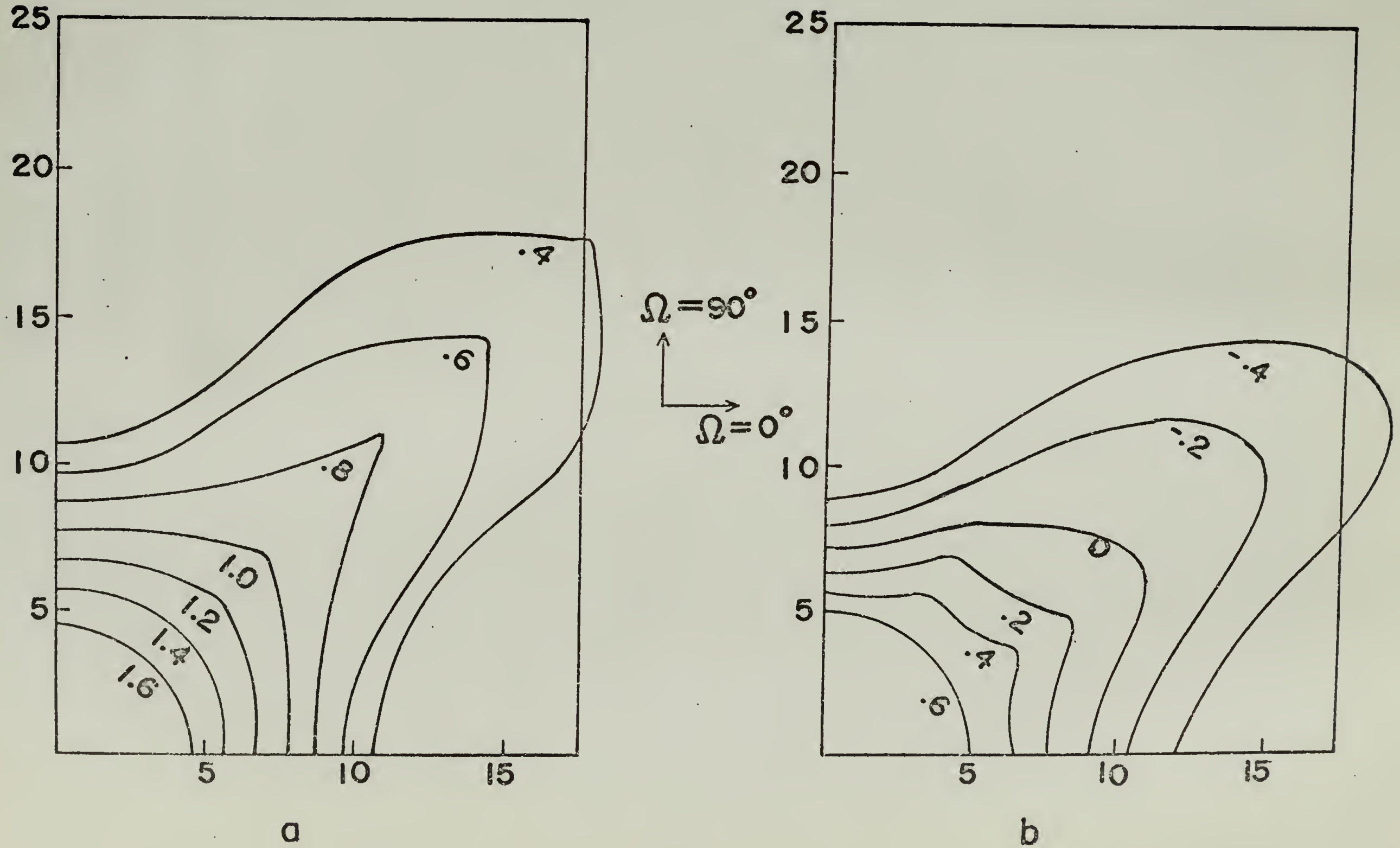
25
20
15
10
5
5
10
15
.4
.6
.8
1.0
1.2
1.4
1.6
Ω=90°
Ω=0°
a
25
20
15
10
5
5
10
15
.4
.2
0
.2
.4
.6
b

Figure 2

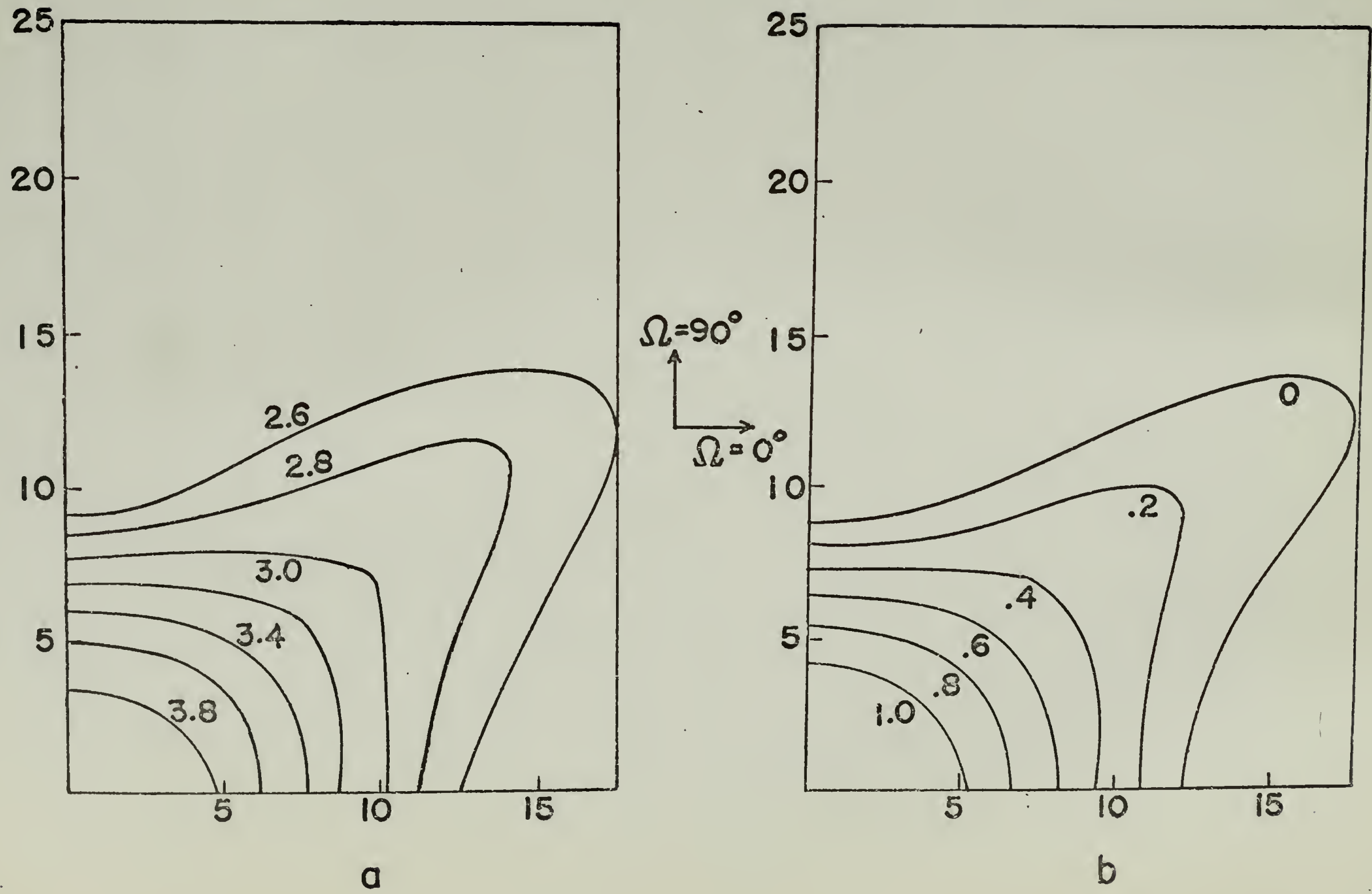
25
20
15
10
5
2.6
2.8
3.0
3.4
3.8
5
10
15
a
Ω=90°
Ω=0°
25
20
15
10
5
0
.2
.4
.6
.8
1.0
5
10
15
b

Figure 3

FURTHER RESEARCH

Low angle light scattering proved to be a useful technique for characterizing the superstructure during the early stages of crystallization and for measuring spherulitic growth rates as seen in Chapters 1 and 2.

The unanswered question in these studies is whether the crystallization started with a predetermined size of rod-like nuclei or whether the lineal growth rate of these rods is different than the spherulitic radial growth rate. To solve this problem one has to determine the size of the rod-like entities during the early stages. At the present time the theories for scattering from rod-like aggregates are not sophisticated enough for an accurate determination of the size of the rods. Furthermore, V_V scattering provided information about the spherulitic crystallization process and was used to explain the observations qualitatively. Recently developed theories can be employed to follow crystallization kinetics and studies of this nature are in progress presently.

In Chapter 3 it was determined that the nuclei for the growth of spherulites are not randomly located but are separated by a certain minimum distance. The computer program used for the simulation of an array of spherulites required that no two nuclei could be closer than this minimum distance. However, in reality this may be a continuous function and the program can be modified to take this into account. The "memory effect" suggested to explain the results can be verified by melting and crystallizing the polymer sample several times on a microscope hot stage and observing the spherulitic superstructure after every crystallization cycle.

Light scattering also proved to be a convenient technique for observing the superstructure formed during the strain induced crystallization of PET as shown in Chapter IV. Patterns from annealed cold drawn samples helped to qualitatively explain the scattering from rows of ellipsoidal spherulites. A theory could now be developed to predict scattering patterns from such row nucleated superstructures.

The stretching of PET above its glass transition temperature was done at only one strain rate. For a complete characterization of the superstructure in strain induced crystallized samples, a number of strain rates should be used. It has been pointed out earlier that a manually operated hand stretcher was used in this study and that a mechanically operated stretcher would be more desirable for any future studies. A mechanical device, however, tends to be bulky and may be difficult to quench fast enough to minimize relaxation of the stretched polymer. Changes occurring upon annealing the samples drawn above Tg were not investigated and would be another area for further research.

All the work done on stretched samples required the elongation of samples by predetermined amounts followed by characterization. A more practical approach would be to set up a small extruder with a slit die to extrude film and to study the superstructure as the polymer is extruded. A photographic light scattering set-up and a birefringence set-up could be used to obtain patterns and measure birefringence at various distances from the die. Another practical approach would be to use a shearing device and to study the crystallization from the shearing melt.

In this work several optical techniques have been successfully used to study the crystallization and deformation of polyethylene

terephthalate and could be extended for similar studies with other polymer systems.

A P P E N D I X

LIST OF COMPUTER PROGRAMS

PROGRAM 1

```
LIST SCATFAN
10    PROGRAM FANIHV
11*   THIS PROGRAM CALCULATES HV LIGHT SCATTERING INTENSITIES
12*   FROM SHEAVES AND IS USED IN CHAPTER II
13    DIMENSION F(129),T(3,3)
14    FUNC(U,V) =SIN(2.*U)/2./V/V*(COS(V)+V*SIN(V)-1.)
16   XT=1./3.
21   INPUT,TCR
22   INPUT,XMU
23   M=20
24   ENS=1.0E+9
25   KK=21
26   ALAMZ=6.328E-5
27   REFIND=1.67
28   TT=TCR*XT
30   PRINT 31,XT
31   FORMAT(5X,*CRITICAL TIME/HALF TIME =*,F4.2)
32   PRINT 33,TCR,TT
33   FORMAT(5X,*T/TCRITICAL=*,F4.2,5X,*T/THALF=*,F5.3)
34   XB=90.*TCR
35   PI=4.*ATAN(1.)
36   RC=(.75*LOG(2.)/(PI*ENS))**(1./3.)
37   R=RC*TT
38   RAD=R*1.E+4
40   PPINT 41,XMU,XB,RAD
41   FORMAT(*MU=*,F3.0,5X,*BETA=*,F4.1,5X,*RADIUS=*,F6.4,* MICRONS*)
44   PRINT 45
45   FORMAT(5X,* THETA *,11X,* I(HV) *,12X,* LOG(I(HV))*)
50    PI =4.*ATAN(1.)
51    C =4.*PI/ALAMZ
52    E =1./SQRT(3.)
53   AMU=XMU
54    AMU =AMU*PI/180.
55    ALAM =ALAMZ/REFIND
56    EM =M
58    MM =M/2-1
60    SMU =SIN(AMU)
64    B=PI*TCR/2.
66    H =2.*B/EM
68    GINC =2.*PI/128.
72    R1 =H*(1.+E)-B
74    R2 =H*(1.-E)-B
100   DO 250 K=1,KK,2
101   XK=K
102   AK=K
104   TH =AK*PI/180.
106   CTH =COS(TH)
108   STH =SIN(TH)
110   U =2.*PI*R/ALAM*STH
112   CRHO2 =CTH/SQRT(CTH*CTH+STH*STH*SMU*SMU)
```

```
114   PREMUL =2.*C*CRMO2*R*R
120   DO 200 I =1,129
122   Y1 =U*COS(AMU-R1)
124   Y2 =U*COS(AMU-R2)
126   EHV =FUNC(R1,Y1) + FUNC(R2,Y2)
130   DO 150 J =1,MM
132   AJ =J
134   TJ =2.*I*AJ
136   RJ1 =R1+TJ
138   RJ2 =R2+TJ
142   YJ1 =U*COS(AMU-RJ1)
144   YJ2 =U*COS(AMU-RJ2)
150   EHV =EHV + FUNC(RJ1,YJ1) + FUNC(RJ2,YJ2)
160   EHV =EHV*H*PREMUL
170   R1 =R1+GINC
180   R2 =R2+GINC
200   F(I) =EHV*EHV/2./PI
205   TWOPI =2.*PI
210   CALL ROMBERG (F,0.,TWOPI,129,8,0,T,AK)
212   CLN =LOG(C)
214   CLOG =CLN/LOG(10.)
216   PRINT 217,XK,C,CLOG
217   FORMAT(5X,F7.2,10X,E10.4,10X,E10.4)
250   CONTINUE
230   XMU=XMU-10.
231   IF(XMU .GT. 0.) 232,301
232   GO TO 49
301   GO TO 21
302   END
```

SUBROUTINE 1

```
402   SUBROUTINE ROMBERG (F,A,B,I,II,Q,T,AK)
404   DIMENSION F(I),T(II,II)
405   IF(AK .EQ. 1.)406,410
406   CNVG=1.0E-25
407   GO TO 412
410   CNVG=1.0E-10
412   K =1
414   J =1
416   C =B-A
420   L =1
422   SUM =0.
424   N =(I-1)/K
430   LL =L+N
432   SUM =SUM + F(L) + F(LL)
434   IF ( LL . EQ . I ) 450 ,440
440   L =LL
442   GO TO 430
450   C =C/2.
452   T(1,J) =C*SUM
454   J =J+1
456   K =K*2
458   IF ( J . EQ . (II+1) ) 460,420
460   D =1.
462   DO 480 M =2,II
463   KK =II-M+1
464   D =D*4.
465   K =1
466   T(M,K) =(D*T(M-1,K+1)-T(M-1,K))/(D-1.)
468   IF ( KK . EQ . 1 ) 490,470
470   DO 480 K =2,KK
472   T(M,K) =(D*T(M-1,K+1)-T(M-1,K))/(D-1.)
474   DIFF =ABSF(T(M,K)-T(M,K-1))
476   IF ( DIFF . LT . CNVG ) 490,480
480   CONTINUE
490   Q =T(M,K)
500   END
600   ENDPROG
```

PROGRAM 2

```
LIST TRUNK
Ø1 PROGRAM TRUNK
Ø2* THIS PROGRAM SIMULATES THE GROWTH OF TRUNCATED SPHERULITES
Ø3* FROM SPECIFIED LOCATION OF NUCLEI IN A GIVEN AREA.
Ø4* IT DETERMINES THE BOUNDARIES OF EACH SPERULITE AND CALCULATES
Ø5* ITS SIZE AND TRUNCATION PARAMETER.  IT THEN CALCULATES (1) THE
Ø6* ARITHMETIC AVERAGE AND AN AVERAGE WEIGHTED TO THE SIXTH POWER
Ø7* OF SIZE FOR THE SPERULITIC RADIUS AND TRUNCATION PARAMETER,
Ø8* (2) THE NUMBER OF NUCLEI PAIRS PER 1 MICRON INTERVAL CONTRIBUTING
Ø9* TO MUTUAL BOUNDARIES AND SEPARATED BY A DISTANCE AS A FUNCTION
1Ø* OF THE DISTANCE.  THIS PROGRAM IS USED IN CHAPTER III.
 12 COMMON XX(35Ø),YY(35Ø),NUC
 13 COMMON SPIX(6ØØ),SPIY(6ØØ),NSPI
 14 COMMON X(1ØØ),Y(1ØØ),IS,N
 15 COMMON LNUM(1ØØ)
 16 COMMON D(1ØØ),SLOPE(1ØØ),GAM(1ØØ),XMID(1ØØ),YMID(1ØØ)
 17 COMMON DI(1ØØ),TH(1ØØ)
 18 COMMON HN(1ØØ),HC(1ØØ),XINT(1ØØ),YINT(1ØØ)
 19 DIMENSION XXINT(2Ø),YYINT(2Ø)
 2Ø DIMENSION SA(2Ø),A(2Ø),STH(2Ø),THETA(2Ø),GAMM(2Ø)
 21 PI=4.*ATAN(1.)
 22 CALL NOMBRE
 24 SUM=Ø.  $ SUM6=Ø.  $ SUM7=Ø.
 25 SUMV=Ø.  $ SUMV6=Ø.
 26 DO 27 LL=Ø,5Ø
 27 LNUM(LL)=Ø
 3Ø DO 45Ø IS=1,NSPI
 32 CALL SELECT
 34 PRINT 35,IS,SPIX(IS),SPIY(IS)
 35 FORMAT(/,*SPHERULITE NO*,I3,5X,*SPIX=*,F6.1,5X,*SPIY=*,F6.1)
 36 K=1
 38 DO 6Ø IJ=1,N
 4Ø X(IJ)=X(IJ)-SPIX(IS)
 41 IF(X(IJ) .EQ. Ø.)42,44
 42 X(IJ)=X(IJ)+.Ø1
 44 Y(IJ)=Y(IJ)-SPIY(IS)
 46 D(IJ)=X(IJ)**2+Y(IJ)**2
 48 IF(IJ .EQ. 1)GO TO 6Ø
 5Ø DIFF=D(IJ)-D(K)
 52 IF(DIFF .GE. Ø.)GO TO 6Ø
 54 K=IJ
 6Ø CONTINUE
 7Ø DO 91 J=1,N
 72 SLOPE(J)=Y(J)/X(J)
 73 GAM(J)=ATAN(SLOPE(J))
 74 GAM(J)=ABSF(GAM(J)*18Ø./PI)
 76 IF(Y(J) .GT. Ø.)77,82
 77 IF(X(J) .GT. Ø.)78,8Ø
 78 GAM(J)=9Ø.-GAM(J)
 79 GO TO 9Ø
 8Ø GAM(J)=27Ø.+GAM(J)
 81 GO TO 9Ø
 82 IF(X(J) .GT. Ø.)83,85
```

```
83 GAM(J)=90.+GAM(J)
84 GO TO 99
85 GAM(J)=270.-GAM(J)
90 XY=0.
91 CONTINUE
92 GAMMA=GAM(K)
94 DO 110 KK=1,N
95 IF(KK .EQ. K)GO TO 93
96 IF(GAM(KK) .LE. GAMMA)102,93
98 GAM(KK)=GAM(KK)-GAMMA
100 GO TO 110
102 GAM(KK)=GAM(KK)+360.-GAMMA
110 CONTINUE
112 DO 136 I=1,N-1
114 DO 135 J=I+1,N
116 IF(GAM(I) .LE. GAM(J))GO TO 135
118 V1=GAM(I)
120 V2=X(I)
122 V3=Y(I)
123 V4=D(I)
124 GAM(I)=GAM(J)
125 D(I)=D(J)
126 X(I)=X(J) $ Y(I)=Y(J)
128 GAM(J)=V1
129 D(J)=V4
130 X(J)=V2 $ Y(J)=V3
135 CONTINUE
136 CONTINUE
140 DO 155 JJ=1,N
141 IF(Y(JJ) .EQ. 0.)142,144
142 HM(JJ)=1000.
143 GO TO 146
144 HM(JJ)=-X(JJ)/Y(JJ)
146 XMID(JJ)=X(JJ)/2.
148 YMID(JJ)=Y(JJ)/2.
150 HC(JJ)=YMID(JJ)-HM(JJ)*XMID(JJ)
155 CONTINUE
156 HC(N+1)=HC(1)
157 HM(N+1)=HM(1)
158 GAM(N+1)=360.
160 KJ=1
161 IN=0
164 PRINT 165
165 FORMAT(/6X,*NO*,6X,*XINT*,7X,*YINT*,7X,*AJ*,5X,*GAMMAJ*
166C,5X,*THETA*)
170 XINT(1)=0. $ YINT(1)=0.
172 JJJ=KJ+1
174 IF(IN .GE. 1)GO TO 177
175 M=N
176 GO TO 180
177 M=N+1
180 DO 300 JJ=KJ+1,M
190 ANGLE=GAM(JJ)-GAM(KJ)
191 IF(ANGLE .EQ. 0.)GO TO 360
192 IF(ANGLE .GE. 179.)GO TO 362
200 XINT(JJ)=(HC(KJ)-HC(JJ))/(HM(JJ)-HM(KJ))
210 YINT(JJ)=XINT(JJ)*HM(KJ)+HC(KJ)
230 TH(JJ)=(XINT(KJ)-XINT(JJ))**2+(YINT(KJ)-YINT(JJ))**2
```

```
235 IF(JJ .EQ. KJ+1)GO TO 300
260 IF(TH(JJ) .LE. TH(JJJ))270,300
270 JJJ=JJ
300 CONTINUE
302 IN=IN+1
304 IF(YINT(JJJ) .EQ. 0.)305,310
305 YINT(JJJ)=YINT(JJJ)+.01
310 STH(IN)=XINT(JJJ)/YINT(JJJ)
312 THETA(IN)=ATAN(STH(IN))
314 THETA(IN)=180.*THETA(IN)/PI
316 IF(YINT(JJJ) .GE. 0.)GO TO 322
318 THETA(IN)=THETA(IN)+180.
320 GO TO 326
322 IF(XINT(JJJ) .GE. 0.)GO TO 326
324 THETA(IN)=THETA(IN)+360.
326 XYXY=0.
330 IF(THETA(IN) .LT. GAMMA)GO TO 336
332 THETA(IN)=THETA(IN)-GAMMA
334 GO TO 340
336 THETA(IN)=THETA(IN)+360.-GAMMA
338
340 XXINT(IN)=XINT(JJJ)+SPHX(IS)
342 YYINT(IN)=YINT(JJJ)+SPHY(IS)
360 SA(IN)=XXIN(KJ)**2+YYIN(KJ)**2
362 A(IN)=SQRT(SA(IN))
364 GAMM(IN)=GAM(KJ)
366 IF(GAMM(IN) .LE. 360.)GO TO 370
367 GAMM(IN)=GAMM(IN)-360.
370 PRINT 372,IN,XXINT(IN),YYINT(IN),A(IN),GAMM(IN),THETA(IN)
372 FORMAT(5X,I2,5X,F6.2,5X,F6.2,5X,F5.2,5X,F5.1,5X,F5.1)
378 KJ=JJJ
390 IF(JJJ .GE. M)400,172
400 CALL COMPUTE(AMEAN,VAR,VARAA,A,GAMM,THETA,IN,LL,LNUM)
410 PRINT 412,AMEAN,VAR,VARAA
412 FORMAT(/5X,*AMEAN=*,F6.2,5X,*VAR=*,F8.4,5X,*VARAA=*,F8.4)
420 SUM=SUM+AMEAN
422 SUM6=SUM6+AMEAN**6
424 SUM7=SUM7+AMEAN**7
426 SUMV=SUMV+VARAA
428 SUMV6=SUMV6+VARAA*(AMEAN**6)
450 CONTINUE
455 XNSPH=NSPH
460 AAVG=SUM/XNSPH
462 AAVG6=SUM7/SUM6
464 VARAVG=SUMV/XNSPH
466 VARAVG6=SUMV6/SUM6
470 PRINT 471,AAVG,AAVG6
471 FORMAT(/5X,*AAVG=*,F8.3,10X,*AAVG6=*,F8.3)
475 PRINT 476,VARAVG,VARAVG6
476 FORMAT(/5X,*VARAVG=*,F9.4,7X,*VARAVG6=*,F9.4)
478 LSUM=0.
480 DO 490 LL=0,50
482 PRINT 484,LL,LNUM(LL)
434 FORMAT(10X,I4,5X,I20)
486 LSUM=LSUM+LNUM(LL)
490 CONTINUE
492 PRINT,LSUM
500 END
```

SUBROUTINE 2

```
LIST NOMBRE
10 SUBROUTINE NOMBRE
11* THIS SUBROUTINE IS USED IN THE MAIN PROGRAM TRUNK.
12* IT SPECIFIES THE TOTAL NUMBER OF SPHERULITES (NUC) AND THE
13* RADIUS OF THE CIRCLE (RCIR) IN WHICH THEY ARE LOCATED.
14* IT ALSO SELECTS THE NUMBER OF SPHERULITES (NSPH) FOR WHICH
15* THE SIZE AND TRUNCATION PARAMETER ARE CALCULATED
16* IN THE PRESENT CASE NUCLEI ARE GENERATED RANDOMLY.
17* IF NUCLEI CENTERS ARE KNOWN, STATEMENTS FROM 70 TO 90 C
18* 70 TO 90 SHOULD BE REPLACED BY READ STATEMENTS.
20 COMMON XX(850),YY(350),NUC
22 COMMON SPHX(600),SPHY(600),NSPH
24 COMMON X(100),Y(100),IS,N
60 NUC=300
62 RCIR=225.
65 DO 90 I=1,NUC
70 XX(I)=RANF(-1)*450.
74 YY(I)=RANF(-1)*450.
76 RADIUS=(225.-XX(I))**2+(225.-YY(I))**2
78 RCONST=225.**2
80 IF(RADIUS .GE. RCONST)GO TO 70
82 DO 90 J=1,I-1
84 DIFF=(XX(I)-XX(J))**2+(YY(I)-YY(J))**2
86 XDIF=4.**2
88 IF(DIFF .LT. XDIF)GO TO 70
90 CONTINUE
95 IJ=0
100 DO 150 I=1,NUC
105 CHECK=(XX(I)-225.)**2+(YY(I)-225.)**2
110 XLIM=190.**2
115 IF(CHECK .GE. XLIM)GO TO 150
125 IJ=IJ+1
130 SPHX(IJ)=XX(I)
135 SPHY(IJ)=YY(I)
150 CONTINUE
160 NSPH=IJ
170 PRINT 171,NUC
171 FORMAT(//5X,*TOTAL NO. OF SPHERULITE CENTERS =*,I4)
175 PRINT 176,NSPH
176 FORMAT(/5X,*NUMBER OF SPHERULITES CONSIDERED=*,I4)
200 END
```

```
LIST SELECT
10 SUBROUTINE SELECT
11* THIS SUBROUTINE IS USED WITH THE MAIN PROGRAM TRUNK.
12* FOR ANY GIVEN SPHERULITE "I" IT SELECTS ITS NEAREST
13* NEIGHBORS.  IN THIS CASE ALL NEIGHBOURING SPHERULITES (N)
14* IN A CIRCLE OF RADIUS 60 UNITONS WERE CONSIDERED
20 COMMON XX(350),YY(350),NUC
22 COMMON SPHX(600),SPHY(600),NSPH
24 COMMON X(100),Y(100),IS,N
30 JI=0
40 DO 100 I=1,NUC
45 DCHECK=(XX(I)-SPHX(IS))**2+(YY(I)-SPHY(IS))**2
50 IF(DCHECK .EQ. 0.)GO TO 100
55 DCONS=60.**2
60 IF(DCHECK .GT. DCONS)GO TO 100
65 JI=JI+1
70 X(JI)=XX(I)
75 Y(JI)=YY(I)
100 CONTINUE
110 N=JI
115 IF(N .LT. 90)GO TO 120
116 PRINT,N
120 END
```

SUBROUTINE 4

```
LIST COMPUTE
 10 SUBROUTINE COMPUTE(AMEAN,VAR,VARAA,A,GAMM,THETA,IN,LL,LNUM)
 11* THIS SUBROUTINE IS USED WITH THE MAIN PROGRAM TRUNK
 12* IT CALCULATES THE AVERAGE SIZE AND THE TRUNCATION
 13* PARAMETER FOR EACH SPHERULITE.
 20 DIMENSION A(20),GAMM(20),THETA(20)
 25 DIMENSION AI(200),DA(200)
 26 DIMENSION LNUM(100)
 30 PI=4.*ATAN(1.)
 32 NINC=130
 34 XINC=NINC
 36 DELAL=360./XINC
 38 AMEAN=0.
 40 J=1
 42 THETA(IN+1)=360.
 44 A(IN+1)=A(1)
 45 GAMM(IN+1)=360.+GAMM(1)
 60 DO 100 I=1,NINC
 70 XI=I-1
 72 ALPHA=XI*DELAL
 74 ERROR=THETA(J)-ALPHA
 76 ERR=DELAL
 78 IF(ERROR .LT. ERR)80,32
 80 J=J+1
 82 GAMAL=(GAMM(J)-ALPHA)*PI/180.
 84 AI(I)=ABSF(A(J)/COS(GAMAL))
 86 AMEAN=AMEAN+AI(I)
100 CONTINUE
102 AMEAN=AMEAN/XINC
104 SQAM=AMEAN**2
120 VAR=0.
130 DO 150 I=1,NINC
132 DA(I)=AI(I)-AMEAN
140 VAR=VAR+DA(I)**2
150 CONTINUE
160 VAR=VAR/XINC
170 VARAA=VAR/SQAM
200 DO 220 L=1,IN
205 A(L)=A(L)*2
210 LL=A(L)
215 LNUM(LL)=LNUM(LL)+1
220 CONTINUE
300 END
310 ENDPROG
400
```

PROGRAM 3

```
LIST RODSCAT
10 PROGRAM RODSCAT
11* THIS PROGRAM CALCULATES HV LIGHT SCATTERING INTENSITIES
12* FROM UNORIENTED AND ORIENTED RODS
13* IT IS USED IN CHAPTER V
14 FORMAT(*LIGHT SCATTERING FROM RODS*)
15 DIMENSION F(500)
20 READ,XL1,H1,XL2,H2
22 PI=4.*ATAN(1.)
24 ALAMZ=.6328
26 REFIND=1.67
28 ALAM=ALAMZ/REFIND
30 XK=2.*PI/ALAM
32 OMEG1=0.
34 OMEG2=PI/2.
36 M=180
38 AM=M
40 DEL=PI/AM
42 INPUT,E
44 PRINT 14
45 FORMAT(
50 PRINT 51,XL1,H1,XL2,H2
51 FORMAT(*L1=*,F5.3,5X,*H1=*,F5.3,5X,*L2=*,F5.3,5X,*H2=*,F5.2)
60 PRINT 61,E
61 FORMAT(*ORIENTATION FACTOR=*,F5.1)
90 DO 400 MU=0,90,15
92 AMU=MU
94 XMU=AMU*PI/180.
96 PRINT 97,AMU
97 FORMAT(*AZIMUTHAL ANGLE=*,F5.2)
200 DO 400 KTH=2,20,2
202 XTH=KTH
204 TH=XTH*PI/180.
206 SUM=0.
210 DO 350 J=0,M
212 XJ=J
214 AL=XJ*DEL
220 U1=SIN(AL+OMEG1)*COS(AL+OMEG1)
224 A1=-SIN(TH)*SIN(AL+XMU)
226 B1=-SIN(TH)*COS(AL+XMU)
232 V1=SIN(XK*A1*XL1/2.)*SIN(XK*B1*H1/2.)/(XK*XK*A1*B1)
234 EHV=4.*U1*V1
264 XX=SIN(AL)*SIN(AL)*E*E+COS(AL)*COS(AL)/E/E
266 ORIEN=1./(SQRT(XX))
290 IF(J .EQ. 0)300,291
291 IF(J .EQ. M)300,303
300 C=1.
```

```
302 GO TO 320
308 HALFJ=J/2
309 HALFJ=J/2
310 DIFF=XJ/2.-HALFJ
312 IF(DIFF .EQ. 0.)316,314
314 C=4.
315 GO TO 320
316 C=2.
320 F(J)=C*ELV*EHV*ORIEN*DEL/3.
330 SUM=SUM+F(J)
350 CONTINUE
352 SUM=SUM*10000.
354 SUMLOG=LOG(SUM)
370 PRINT 371,XTH,SUM,SUMLOG
371 FORMAT(F7.2,10X,E12.4,10X,E12.4)
400 CONTINUE
500 END
502 ENDPROG
510 2.,.02,.2,.02
```

PROGRAM 4

```
LIST SHISH
10 PROGRAM KEBAB
11* THIS PROGRAM CALCULATES MV LIGHT SCATTERING INTENSITIES
12* FROM SHISH KEBABS AND IS USED IN CHAPTER V
15 DIMENSION P(500),T(300)
17 FORMAT(*LIGHT SCATTERING CALCULATIONS FOR SHISH KABABS*)
19 FORMAT(*KABABS ARE RANDOMLY SPACED*)
20 READ,XL1,H1,XL2,H2
22 PI=4.*ATAN(1.)
24 ALAMZ=.6328
26 REFIND=1.67
28 ALAM=ALAMZ/REFIND
30 XK=2.*PI/ALAM
32 OMEG1=0.
34 OMEG2=PI/2.
36 M=180
38 AM=M
40 DEL=PI/AM
42 INPUT,E
44 XINTROD=.02
46 PRINT 17
48 PRINT 19
50 PRINT 51,XL1,H1,XL2,H2
51 FORMAT(*L1=*,F5.3,5X,*H1=*,F5.3,5X,*L2=*,F5.3,5X,*H2=*,F5.2)
53 PRINT 59,XINTROD
59 FORMAT(*MINIMUM INTER ROD DISTANCE=*,F5.3)
60 PRINT 61,E
61 FORMAT(*ORIENTATION FACTOR=*,F5.2)
100 DO 118 I=1,20
102 P(I)=RANF(-1)*XL1/2.
104 IF(I .EQ. 1)118,106
106 DO 112 II=1,(I-1)
108 DP=ABSF(P(I)-P(II))
110 IF(DP .LT. XINTROD)102,112
112 CONTINUE
118 CONTINUE
120 DO 138 K=21,40
122 P(K)=RANF(-1)*(-XL1/2.)
126 DO 132 KK=1,(K-1)
128 DP=ABSF(P(K)-P(KK))
130 IF(DP .LT. XINTROD)122,132
132 CONTINUE
138 CONTINUE
180 DO 400 MU=0,90,15
182 ANU=MU
184 XMU=ANU*PI/180.
186 PRINT 187,ANU
187 FORMAT(*AZIMUTHAL ANGLE=*,F5.1)
```

```
190 PRINT 191
191 FORMAT(3X,*THETA*,15X,*ENV*,17X,*LOGENV*)
200 DO 400 KTH=2,30,2
202 XTH=KTH
204 TH=XTH*PI/180.
206 SUM=0.
210 DO 350 J=0,M
212 XJ=J
214 AL=XJ*DEL
216 F2=0.
220 U1=SIN(AL+0.5EG1)*COS(AL+0.5EG1)
222 U2=SIN(AL+0.5EG2+PI/2.)*COS(AL+0.5EG2+PI/2.)
224 A1=-SIN(TH)*SIN(AL+XMU)
226 B1=-SIN(TH)*COS(AL+XMU)
228 A2=SIN(TH)*COS(AL+XMU)
230 B2=-SIN(TH)*SIN(AL+XMU)
232 V1=SIN(XK*A1*XL1/2.)*SIN(XK*B1*H1/2.)/(XK*XK*A1*B1)
234 ENV1=4.*U1*V1
236 V2=SIN(XK*B2*H2/2.)*(SIN(XK*A2*XL2/2.)-SIN(XK*A2*H1/2.))
238C/(XK*XK*A2*B2)
240 DO 244 IK=1,40
242 F2=F2+COS(XK*SIN(TH)*SIN(AL+XMU)*P(IK))
244 CONTINUE
260 ENV2=4.*U2*V2*F2
262 ENV=ENV1+ENV2
264 XX=SIN(AL)*SIN(AL)*E*E+COS(AL)*COS(AL)/E/E
266 ORIEN=1./(SQRT(XX))
290 IF(J .EQ. 0)300,291
291 IF(J .EQ. M)300,308
300 C=1.
302 GO TO 320
308 HALFJ=J/2
309 HALFJ=J/2
310 DIFF=XJ/2.-HALFJ
312 IF(DIFF .EQ. 0.)316,314
314 C=4.
315 GO TO 320
316 C=2.
320 F(J)=C*ENV*ENV*ORIEN*DEL/3.
330 SUM=SUM+F(J)
350 CONTINUE
352 SUM=SUM*100000.
354 SUMLOG=ALOG(SUM)
370 PRINT 371,XTH,SUM,SUMLOG
371 FORMAT(F7.2,10X,E12.4,10X,E12.4)
400 CONTINUE
500 END
502 ENDPROG
510 2.,.02,.2,.02
```